GEAP-22212
UC-78
SEPTEMBER 1982

FLOW-INDUCED VIBRATION CHARACTERISTICS OF BWR/6 JET PUMPS

L. V. LACROIX

U.S. DEPARTMENT OF ENERGY
PRIME CONTRACT DE-AC02-77ET34209-28

GENERAL ELECTRIC

GEAP 22212
UC-78
September 1982

GEAP--22212

DE83 003976

FLOW-INDUCED VIBRATION CHARACTERISTICS OF BWR/6 JET PUMPS

L. V. LaCroix

Reviewed: Martin R. Torres
M. R. Torres, Manager
FIV Experiments

Reviewed: C. H. Solanas
C. H. Solanas, Manager
Hydrodynamics & Mechanical
Component Design

Approved: E. Kiss
E. Kiss, Manager
Applied Mechanics

U.S. DEPARTMENT OF ENERGY
PRIME CONTRACT DE-AC02-77ET34209-28

GENERAL ELECTRIC

DISCLAIMER

Printed in the United States of America

Available from
National Technical Information Service
U.S. Department of Commerce
5285 Port Royal Road
Springfield, VA 22161

Price: Code A04
Microfiche A01

TABLE OF CONTENTS

TABLE OF CONTENTS (Continued)

LIST OF ILLUSTRATIONS

LIST OF ILLUSTRATIONS (Continued)

LIST OF ILLUSTRATIONS (Continued)

LIST OF ILLUSTRATIONS (Continued)

LIST OF TABLES

1. INTRODUCTION

The purpose of this report is to document the results of two recent jet pump tests at the General Electric Large Steam-Water Test Facility at Moss Landing, California. A BWR/6-251 standard plant jet pump and a BWR/6-218 standard plant jet pump were tested for flow-induced vibration (FIV) characteristics at a variety of test conditions, both prototypical and nonprototypical. The two separate tests were conducted during February and March 1978 in conjunction with regularly scheduled jet pump thermal and hydraulic performance tests.

The primary purpose of jet pump testing at Moss Landing has been the calibration of jet pump thermal and hydraulic performance characteristics. Early prototypical jet pump vibration tests were conducted at Moss Landing in 1970[1] in conjunction with these performance tests. Recently, more in-depth vibration investigations have been performed.

Documented degradation of jet pump support structures in a domestic plant occurred early in 1974. These field difficulties prompted additional interest in jet pump FIV characteristics. A comprehensive test program was undertaken in response to the 1974 field problems. The results of this test program were published in 1976.[2] At that time, it was shown that high-level FIV could occur if a jet pump was improperly installed. It was also shown that the high-level FIV could occur in properly installed jet pumps but only at non-operational (off-design curve) conditions.

Experience gained from other FIV test programs, in particular the feedwater sparger tests,[3] resulted in a hypothesis that the jet pump slip-fit between the inlet mixer and diffuser was the major contributor to the high-level FIV. The differential pressure across the slip joint was observed to be a controlling parameter.

Early in 1976, a BWR/5-201 standard plant jet pump was instrumented for FIV and exhaustively tested at Moss Landing. Contrary to previous experience, this jet pump exhibited high-level FIV at normal reactor operating conditions with proper installation. Further testing demonstrated that elimination of the slip joint (filling the gap with packing material) eliminated the high-level FIV. Plans were then made to retest the BWR/5-201 jet pump in 1978 to further under-

stand the unique FIV mechanism and to evaluate a number of potential "fixes" which were proposed to eliminate high-level FIV. The results of that test program were published in January 1979.[4]

2. JET PUMP DESCRIPTION AND OPERATION

The function of the jet pump in a boiling water reactor is to induce flow (suction flow) via a high velocity jet flow (drive flow, recirculation pump flow) to produce the required total flow (core flow) with sufficient head to recirculate the coolant through the reactor core. Although there are no moving parts in the jet pump, it consists of three separate sections: (1) riser; (2) inlet mixer assembly; and (3) diffuser. In the BWR/6-251 reactor, there are 24 jet pumps (two jet pumps per riser) located in the annulus between the reactor core and the reactor pressure vessel. In the BWR/6-218 reactor, there are 20 jet pumps similarly arranged. A typical jet pump pair is shown in Figure 2-1. In the Moss Landing test facility, space limitations required that a single jet pump, rather than a pair, be tested. The second branch at the top of the riser pipe was blanked.

The riser penetrates and is rigidly connected to the reactor pressure vessel wall at the point of penetration and again by a support bracket near the top of the riser pipe. The inlet mixer assembly is loaded into a mating socket in the riser by a beam-bolt assembly (Figure 2-2). The loading is accomplished by a hydraulic tensioner and is typically 30,000 lb to achieve a tight hydraulic seal and mechanical rigidity while allowing easy removal for inspection and/or repair. The middle of the mixer assembly is secured to the riser pipe by means of a restrainer bracket. Two adjusting screws and a self-tightening wedge assembly secure the mixer within the restrainer bracket with three-point contact (Figure 2-3). In the Moss Landing test facility, a prototypical restrainer bracket was modified to allow single jet pump operation with a wide variety of mixer geometries.

In the reactor, the jet pump diffuser is welded at its lower end to the shroud support shelf, which connects the reactor core to the pressure vessel wall. Because of the differential thermal expansion between the dissimilar materials of the reactor vessel, jet pump and core, the jet pump diffuser is not attached to the mixer. Rather, the mixer is inserted into the top of the diffuser with a nominal 0.008-in. radial clearance (gap) between the two components to allow relative axial movement. This insertion region is the slip joint. A typical

jet pump assembly in a BWR is shown in Figure 2-4. In the Moss Landing test facility, the jet pump diffuser was attached to the inside of the test vessel by means of a universal clamping arrangement employing standard pump packing material to achieve a tight hydraulic seal.

In jet pump functional operation, a conversion of drive flow momentum to suction flow pressure head occurs in the inlet mixer region. High-velocity fluid emerging from the nozzles has high momentum. Low energy fluid around the high-velocity jet is drawn into the mixer by the pressure difference existing between the suction fluid and the driving fluid with momentum being transferred to the low energy suction fluid. A turbulent, high-velocity stream then enters the diffuser inlet. In the diffuser, the velocity head is converted to the pressure head required for the core flow. A schematic representation of the internal jet pump pressure is shown in Figure 2-5a. From this figure, it is apparent that the differential pressure between the fluid inside and outside the jet pump at the slip joint (i.e., slip-joint differential pressure) is a function of the location of the slip joint along the jet pump axis. In general, the slip-joint differential pressure (SJDP) is positive, resulting in leakage flow out of the jet pump as shown in Figure 2-5b.

Significant parameters describing the hydraulic condition of a jet pump are: (1) M-ratio (M); (2) drive flow (W_D); (3) total flow (W_T); and (4) suction flow (W_S) (Figure 2-6), with the flow in units of lb/sec or lb/hr. The M-ratio is defined as the ratio of suction flow to drive flow:

$$M = W_S/W_D. \tag{2-1}$$

The remaining parameters are interrelated as follows:

$$W_S = W_T - W_D \tag{2-2}$$

$$M = W_T/W_D - 1 \tag{2-3}$$

Note that only two of these parameters are required to completely describe the hydraulic conditions of a given jet pump. Since the M-ratio and drive flow are most directly related to BWR operation, they have traditionally been used as the hydraulic variables for establishing test conditions. The operating

curve of M-ratio and drive flow for the BWR/6-218 jet pump is shown in Figure 2-7a. The two curves represent the predicted[5] reactor recirculation system performance at beginning of life (BOL) and end of life (EOL). The EOL prediction is the design condition[10] for the plant. Figure 2-7b shows the relationship between core flow (total flow) and drive flow. Figure 2-8 shows the predicted[5,11] reactor recirculation system performance curves for the BWR/6-251 plant. There are actually three different plant designs designated BWR/6-251, classed according to thermal power rating: 3800 MW, 4069 MW, and 4146 MW. All contain the same size jet pumps. The test conditions at Moss Landing were established to simulate the performance of the 4146 MW plant. However, Figure 2-8 shows both the 4146 MW and 3800 MW performance curves at both BOL and EOL for comparison.

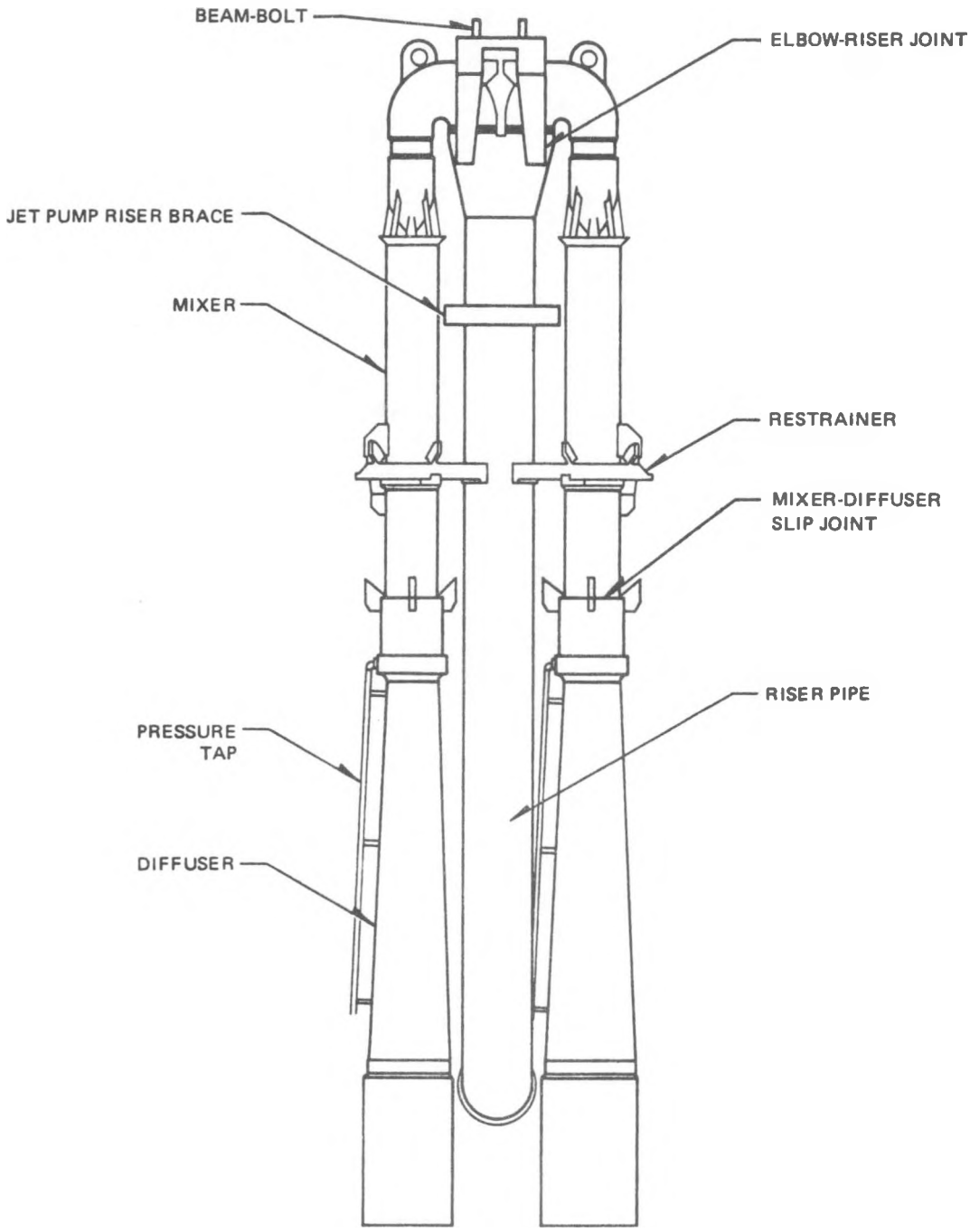

Figure 2-1. Complete BWR Jet Pump Assembly

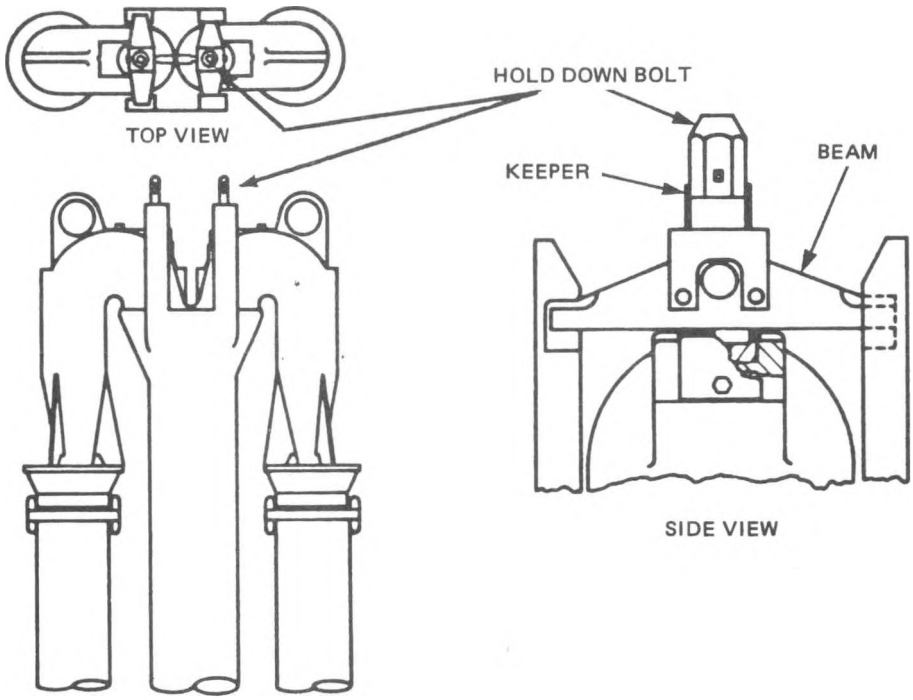

Figure 2-2. Beam-Bolt Assembly for a BWR Jet Pump

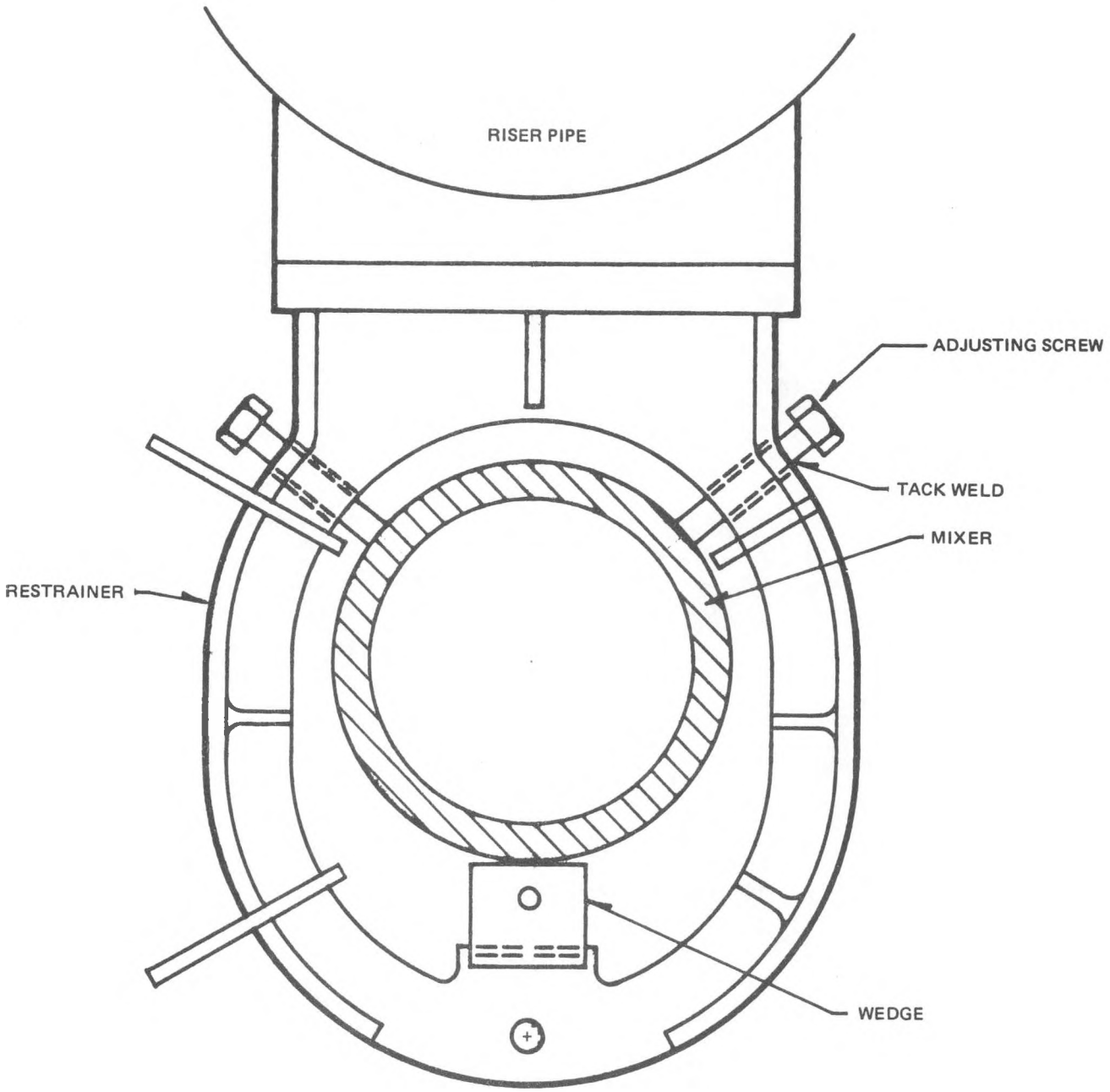

Figure 2-3. Moss Landing Restrainer Used with BWR/6 Jet Pump Test (Not to Scale)

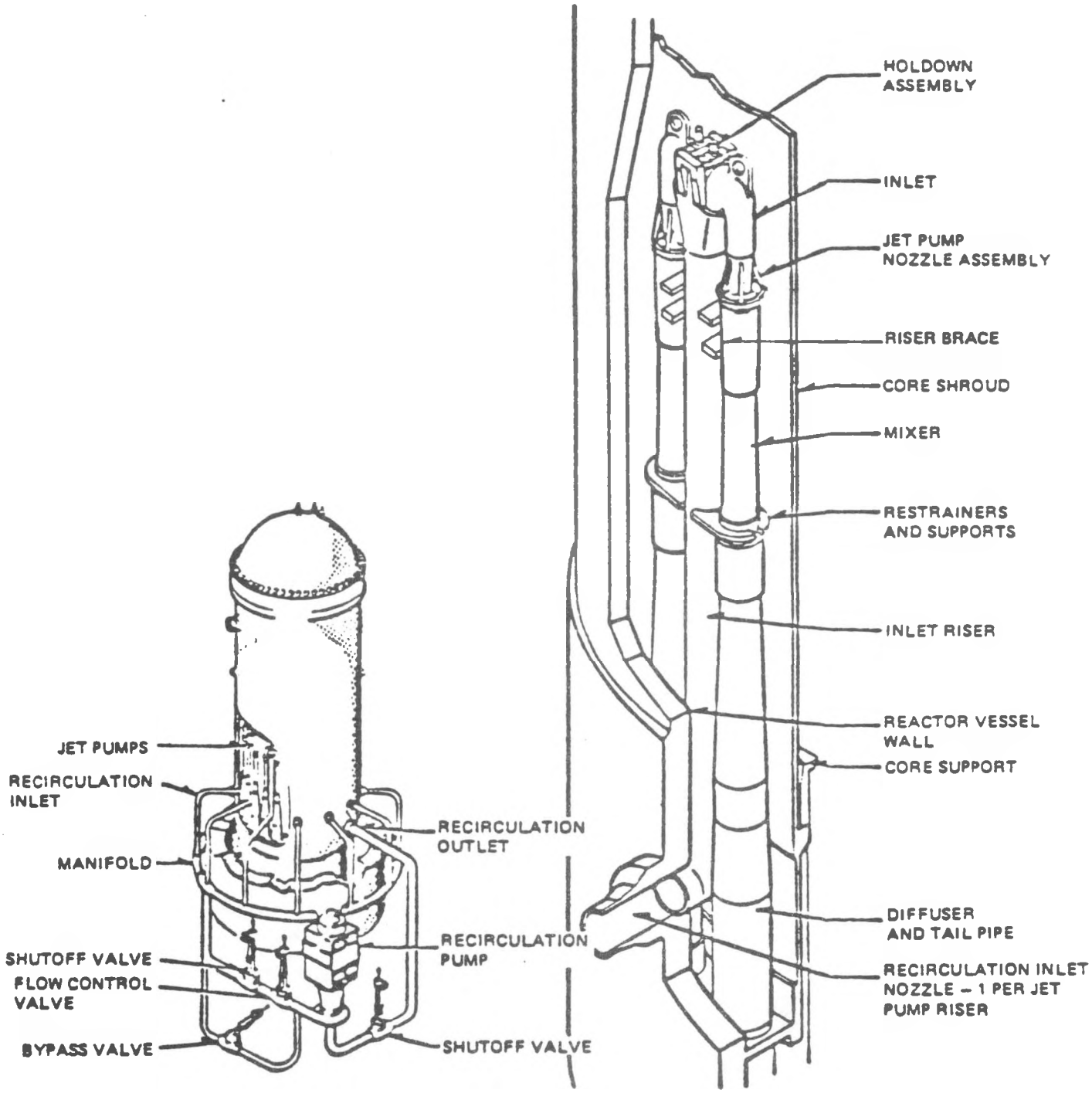

Figure 2-4. Jet Pump Assembly in a BWR

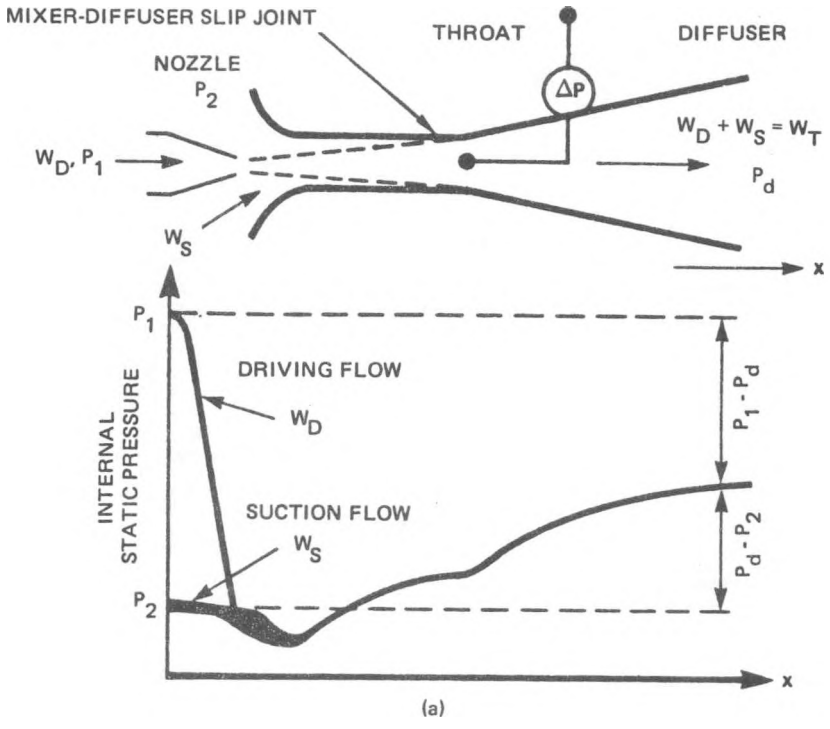

Figure 2-5a. Internal Jet Pump Pressure

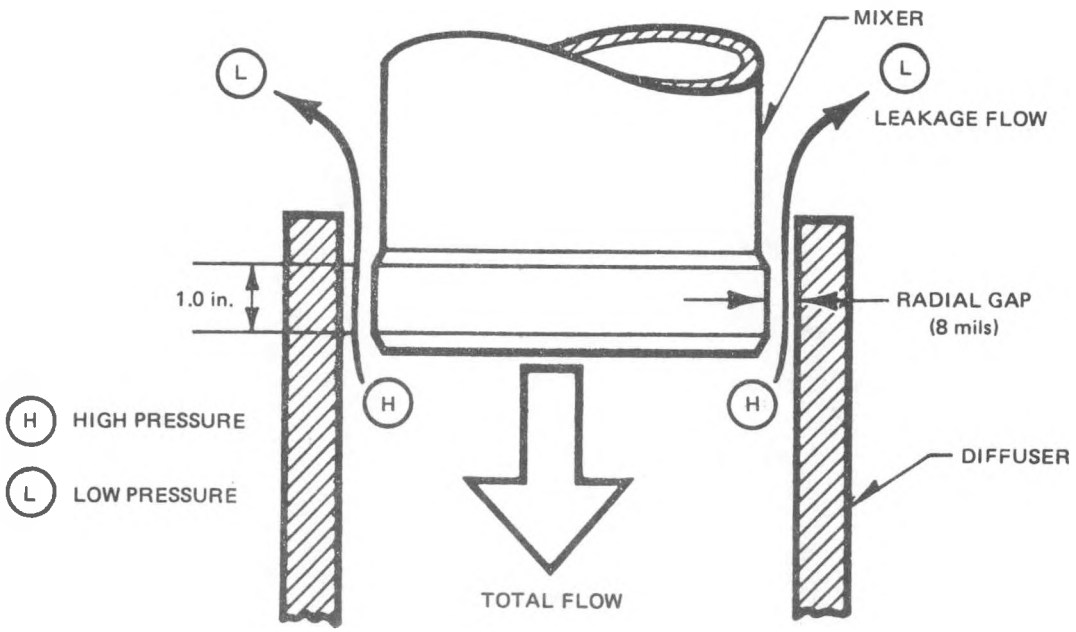

Figure 2-5b. Leakage Flow Path at the Jet Pump Slip Joint

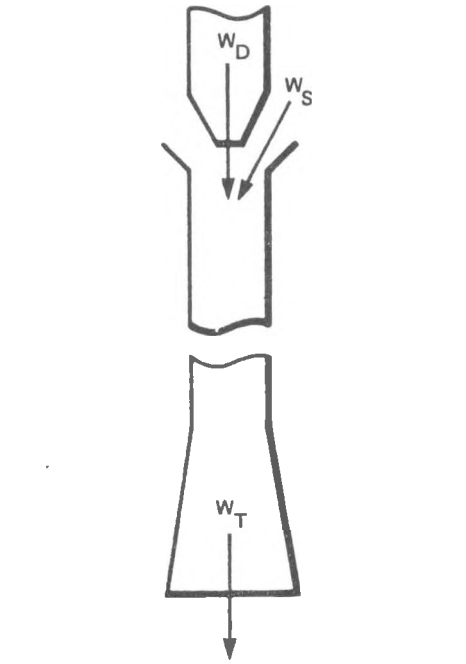

Figure 2-6. Parameters Describing Jet Pump Hydraulic Condition

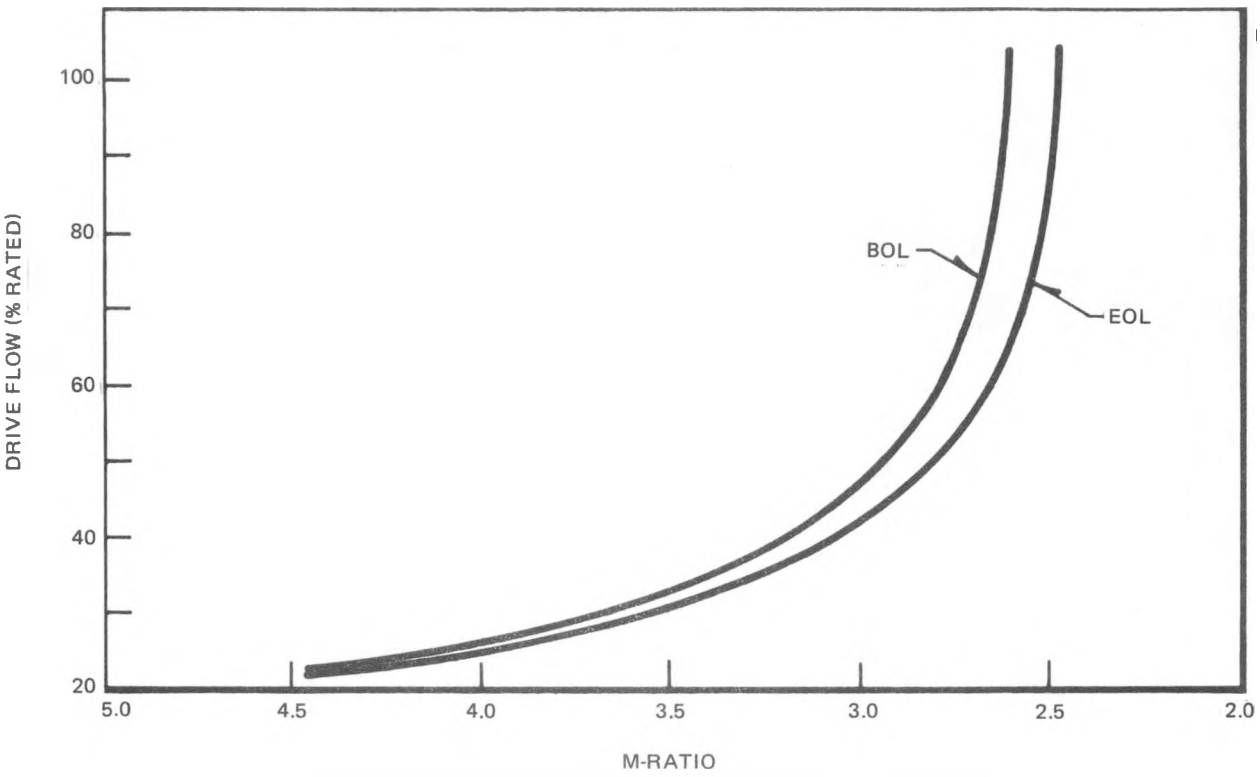

Figure 2-7a. BWR/6-218 Predicted Recirculation Performance-Drive Flow versus M-Ratio

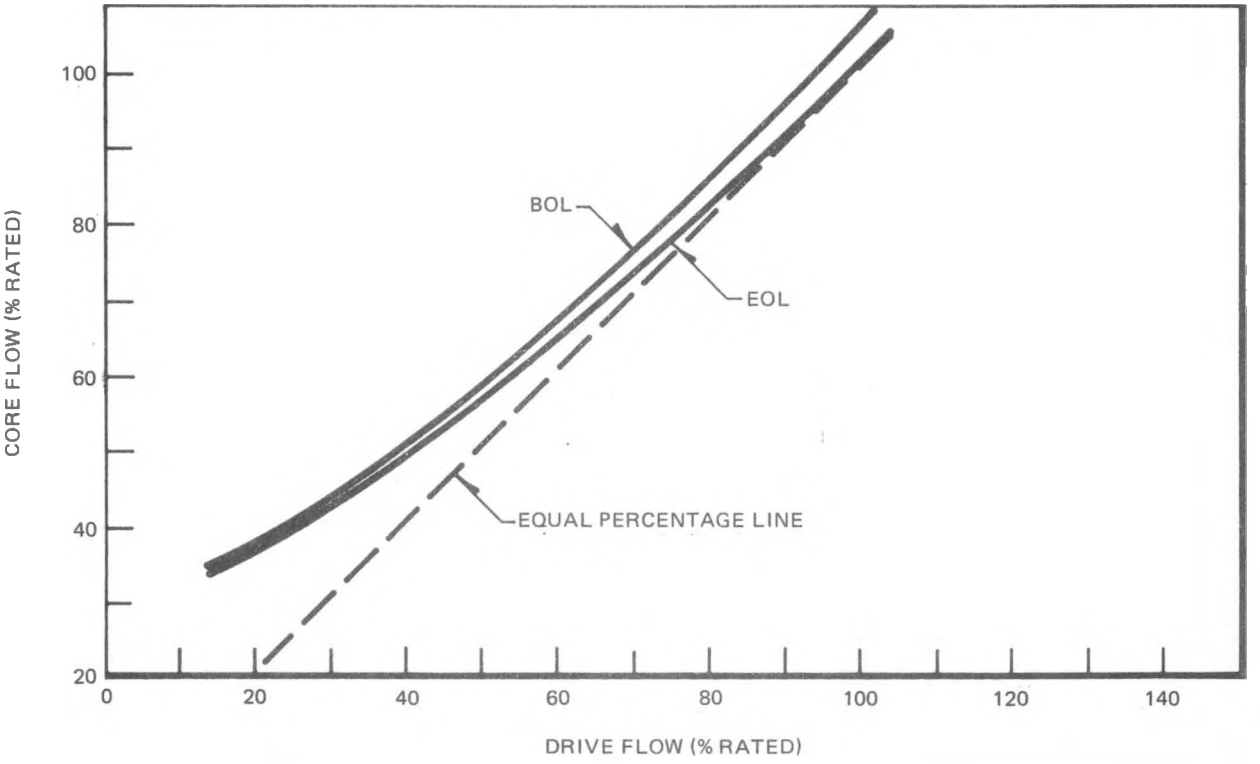

Figure 2-7b. BWR/6-218 Predicted Recirculation System Performance-Core Flow versus Drive Flow

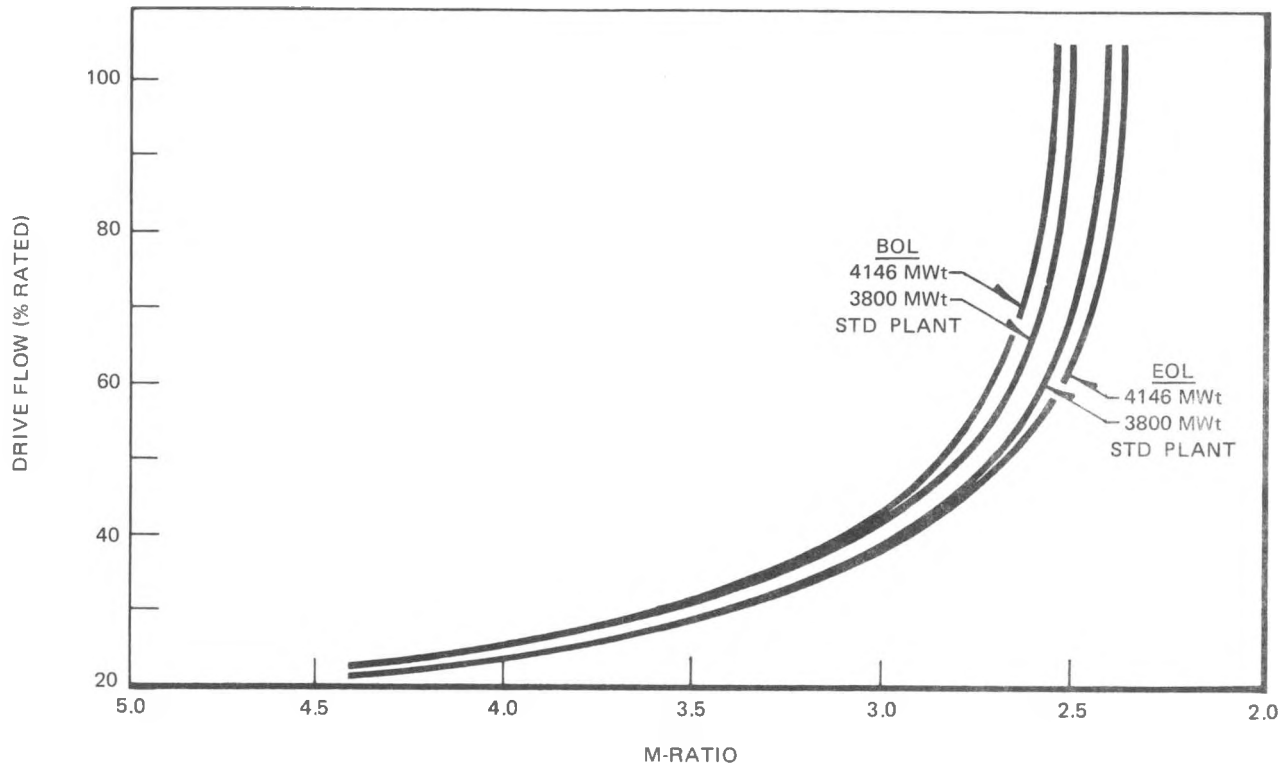

Figure 2-8a. BWR/6-251 Predicted Recirculation System Performance-Drive Flow versus M-Ratio

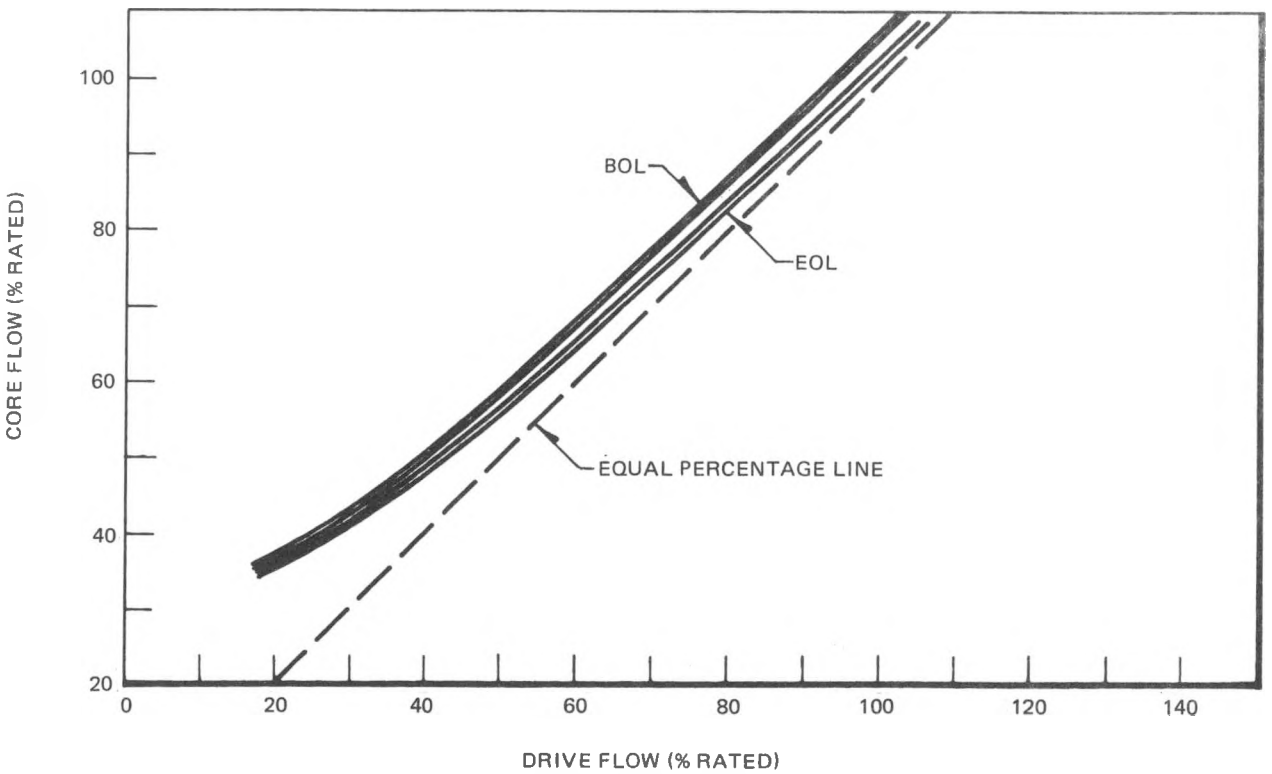

Figure 2-8b. BWR/6-251 Predicted Recirculation System Performance-Core Flow versus Drive Flow

3. TEST FACILITY DESCRIPTION

The General Electric Large Steam-Water Test Facility is located at the Pacific Gas and Electric fossil power plant at Moss Landing, California. The test facility consisted of a 42-in. i.d. pressure vessel, recirculation pump and associated steam/water piping and controls capable of operating at BWR thermal-hydraulic conditions (~550°F, 1000 psig). Boiler feedwater and live steam needed to pressurize and operate the test facility were provided by PG&E. The test vessel with jet pump installed is shown in Figure 3-1.

A schematic flow diagram of the test facility is shown in Figure 3-2. The drive flow (recirculation pump flow) and total flow (core flow) were regulated by individual flow control valves. Flow rates were determined from the differential pressures across calibrated orifice plates. Static and differential pressures throughout the test vessel were monitored and used to provide the data needed to compute SJDP and jet pump hydraulic performance characteristics. Both drive flow and total flow rates were variable to allow jet pump operations over a wide range of design and off-design hydraulic conditions.

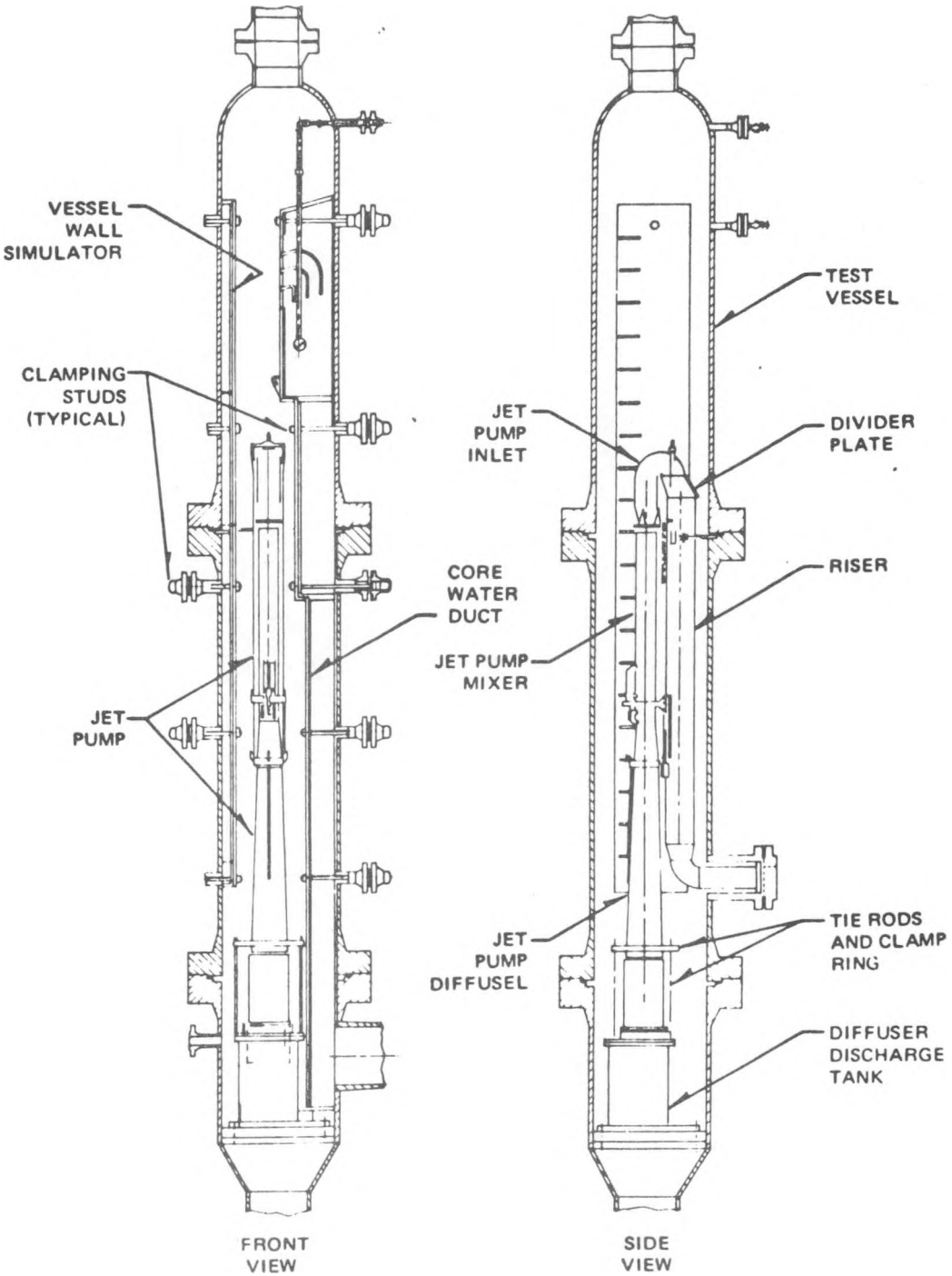

Figure 3-1. Jet Pump FIV Test at Moss Landing

1 RECIRCULATION PUMP
2 DRIVE FLOW (W_D) ORIFICE
3 W_D ORIFICE DIFFERENTIAL PRESSURE
4 W_D FLOW CONTROL VALVE
5 TOTAL FLOW (W_T) CONTROL VALVE
6 W_T ORIFICE
7 W_T ORIFICE DIFFERENTIAL PRESSURE
8 MOSS LANDING TEST VESSEL
9 MIXER-DIFFUSER SLIP JOINT

NOTE:
1. (R_a) REPRESENTS AN ABSOLUTE OR DIFFERENTIAL PRESSURE MEASUREMENT
2. W_S REPRESENTS SUCTION FLOW

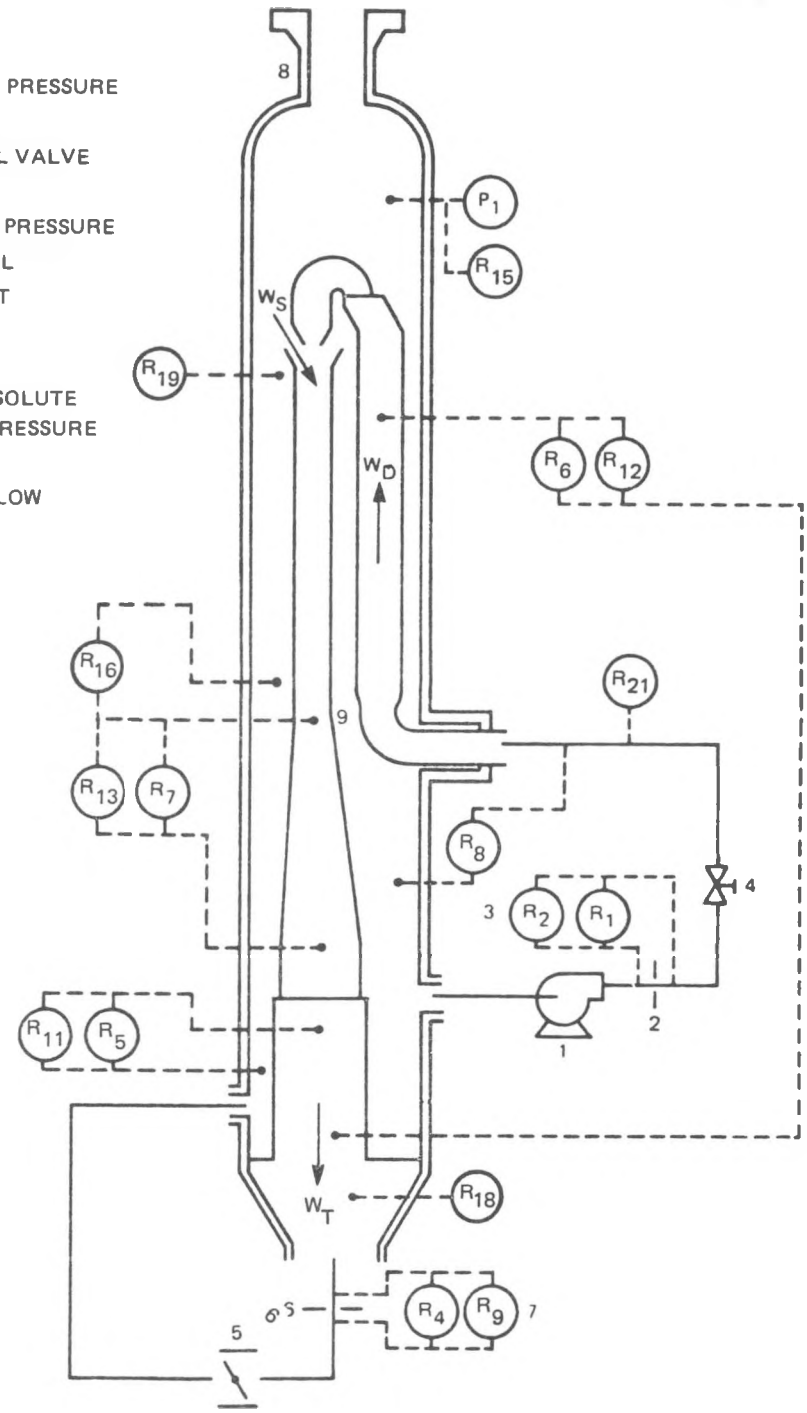

Figure 3-2. Schematic of Moss Landing Flow Facility

4. TEST PROGRAM

4.1 TEST OBJECTIVE

The test objective was to determine the FIV characteristics of a BWR/6-251 and a BWR/6-218 standard plant jet pump at typical BWR thermal-hydraulic operating conditions and at number of off-design test conditions. This test objective was to be accomplished in conjunction with the routine thermal-hydraulic performance tests which, historically, have been conducted for each new jet pump design.

4.2 TEST PLAN

The overall test plan was to obtain as much FIV information as practical under a wide variety of jet pump operating conditions. The test plan, instrumentation and conditions were identical for the two jet pumps tested, and are described generally herein. For each jet pump tested, four separate test conditions were planned (shown in Table 4-1 and 4-2).

In order to maximize the information obtained in these tests, two types of test data were collected: steady-state and transient. Steady-state data were collected at 8-10 setpoints for each of the test conditions shown in Tables 4-1 and 4-2. Each setpoint represented a different M-ratio within the indicated test condition. These setpoints were established for thermal-hydraulic performance characterization and spanned the entire operating range of the test facility. At each setpoint, a complete record of the test facility thermal-hydraulic condition, as well as analog vibration data, was obtained.

Following steady-state testing at each test condition, transient vibration data were obtained. This was accomplished by continuously varying the total flow while maintaining a constant drive flow at one of the test conditions of Tables 4-1 and 4-2. During the transient vibration data, SJDP and a total flow signal were continuously recorded. Additionally, a representative vibration signal and the SJDP were recorded on an analog x-y recorder during the transient. These transient data proved to be redundant with the steady-state data and are, therefore, not discussed further.

4.3 TEST PROCEDURE

Detailed test facility operating procedures were prepared and executed by the General Electric component(s) responsible for the Large Steam-Water Test Facility. Detailed below is a description of the hardware and test instrumentation associated with the acquisition and analysis of vibration test data.

4.3.1 Test Hardware

The jet pump installation was accomplished by first locating the centerline of the jet pump relative to the riser pipe within the test vessel. This was done with the aid of a calibrated jib and plumb line. A tailpipe adaptor was then bolted to the diffuser discharge tank (Figure 3-1) concentric with the plumb line. The diffuser was then fitted into the tailpipe adaptor and secured with a collar around the tapered midsection and threaded rods to the diffuser discharge tank. Packing material was forced into the annulus between the diffuser and tailpipe adaptor and secured with a metal ring.

Following installation of the diffuser in the test vessel, the mixer was installed and centered within the diffuser at the slip joint by means of the adjusting screws and wedge (Figure 2-3). The centering was done to achieve a uniform 0.006 to 0.008-in. clearance between the mixer and the diffuser at the slip joint. The jet pump installation at Moss Landing is shown in Figure 4-1.

4.3.2 Test Instrumentation

Vibration instrumentation was divided into two classes: (1) acceleration sensitive, and (2) strain sensitive. The instrumentation was arranged to detect vibrations in the radial and tangential directions. Figure 4-2 defines this orientation nomenclature, consistent with BWR standard plant orientation.

The acceleration-sensitive devices consisted of six piezoelectric accelerometers, four on the inlet mixer and two on the diffuser near the slip joint. The exact locations and identifications of all sensors is shown in Figure 4-3 for BWR/6-251 jet pump test, and in Figure 4-4 for the BWR/6-218 jet pump test.

The strain-sensitive devices consisted of four weldable strain gage groupings on the riser support bracket arranged to detect tension (radial) and bending (tangential) strain in each arm (Figures 4-3 and 4-4).

In addition to this dynamic instrumentation, three analog signals representing the differential pressures across the slip joint, drive flow orifice and total flow orifice were utilized. Table 4-3 lists the vibration sensors used during the test.

4.3.3 Data Acquisition Scheme

Figure 4-5 shows the basic data acquisition arrangement employed in these tests. The overriding test philosophy employed was to maximize the quality of test data by minimizing the number of electronic "black boxes" in the signal path between the vibration sensors and the data recording devices. A 14-track FM tape recorder was used to acquire all vibration test data. For each steady-state test condition, data were recorded continuously for a minimum of 5 minutes (when possible). The six accelerometer signals were recorded on odd-numbered channels of the tape recorder, while the four strain gage signals were recorded on even-numbered channels. This scheme was chosen to reduce phase differences among each transducer type, which can arise when reproducing data on a tape recorder with different reproduce head spacing than the original. Additionally, the SJDP, drive flow and total flow transducer signals and an accelerometer mounted on the outside of the test vessel were recorded on the remaining channels.

In addition to the 14 data channels, a voice track was employed to provide a continuous commentary for future reference as well as individual channel identification, amplifier gains, tape speed, test condition identification, etc. This latter information was also recorded manually on test record sheets, with each test condition identified by elapsed tape footage and test facility data acquisition computer run number (steady-state data only).

Calibration information was recorded, as a minimum, at the beginning and end of each test condition (Tables 4-1 and 4-2), at the beginning and end of each reel of tape, and/or at the beginning and end of each test work day. Calibration signals of 0, 0.01, 0.10 and 1.0 Vac at 100 Hz were recorded on all tape recorder

channels simultaneously. Additionally, calibration signals representing the full-scale output from each charge amplifier and a known strain from each strain gage bridge conditioner were recorded, both on FM tape and manually on the test record sheets. During transient testing, the SJDP transducer and a selected acceleration signal were recorded on-line on an X-Y recorder. A complete list of data acquisition/analysis instrumentation is included in Appendix A.

Table 4-1

HYDRAULIC TEST CONDITIONS FOR THE BWR/6-251

JET PUMP VIBRATION TESTS

Test Condition	Drive Flow (% of 1.45×10^6 lb/hr)	M-Ratio Range	Pressure (psia)	Temperature (^{o}F)
01	80	1.3 - 2.9	1046	532.0
02	100	1.3 - 2.9	1046	532.0
03	105	1.3 - 2.9	1046	532.0
06	67	1.3 - 2.9	1046	532.0

Table 4-2

HYDRAULIC TEST CONDITIONS FOR THE BWR/6-218

JET PUMP VIBRATION TESTS

Test Condition	Drive Flow (% of 1.216×10^6 lb/hr)	M-Ratio Range	Pressure (psia)	Temperature (^{o}F)
41	80	1.4 - 3.2	1046	532.5
42	100	1.4 - 3.2	1046	532.5
43	105	1.4 - 3.2	1046	532.5
46	50	1.4 - 3.2	1046	532.5

Table 4-3

VIBRATION SENSORS FOR BWR/6 JET PUMP TESTS

ID	Type	Location[1]	Orientation[2]
A1	Accelerometer	Top of Mixer - West	Tangential
A2	Accelerometer	Top of Mixer - South	Radial
A3	Accelerometer	Bottom of Mixer - West	Tangential
A4	Accelerometer	Bottom of Mixer - South	Radial
A5	Accelerometer	Top of Diffuser - West	Tangential
A6	Accelerometer	Top of Diffuser - South	Radial
A7	Accelerometer	On Test Vessel - North	--
S11	Strain Gage	Riser Brace - bending	Tangential
S12	Strain Gage	Riser Brace - tension	Radial
S13	Strain Gage	Riser Brace - bending	Tangential
S14	Strain Gage	Riser Brace - tension	Radial

[1]See Figures 4-3 and 4-4 for exact locations.

[2]See Figure 4-2 for terminology.

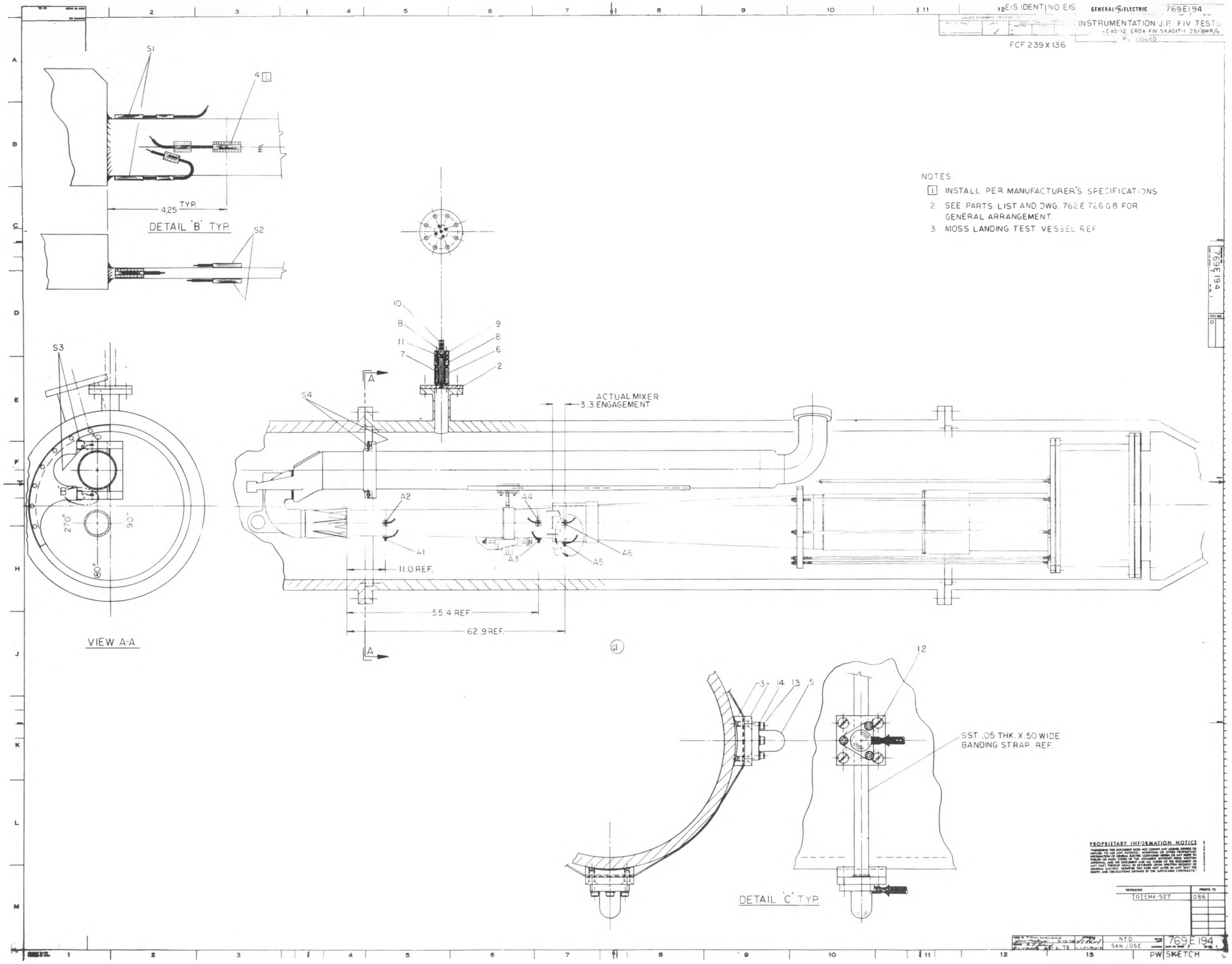

Figure 4-3. Jet Pump FIV Instrumentation Test - BWR/6-251

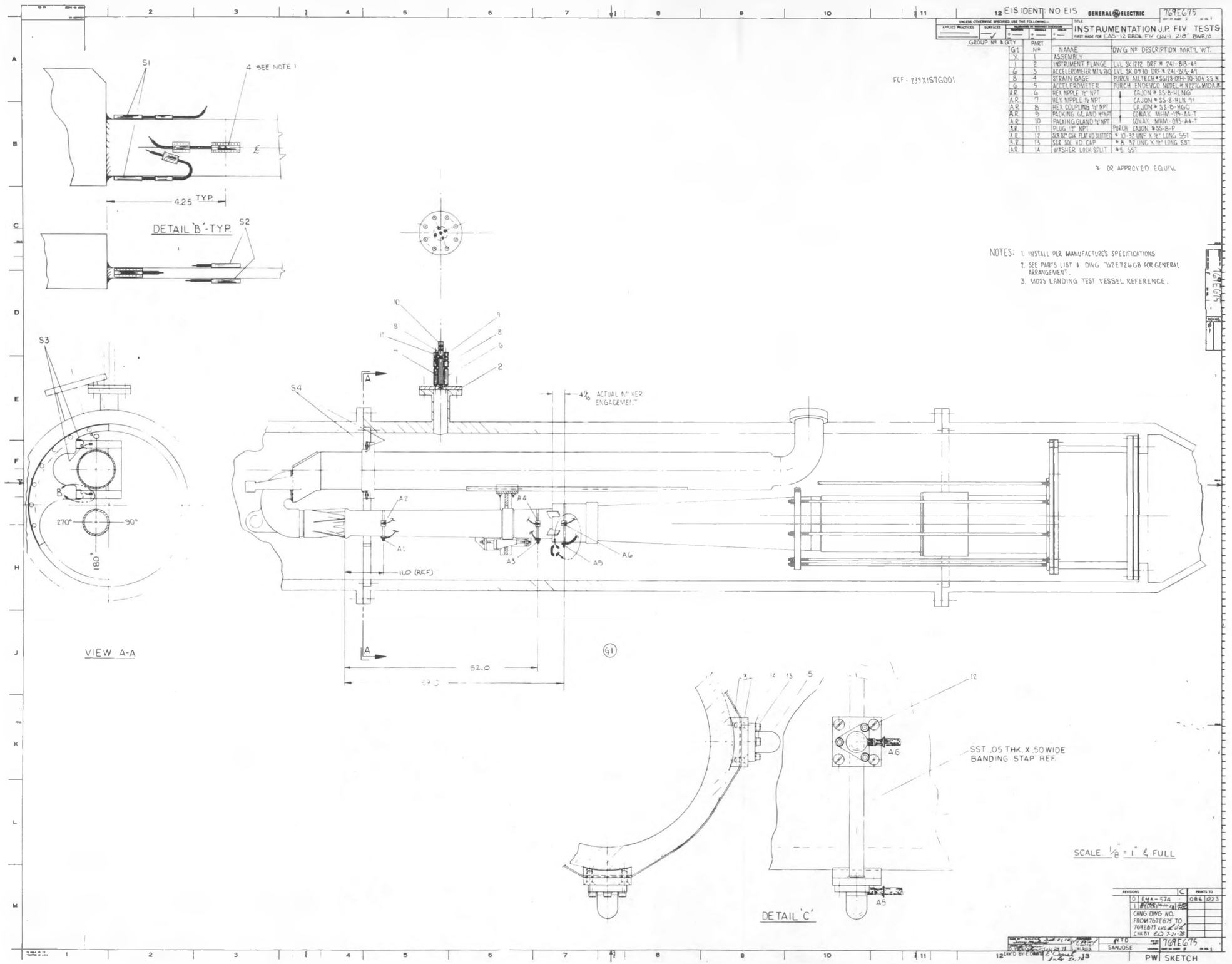

GROUP NO.	QTY	PART NO.	NAME	DWG NO. DESCRIPTION MATL WT.
	X	1	ASSEMBLY	
	1	2	INSTRUMENT FLANGE	LVL SK1712 DRF # 24I-B13-49
G	3	3	ACCELEROMETER MTG PAD	LVL SK 0930 DRF # 24I-B25-49
B	4	4	STRAIN GAGE	PURCH AILTECH # SG128-01H-30-304 SS #
G	5	5	ACCELEROMETER	PURCH ENDEVCO MODEL # 2272G MIDA #
A.R.	6		HEX NIPPLE ¾" NPT	CAJON # SS-8-HLNG
A.R.	7		HEX NIPPLE ½ NPT	CAJON # SS-8-HLN 91
A.R.	8		HEX COUPLING ½" NPT	CAJON # SS-8-HGC
A.R.	9		PACKING GLAND ½"NPT	CONAX MHM-125-AA-T
A.R.	10		PACKING GLAND ¾"NPT	CONAX MHM-093-AA-T
A.R.	11		PLUG ½" NPT	PURCH CAJON # SS-8-P
A.R.	12		SCR 82° CSK FLAT HD SLOTTED	# 10-32 UNF X ¾" LONG SST
A.R.	13		SCR SOC HD CAP	# 8 32 UNC X ½" LONG SST
A.R.	14		WASHER LOCK SPLIT	#5 SST

OR APPROVED EQUIV.

Figure 4-4. Jet Pump FIV Instrumentation Test - BWR/6-218

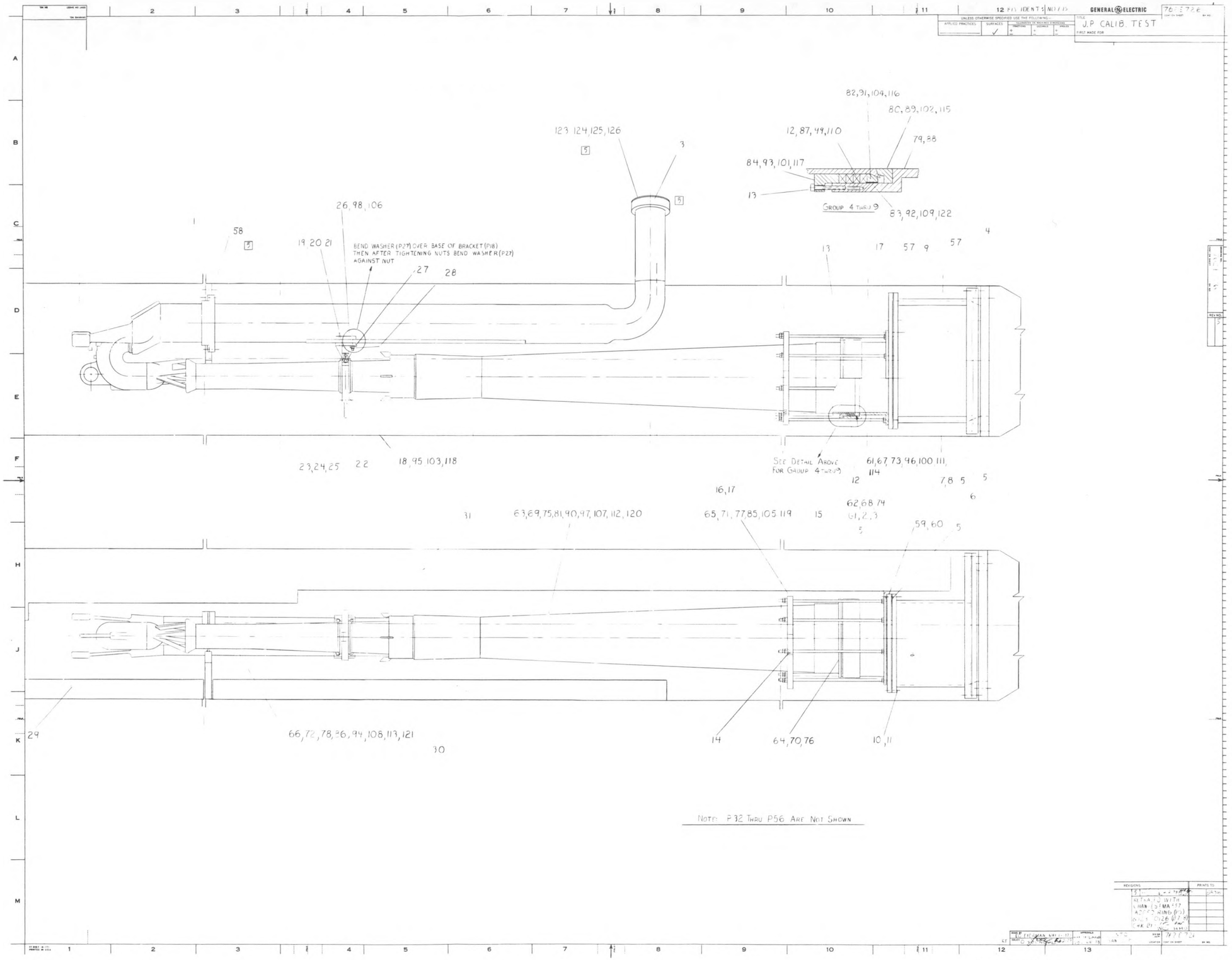

NOTE: P32 THRU P56 ARE NOT SHOWN

Figure 4-1. Jet Pump Calibration Test

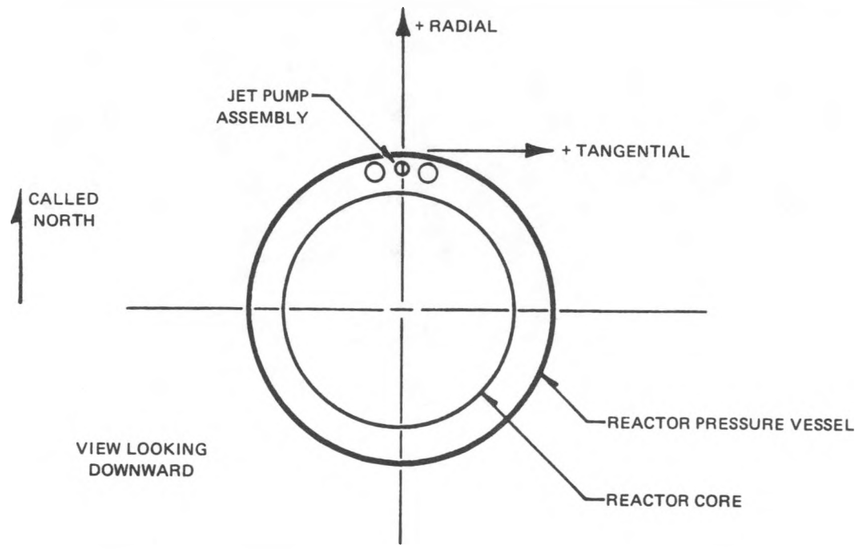

Figure 4-2. Terminology Used to Define Instrumentation Orientation for Jet Pump Testing

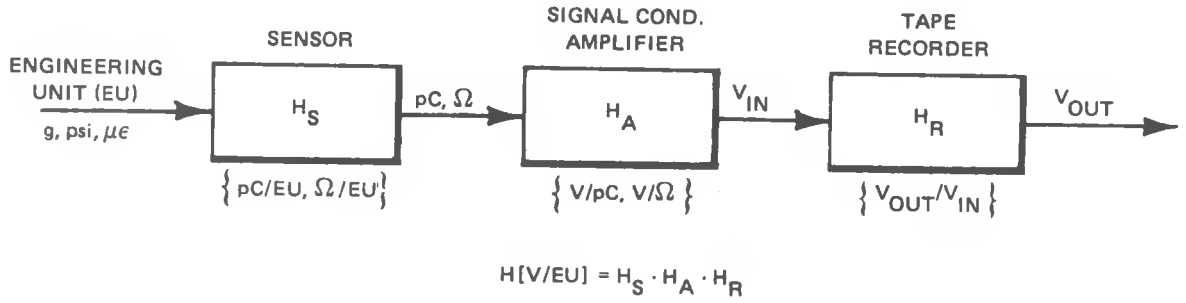

Figure B-1. Data Acquisition Block Diagram

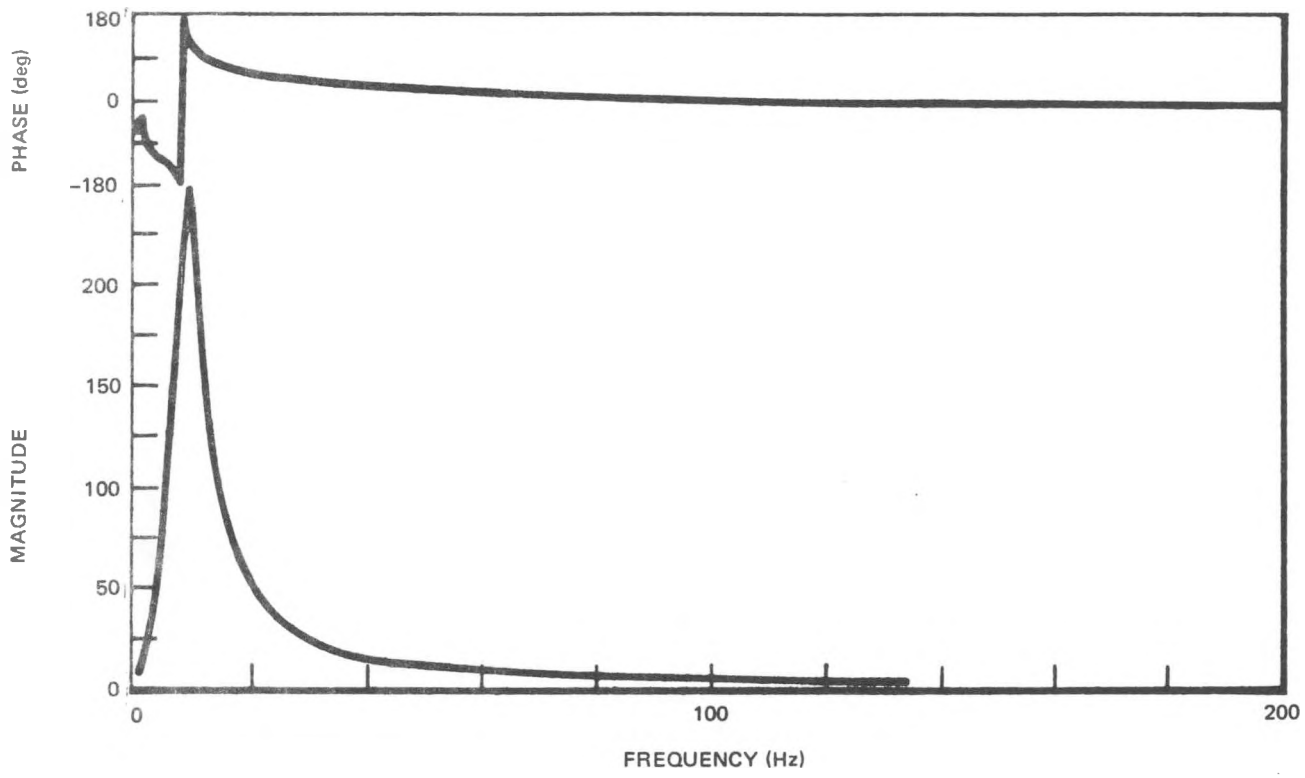

Figure B-2. Transfer Function for B&K Model 2635 Integrating Charge Amplifier (white noise excitation)

The strain gage sensitivities were calculated from the first principles using gage factors supplied by the manufacturer. These gage factors were subject to a 3% error according to the manufacturer. Therefore, a 5% estimated error is assigned to the strain gage sensitivities.

The signal conditioning amplifier transfer function, H_A, was determined from the formula:

$$H_A = V_{FS}/S \cdot E_{FS} \qquad \text{(B-2)}$$

where

V_{FS} = full-scale amplifier output;
E_{FS} = full-scale engineering units setting; and
S = sensitivity setting.

The full-scale amplifier outputs were recorded for each test condition. The amplifiers themselves were calibrated to an accuracy of better than 1% prior to the test. Minor adjustments to the amplifier gains were made throughout the test period to maintain this level of accuracy.

The tape recorder transfer function, H_R, was determined by comparing the recorded calibration signals to the standard used to apply the calibration. Differences less than 1% were not corrected.

From the foregoing discussion, it is estimated that the overall errors associated with the accelerometers were no more than 5%, while strain gage data are subject to errors as large as 10%. These error estimates do not apply to the displacement data for reasons explained below.

Displacement data were obtained from acceleration data by integrating the acceleration data twice in the time domain using a B&K Model 2635 charge amplifier. The use of this device resulted in an additional transfer function H_I, in the data analysis chain of Figure 5-1. This transfer function has a nominal magnitude of $1/\omega^2$, where ω is the angular frequency of the input signal ($\omega = 2\pi f$). However, due to a 10 Hz high-pass filter built into the amplifier, the actual transfer function is as shown in Figure B-2 (note the apparent spectral line at 10 Hz). Analog signals processed in this manner would, therefore, exhibit strong 10 Hz characteristics unless higher frequency components were dominant in the signal. For this reason, instantaneous displacement time histories were not included in this report.

Appendix B

DATA REDUCTION AND ANALYSIS TECHNIQUE

The instruments used to analyze the test data are summarized in Table A-2. The following discussion addresses the specific techniques used to convert the analog test data into meaningful engineering units. The backbone of the data reduction and analysis technique was the Nicolet Scientific Corporation Model 660 Dual-Channel FFT Analyzer (called 2FFT). This instrument was used to calibrate all other instruments in the data reduction/analysis chain.

The first step in converting analog test data to engineering units is shown in the signal flow chart of Figure B-1. In this figure, the basic engineering unit to be determined (g, psi, με, etc.) is represented by the input to the first "black box," which is the sensor or transducer attached to the test hardware. The sensor converts the engineering unit into an electrical signal (charge, voltage, etc.) with the transfer function H_S. This signal then enters the second box, which is the signal conditioning amplifier, and leaves as a voltage signal via the transfer function H_A. This voltage signal is then recorded on FM tape for later retrieval. Due to small inaccuracies in the tape recorder electronics, a transfer function, H_R, is assigned to the tape recorder as well. The voltage (V) measured at the output of the tape recorder is thus related to the original engineering unit (EU) by the product of the three transfer functions:

$$V/EU = H_S \cdot H_A \cdot H_R \qquad \text{(B-1)}$$

This conversion factor was input into the 2FFT for each sensor analyzed to produce the spectra and time histories shown in the report.

The three component transfer functions (H_S, H_A and H_R) were determined independently by calibration. For the accelerometers, H_S was obtained by comparing each accelerometer against a calibrated laboratory standard accelerometer and correcting for operation at high temperature. The resulting sensitivites differed substantially from the original data provided by the manufacturer. These differences were attributed to long-term exposure to high temperature (530°F) prior to the test. Therefore, the most recent calibration data were used. The estimated error in these calibrations is 2%, which includes uncertainties in the temperature coefficient of sensitivity provided by the manufacturer.

Table A-2

DATA ANALYSIS INSTRUMENTATION

	Instrument	Manufacturer	Model	Minimum Accuracy
1.	Integrating Amplifier	B&K Instruments, Inc.	2635	Note (1)
2.	Digital Plotter	Tektronix, Inc.	4662	Note (1)
3.	Digital Multimeter	Dana Laboratories, Inc.	5900	DC: ±0.001% of Reading ±0.001% of Full Scale AC: ±0.03% of Reading ±0.002% of Full Scale
4.	Dual Channel Spectrum Analyzer	Nicolet Scientific Corp.	660	All Digital: 12 Bit A/D Conversion, 3 Digit + Exponent Amplitude Resolution, 400 Line Frequency Resolution

Note: (1) These instruments were calibrated against 3 and/or 4 prior to each use. When several instruments were used in series (Appendix B), the series arrangement was calibrated against 3 and/or 4. Overall accuracy of at least 1% was maintained for all system transfer functions.

Table A-1

DATA ACQUISITION INSTRUMENTATION

	Instrument	Manufacturer	Model	D Characteristics	Reference[1]
1.	Piezoelectric Accelerometer	Endevco	N2276M10	Sensitivity: 20pC/g Nominal Frequency Response: 2-2000 Hz ±5% Temperature: 50-650°F Pressure: 2500 psig	3
2.	Weldable Strain Gage	Ailtech	SG128	Gage Factor: 2.0 Nominal Resistance: 120Ω Nominal Temperature: Compensated 75-600°F	4
3.	Charge Amplifier	Endevco	2735	Gain: 0-10V/psi ±1.5% F.S. Frequency Response: 2-20,000 Hz ±5%	1
4.	Bridge Conditioner	Validyne Engineering Corp.	SG71	Gain: 1-50 Mv/V Frequency Response: DC-10K Hz ±5%	2
5.	Tape Recorder	Honeywell	5600E	Mode: FM Record/Reproduce Frequency Response: DC-1250 Hz at 3-3/4 ips Harmonic Distortion: <1.2% Linearity: ±0.3% of Full Scale Tape Speed Used: 3-3/4 ips	1-4

[1]This column cross-references the data acquisition signal conditioning to transducer type used in the test.

Appendix A

INSTRUMENTATION FOR BWR/5-201 JET PUMP FIV TEST

The data acquisition instruments used in the test are summarized in Table A-1. This table lists only those instruments in the direct path between the test data and the FM tape recorder.

The data analysis instruments used in the test are summarized in Table A-2. This table lists only those instruments used to process the test data upon completion of the test.

7. REFERENCES

1. M. R. Torres, 1978 - 1979 Test Program for High Flow Hydraulic Facility, March 1978 (NEDE-24102).

2. L. S. Dorfman and M. R. Torres, BWR Jet Pump Flow-Induced Vibration Characteristics, March 1976 (NEDE-20890).

3. M. R. Torres, Feedwater Sparger Cold Flow Vibration Tests, June 1974 (NEDO-20554).

4. L. V. LaCroix, Flow-Induced Vibration Characteristics of the BWR/5-201 Jet Pump, January 1979 (NEDE-24153).

5. J. R. Pallette, M-Ratio vs Drive Flow, letter to L. V. LaCroix, December 29, 1978.

6. H. M. Ondang, Design Record File #505-DEV.0034.

7. H. M. Ondang, Design Record File #505-DEV.0033.

8. M. R. Torres, Jet Pump Slip Joint Mechanistic Test, ATR 241-MRT.01, FIVE Transmittal No. 78-07, June 1978.

9. M. R. Torres, Ph.D. Thesis, Stanford University (work in progress).

10. Recirculation System Performance Data Sheets, General Electric Company Document No. 384HA163AB Rev. 2 (BWR/6-251 Plant).

11. Recirculation System Performance Data Sheets, General Electric Company Document No. 383HA825AB Rev. 2 (BWR/6-218 Plant).

6. CONCLUSIONS

The two BWR/6 jet pumps tested at Moss Landing exhibited similar FIV characteristics. Several important features bear underscoring:

a. The BWR/6-251 and BWR/6-218 jet pumps exhibited low level random type FIV characteristics at normal BWR operating conditions.

b. The BWR/6-251 and BWR/6-218 jet pumps exhibited high level, periodic type FIV characteristics at nonprototypical operating conditions.

c. Operation of the BWR/6 jet pumps at high-level FIV conditions resulted in damage to the jet pumps and associated support hardware.

d. The FIV susceptibility of the BWR/6 jet pumps increases with service life as a result of increased core resistance (SJDP) during the fuel cycle (Figures 5-18 and 5-35).

It is clear that the FIV behavior of a jet pump is extremely complex. In order to fully understand the mechanism which governs FIV in jet pumps and similar structures, additional study is required. Efforts to quantify the FIV mechanism, both experimentally and analytically, are currently in progress[8,9] and should be continued.

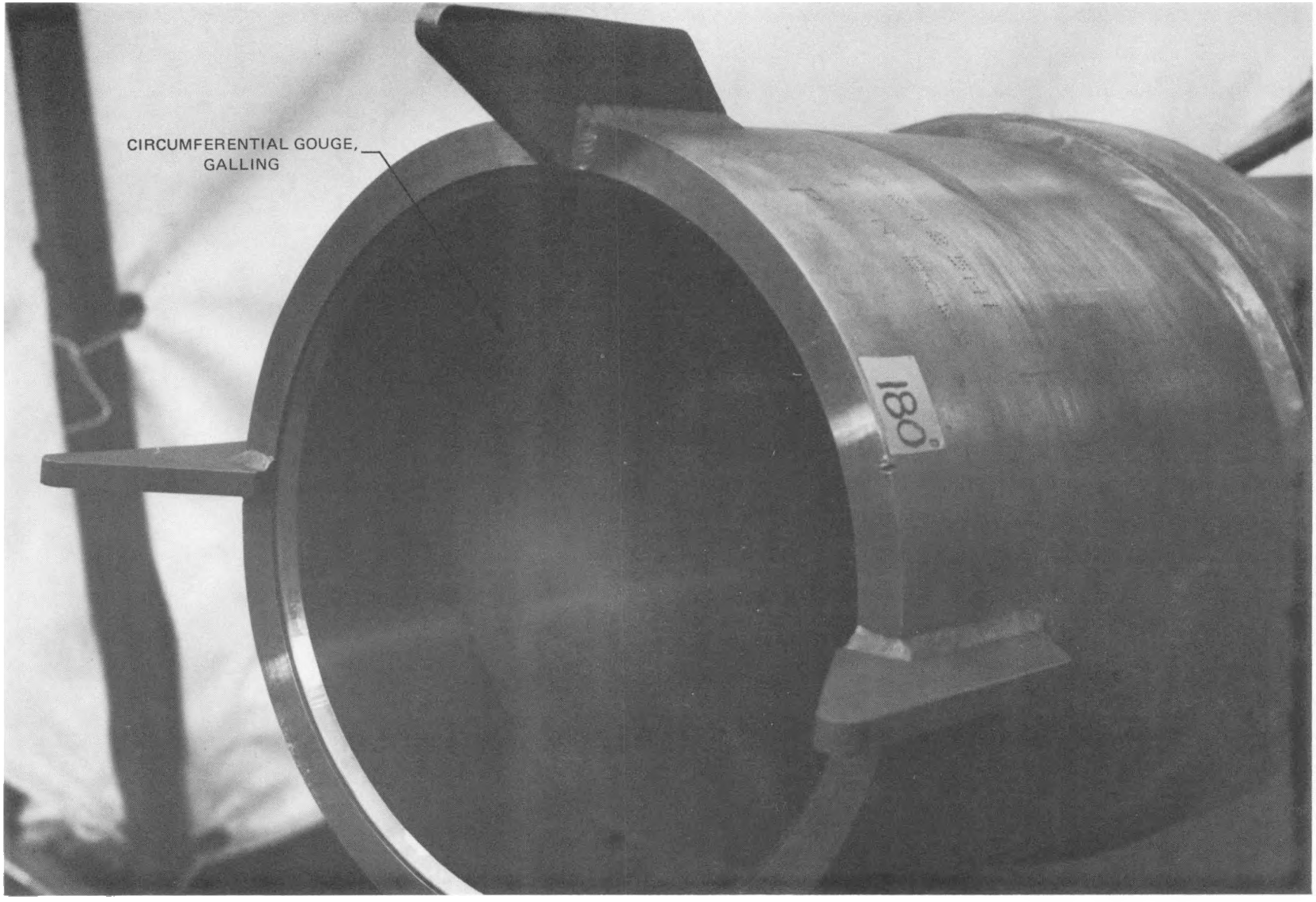

Figure 5-49. BWR/6-218 Diffuser - Slip Joint Region Circumferential Gouge from Impact with Mixer (See Figure 5-48)

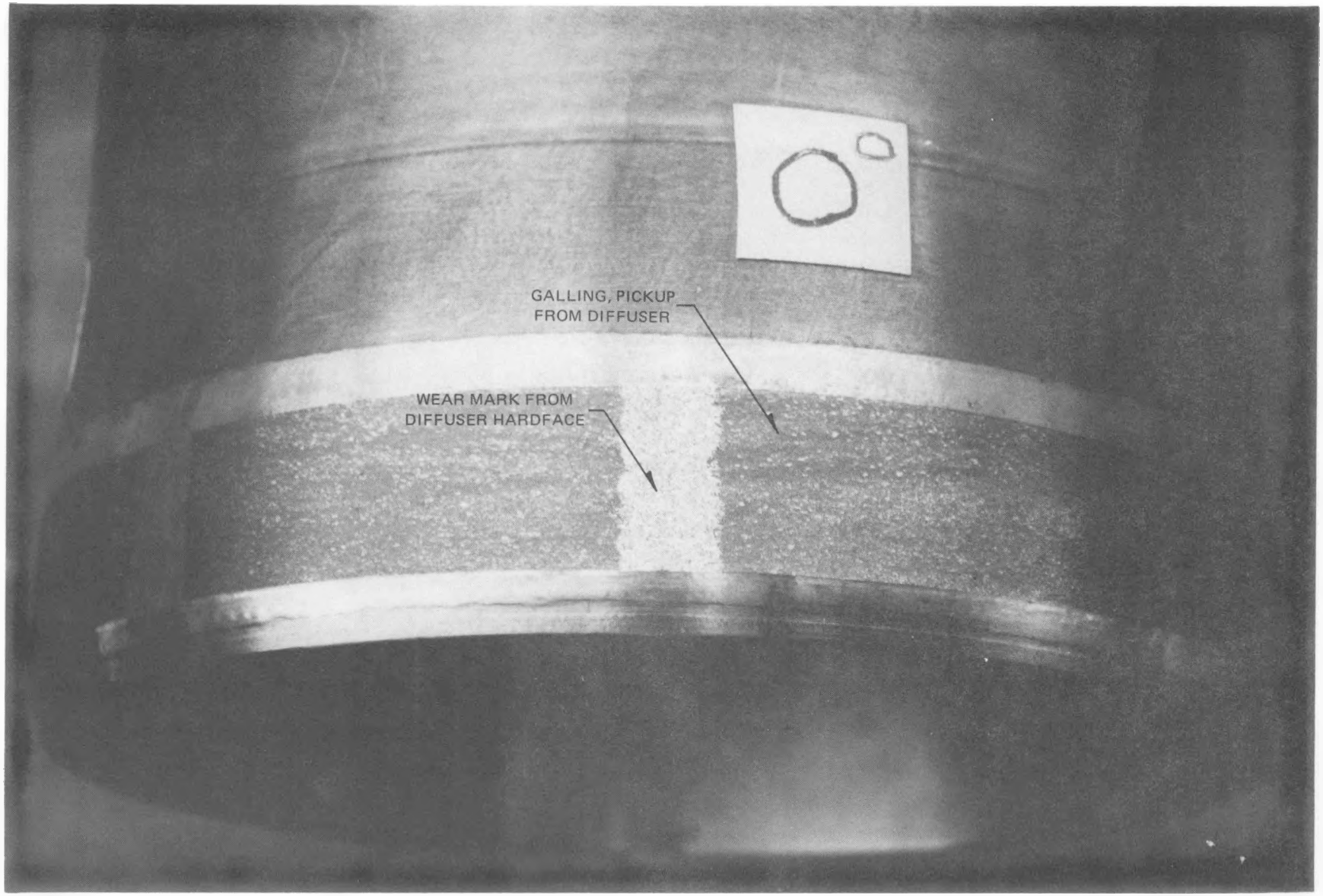

Figure 5-48. BWR/6-218 Mixer - Slip Joint Region Material Pickup from Diffuser (See Figure 5-49)

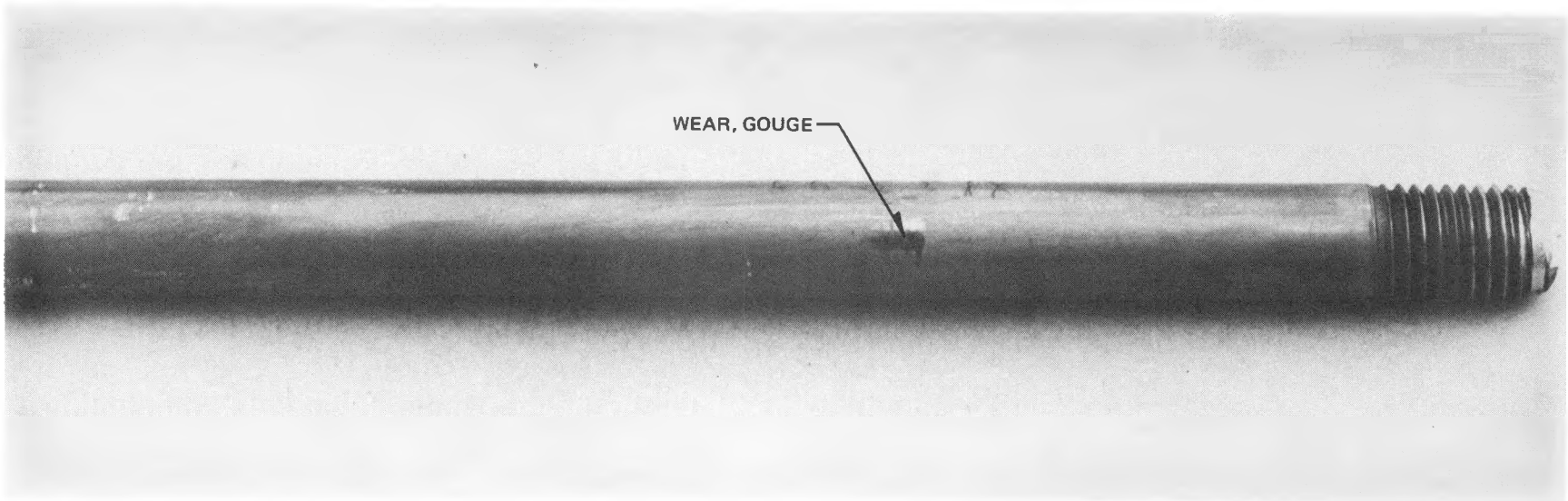

Figure 5-47. BWR/6-218 Wedge Aligning Rod - Wear and Gouging from Vibration (Axial) of Wedge

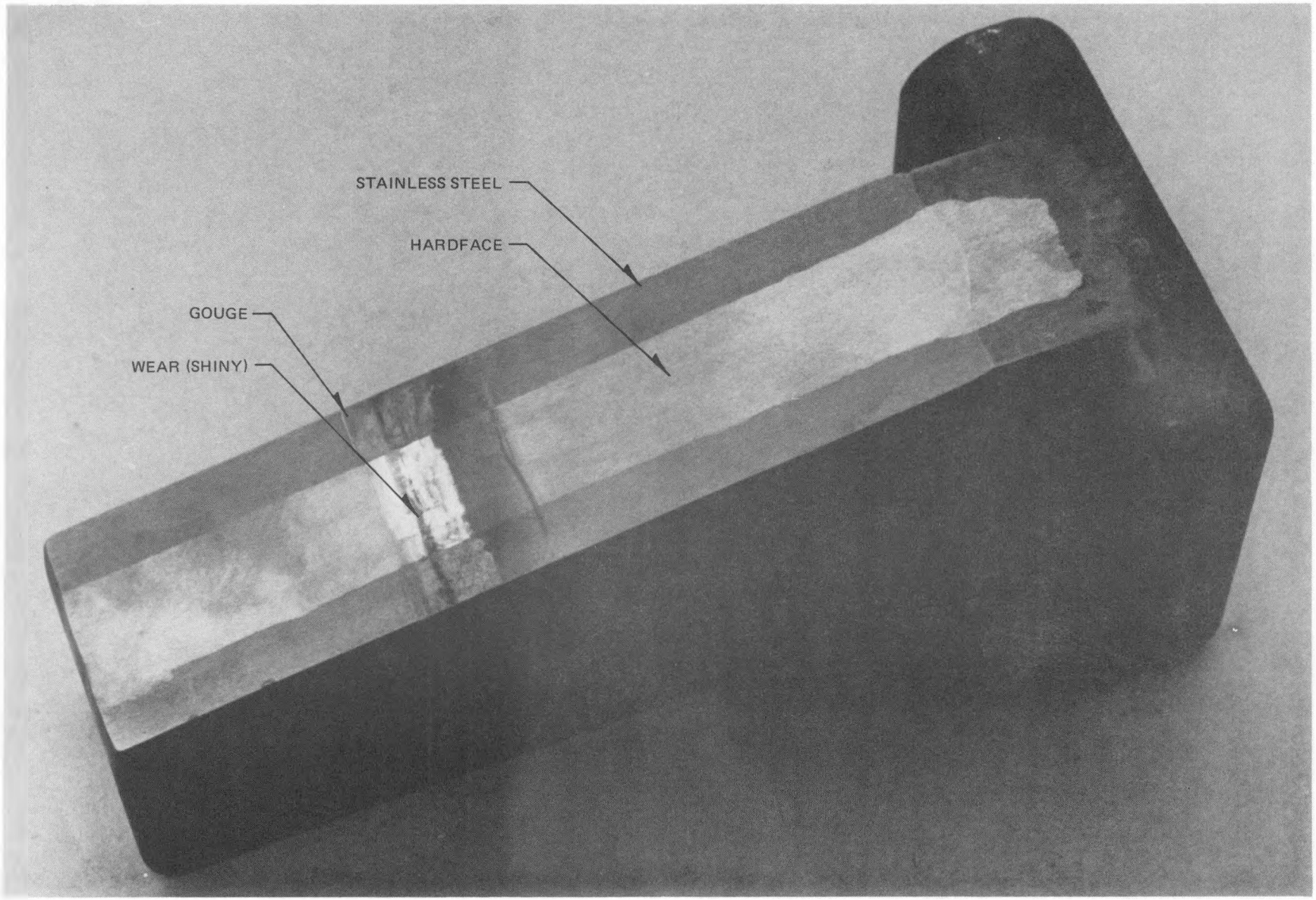

Figure 5-46. BWR/6-218 Wedge - Tapered Side Wear and Gouging from Contact with Restrainer Bracket

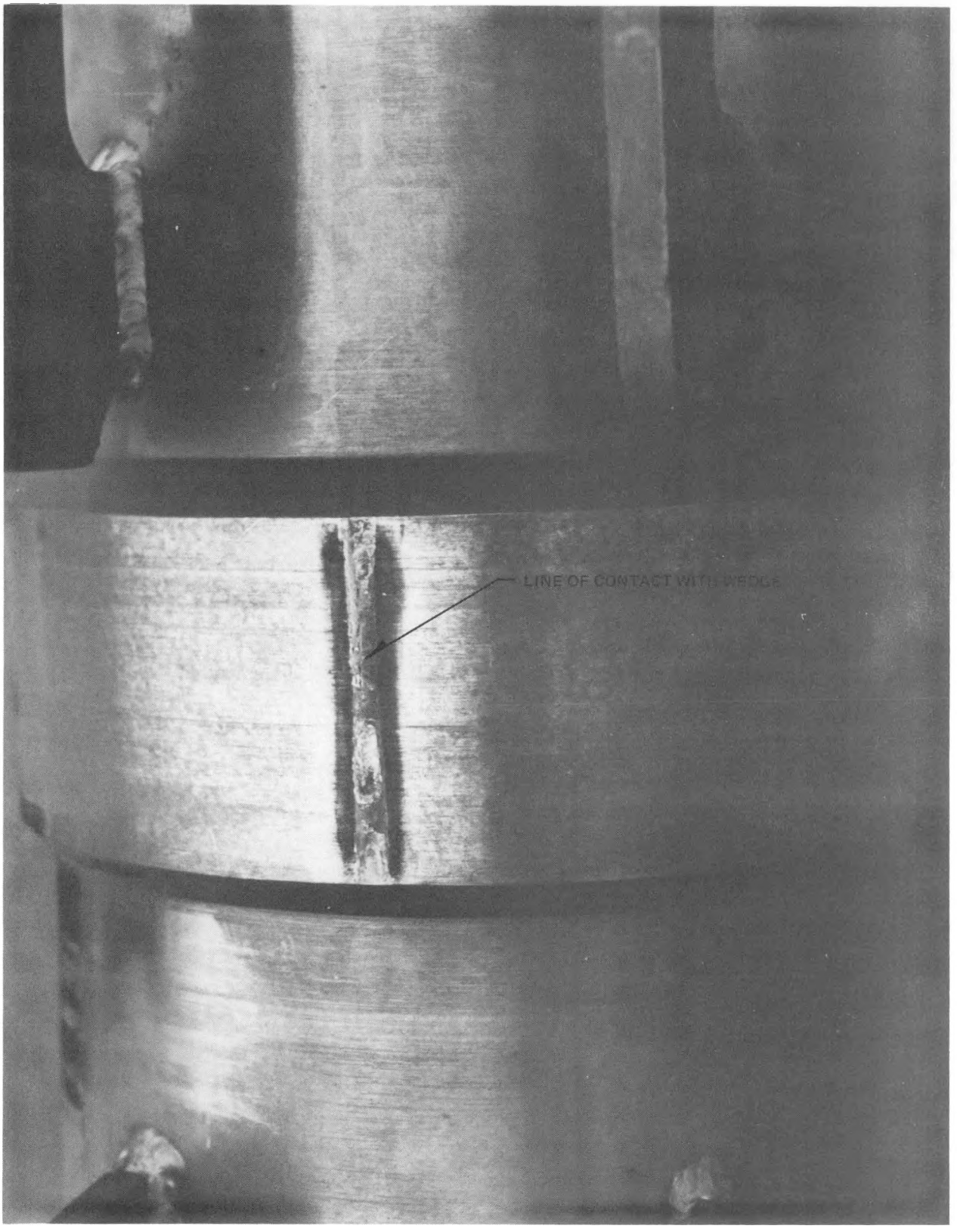

Figure 5-45. BWR/6-251 Mixer - Wear Impression of Wedge on West Side

Figure 5-44. BWR/6-218 Mixer - Impression of Adjusting Screw on Southeast Side

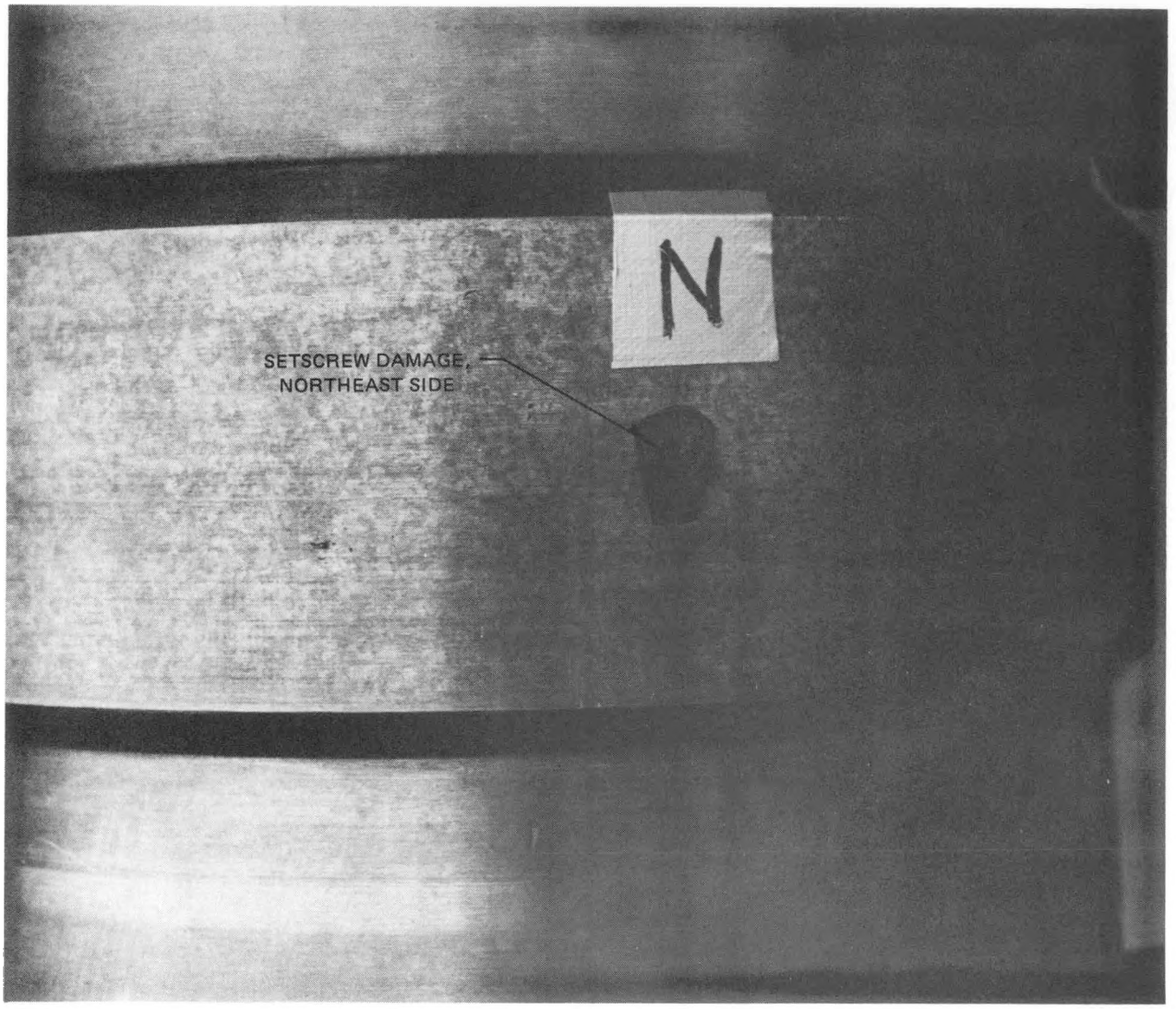

Figure 5-43. BWR/6-218 Mixer - Impression of Adjusting Screw on Northeast Side

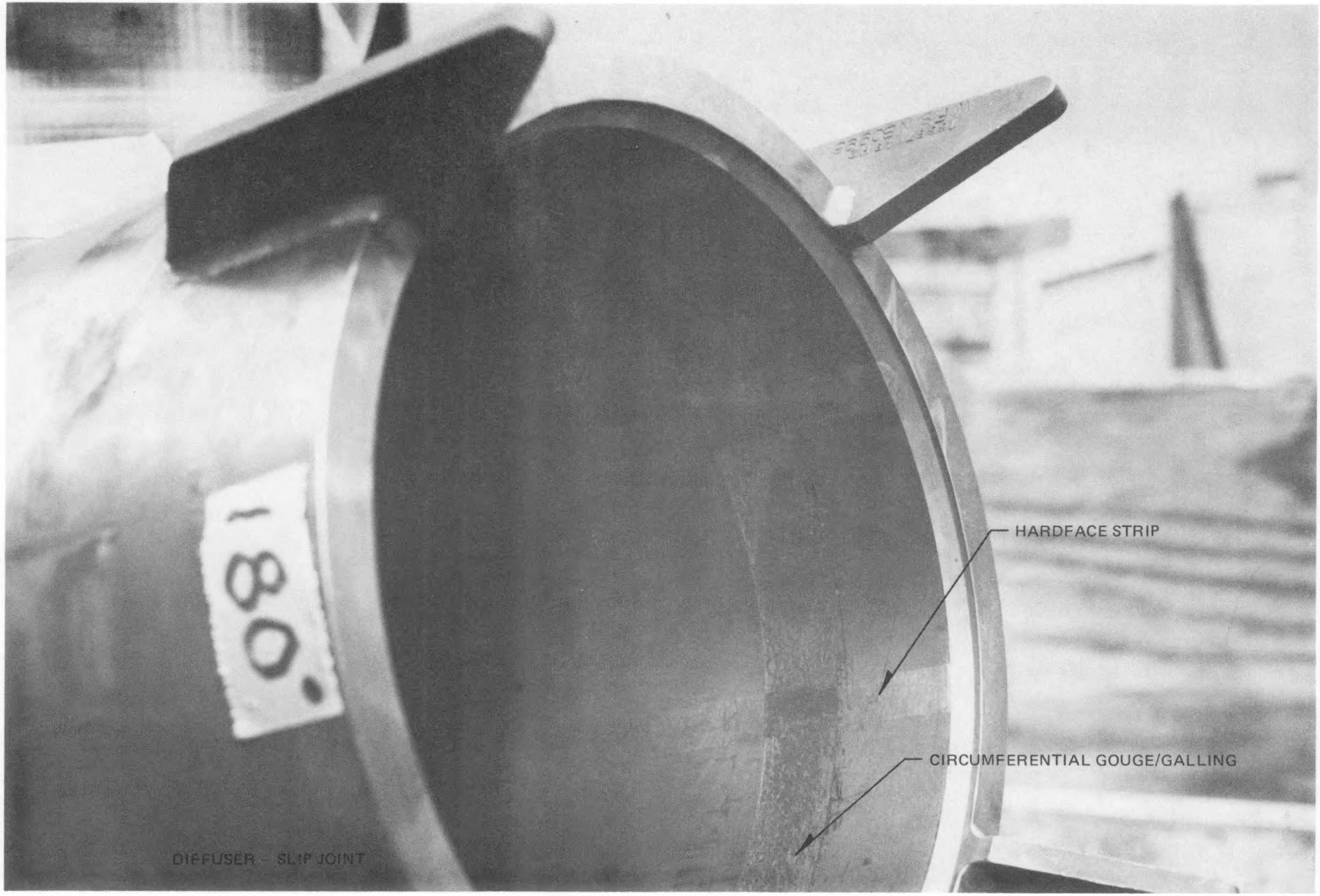

Figure 5-42. BWR/6-251 Diffuser - Slip Joint Region Circumferential Gouge from Impact with Mixer (See Figure 5-41)

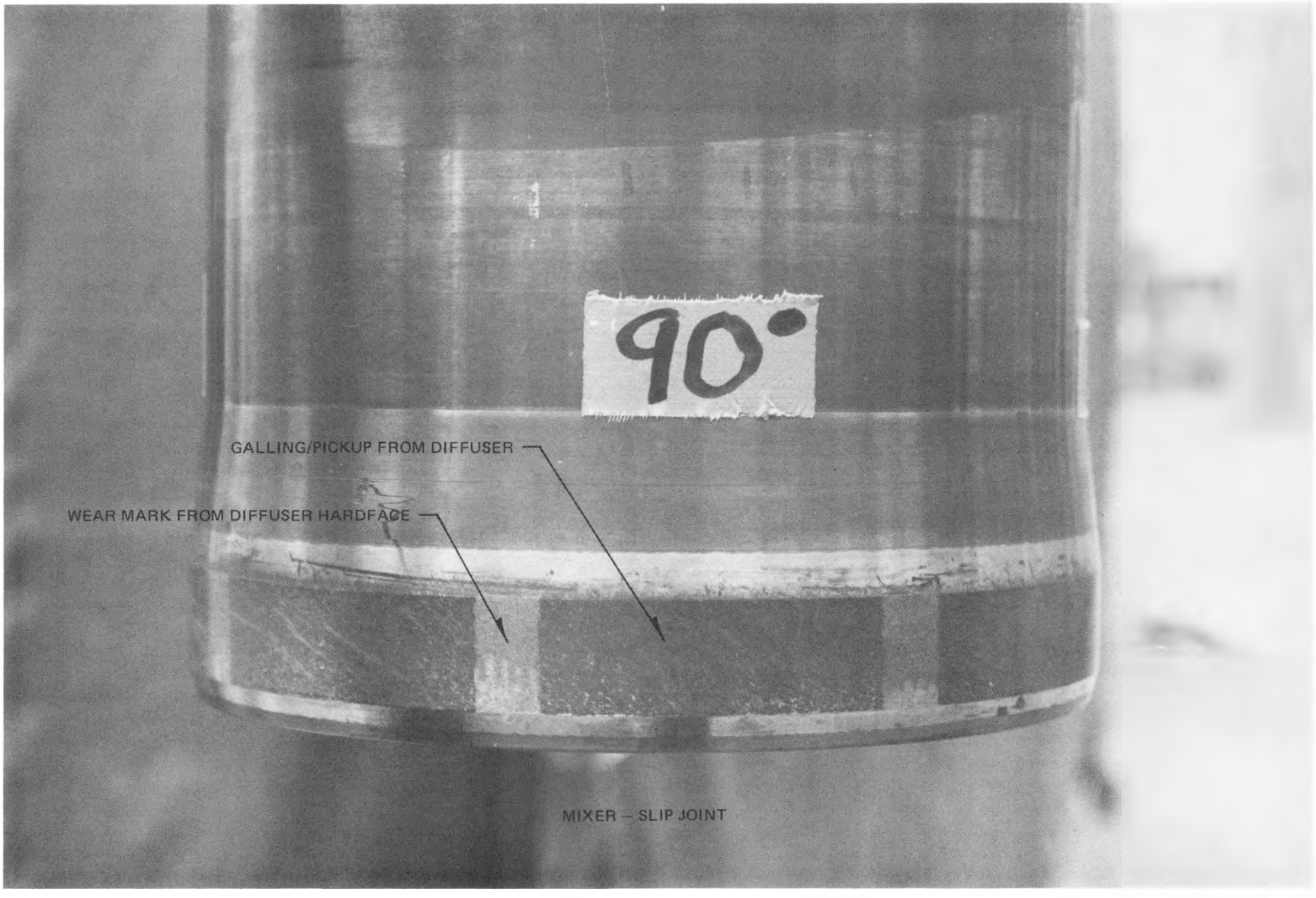

Figure 5-41. BWR/6-251 Mixer - Slip Joint Region Material Pickup from Diffuser (See Figure 5-42)

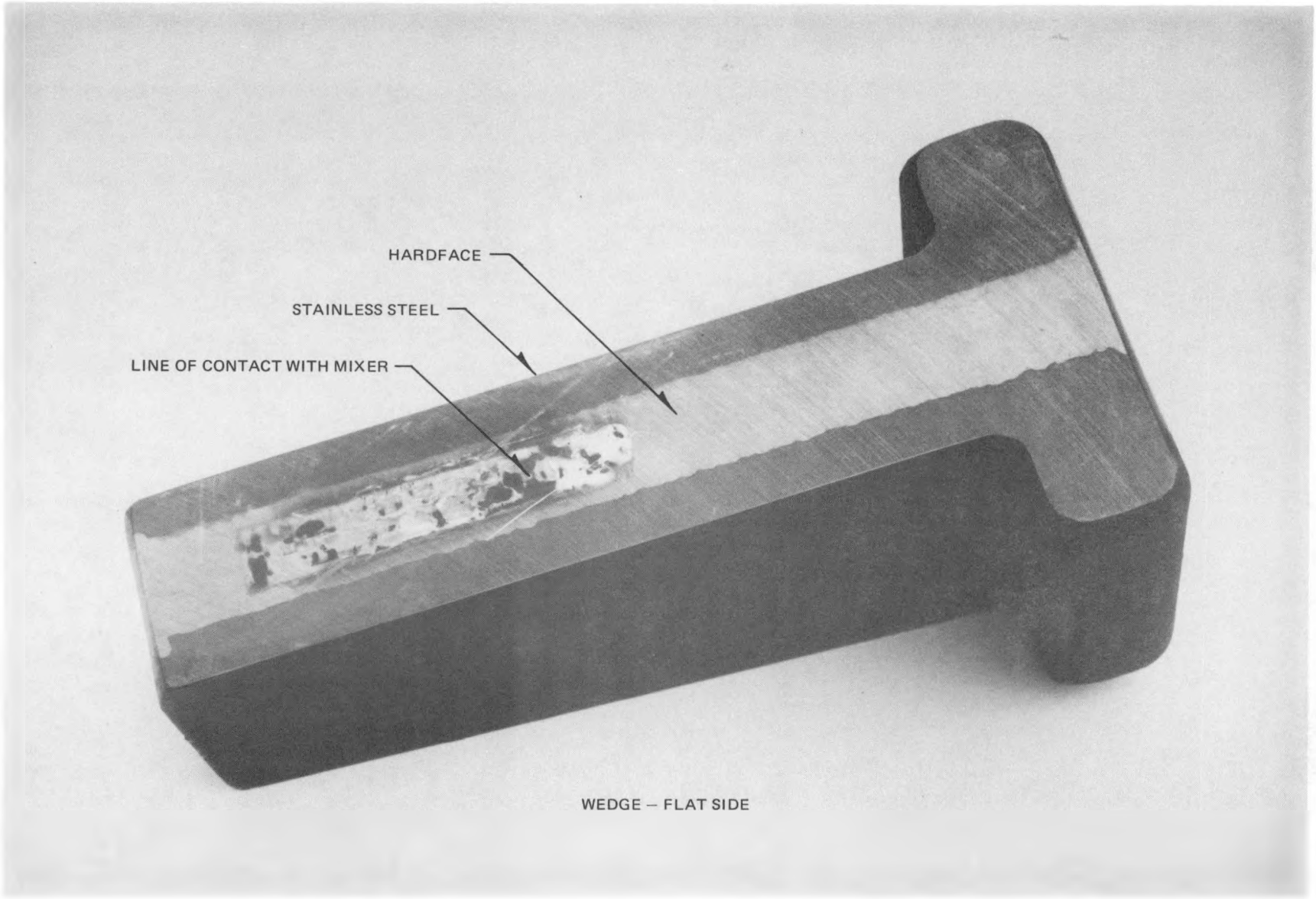

Figure 5-40. BWR/6-251 Wedge - Flat Side Wear from Contact with Mixer (See Figure 5-38)

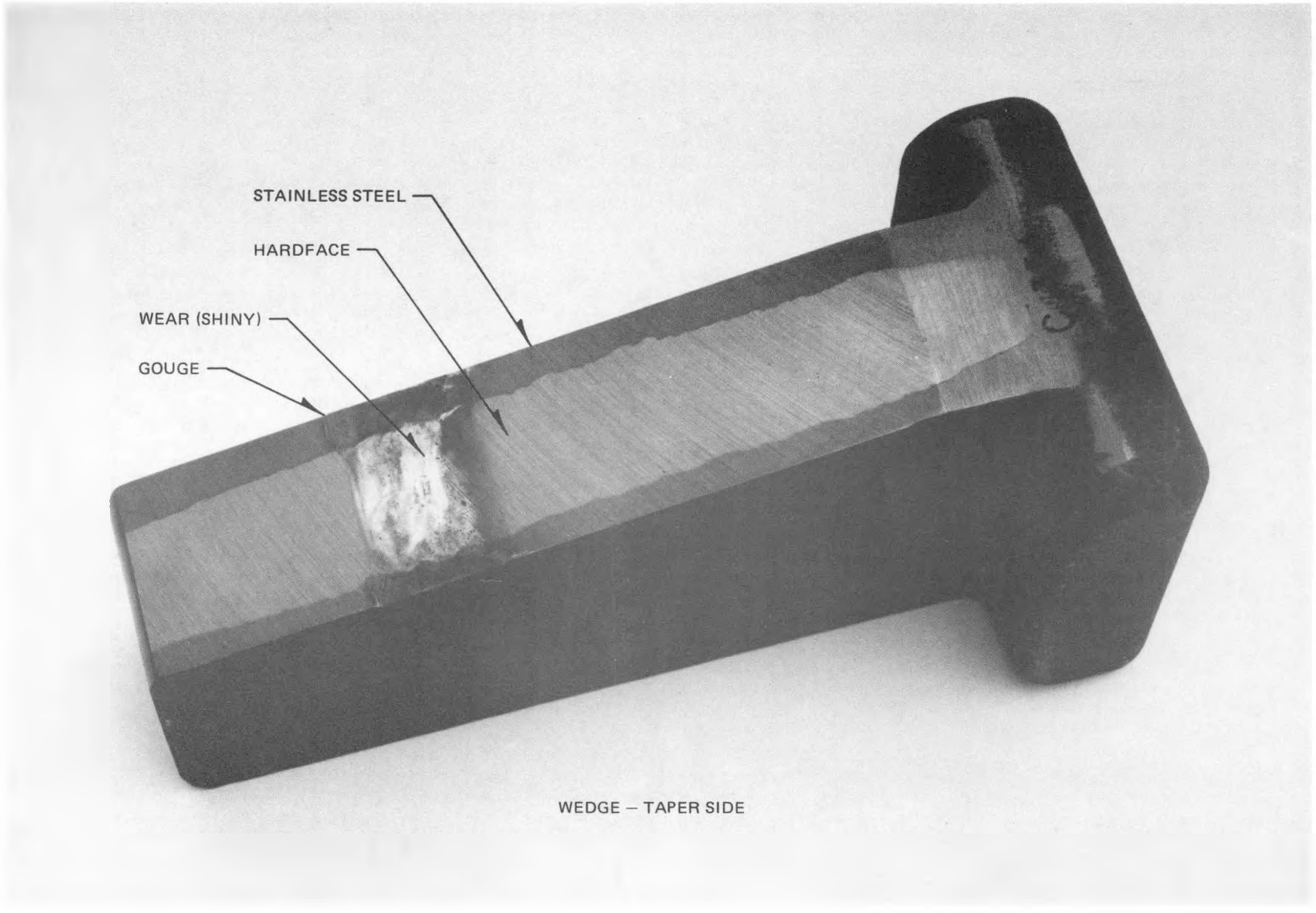

Figure 5-39. BWR/6-251 Wedge - Tapered Side Wear and Gouging from Contact with Restrainer Bracket

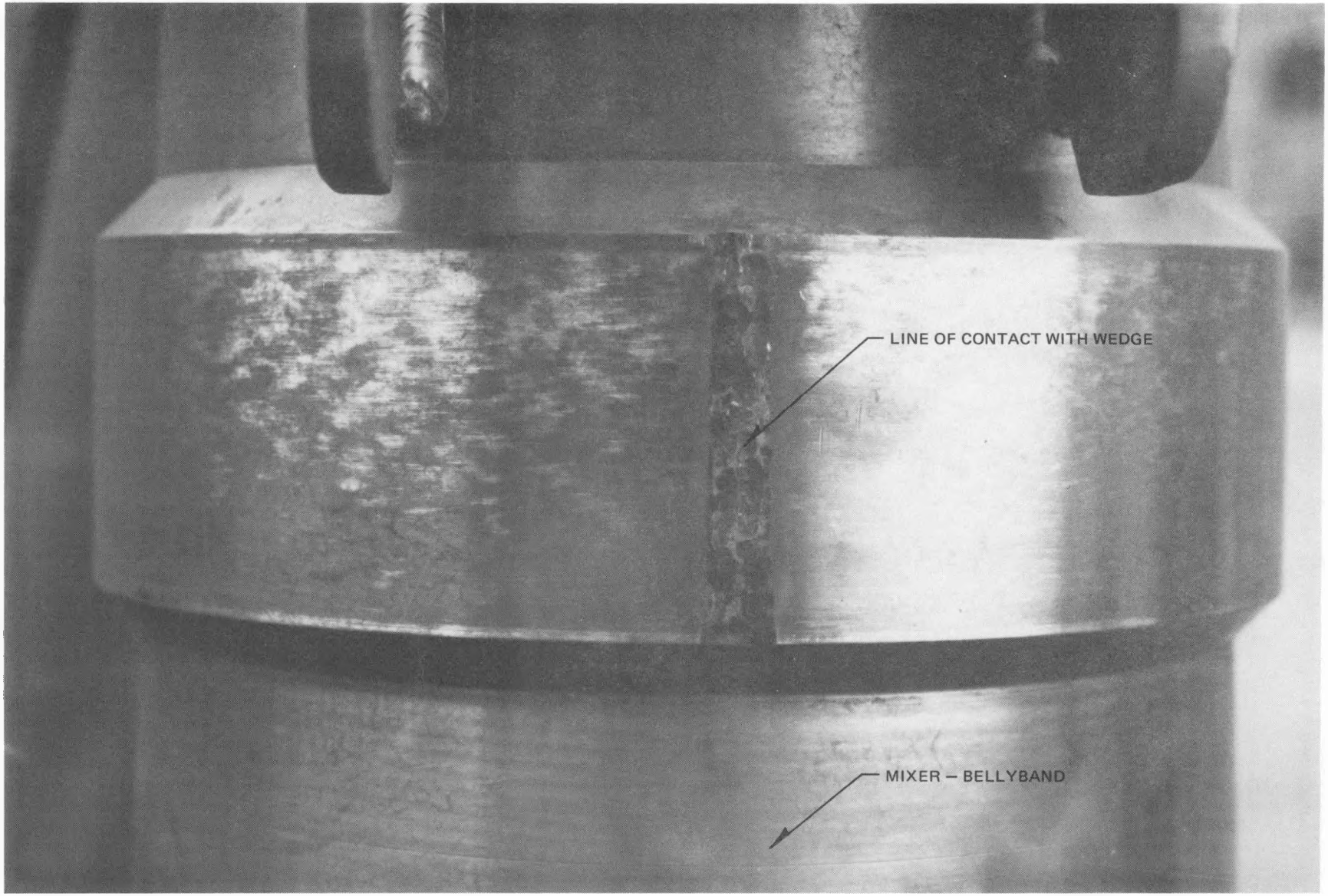

Figure 5-38. BWR/6-251 Mixer - Wear Impression of Wedge on West Side (See Figure 5-40)

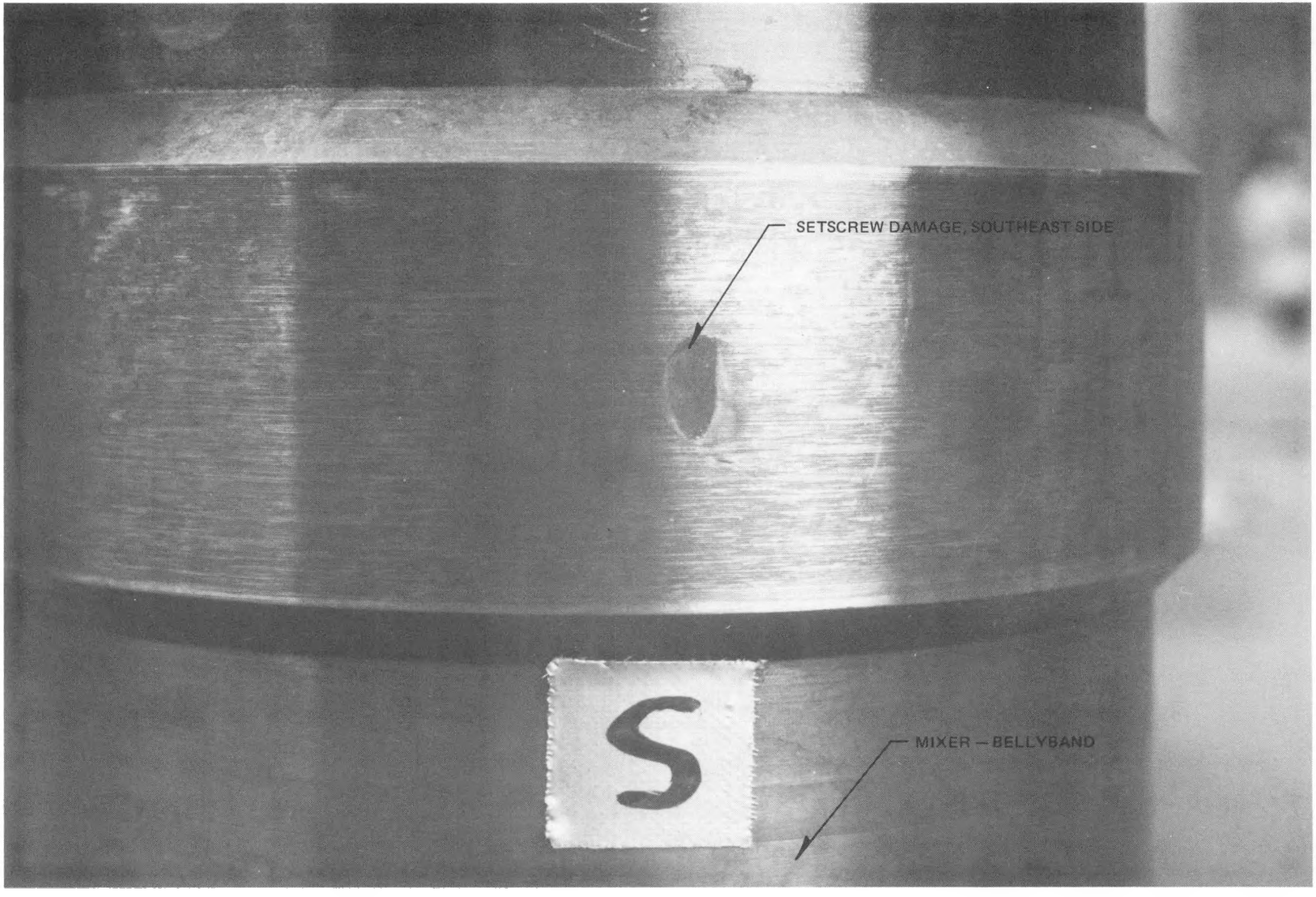

Figure 5-37. BWR/6-251 Mixer - Impression of Adjusting Screw on Southeast Side

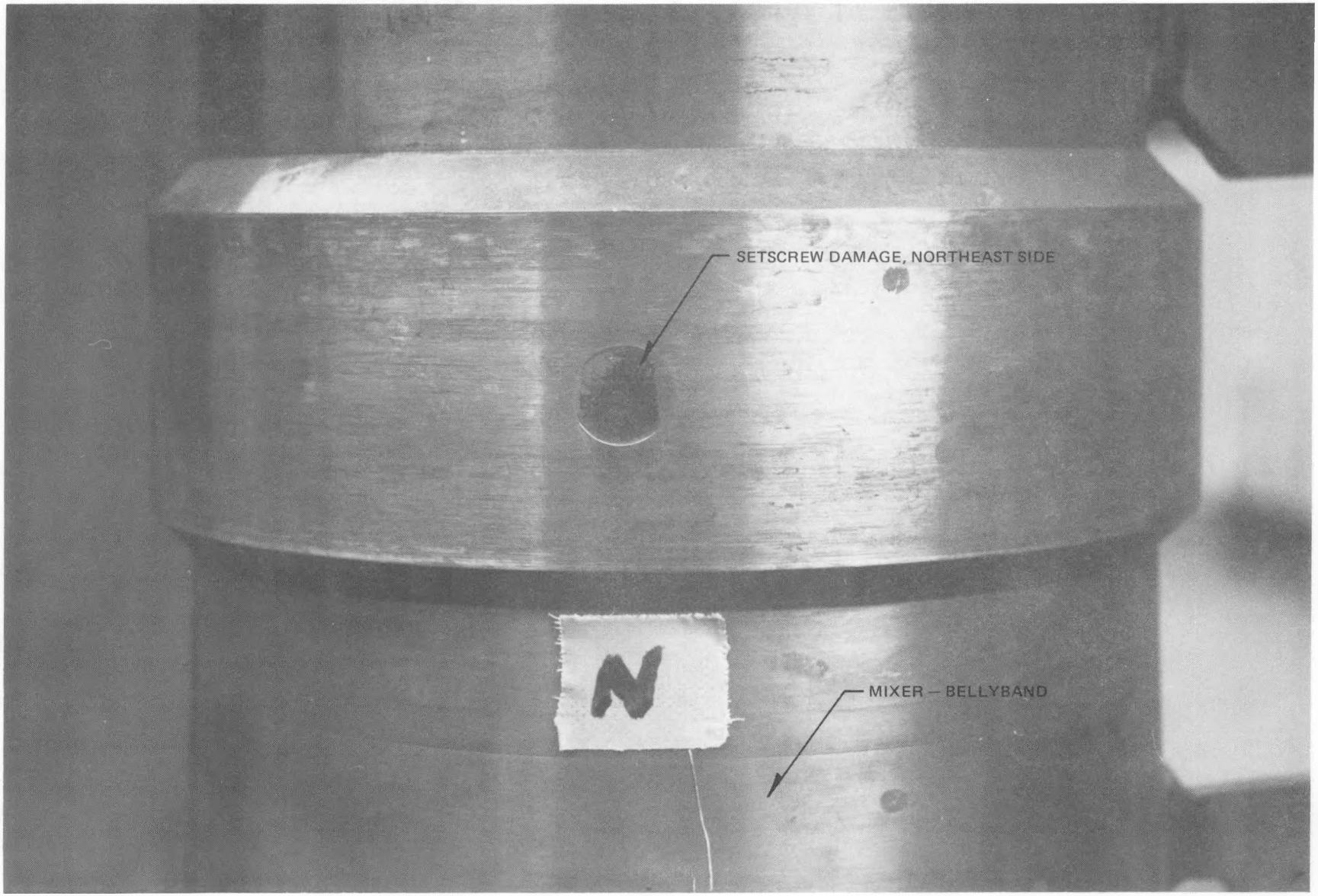

Figure 5-36. BWR/6-251 Mixer - Impression of Adjusting Screw on Northeast Side

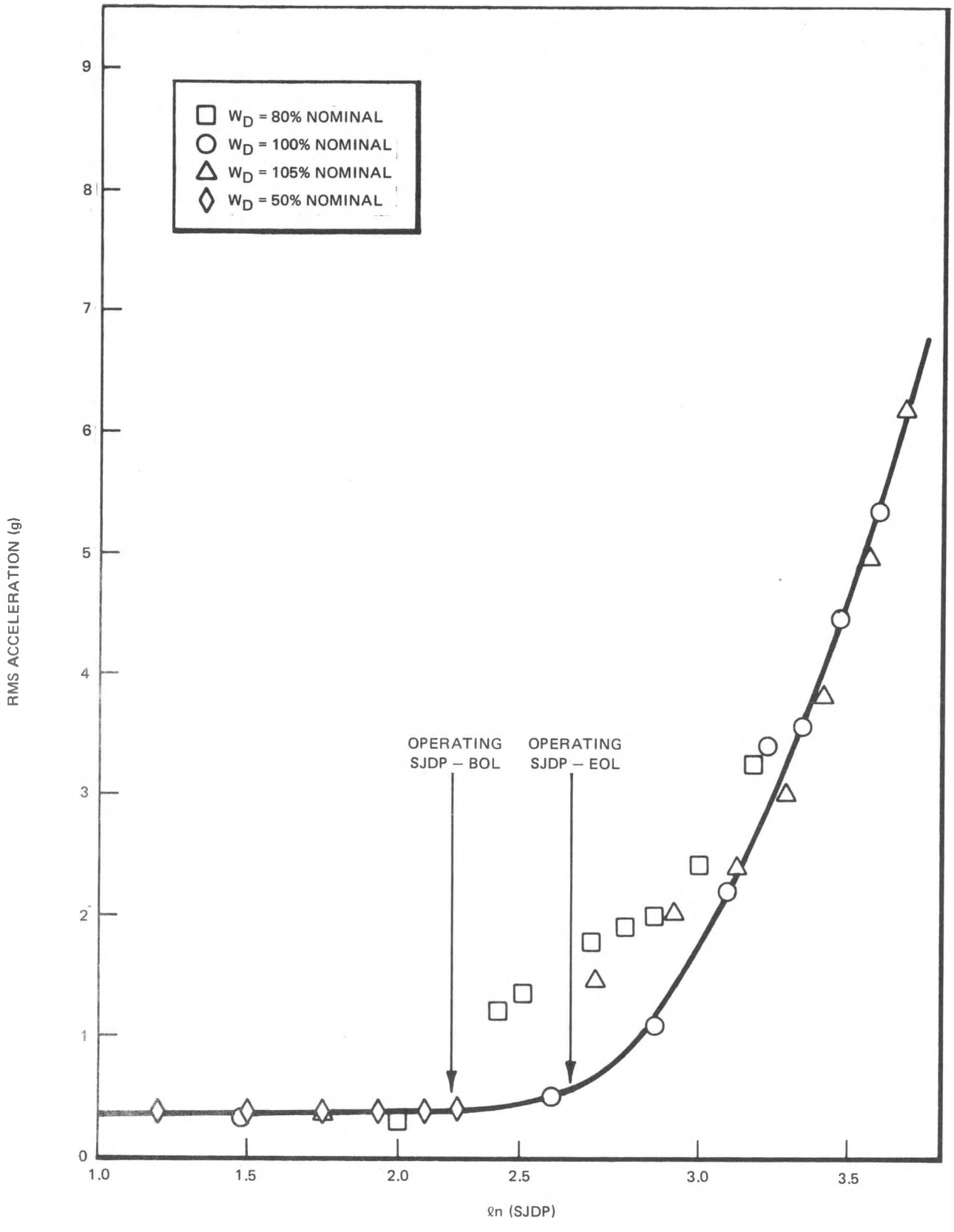

Figure 5-35. Vibration Characteristic for the BWR/6-218 Jet Pump

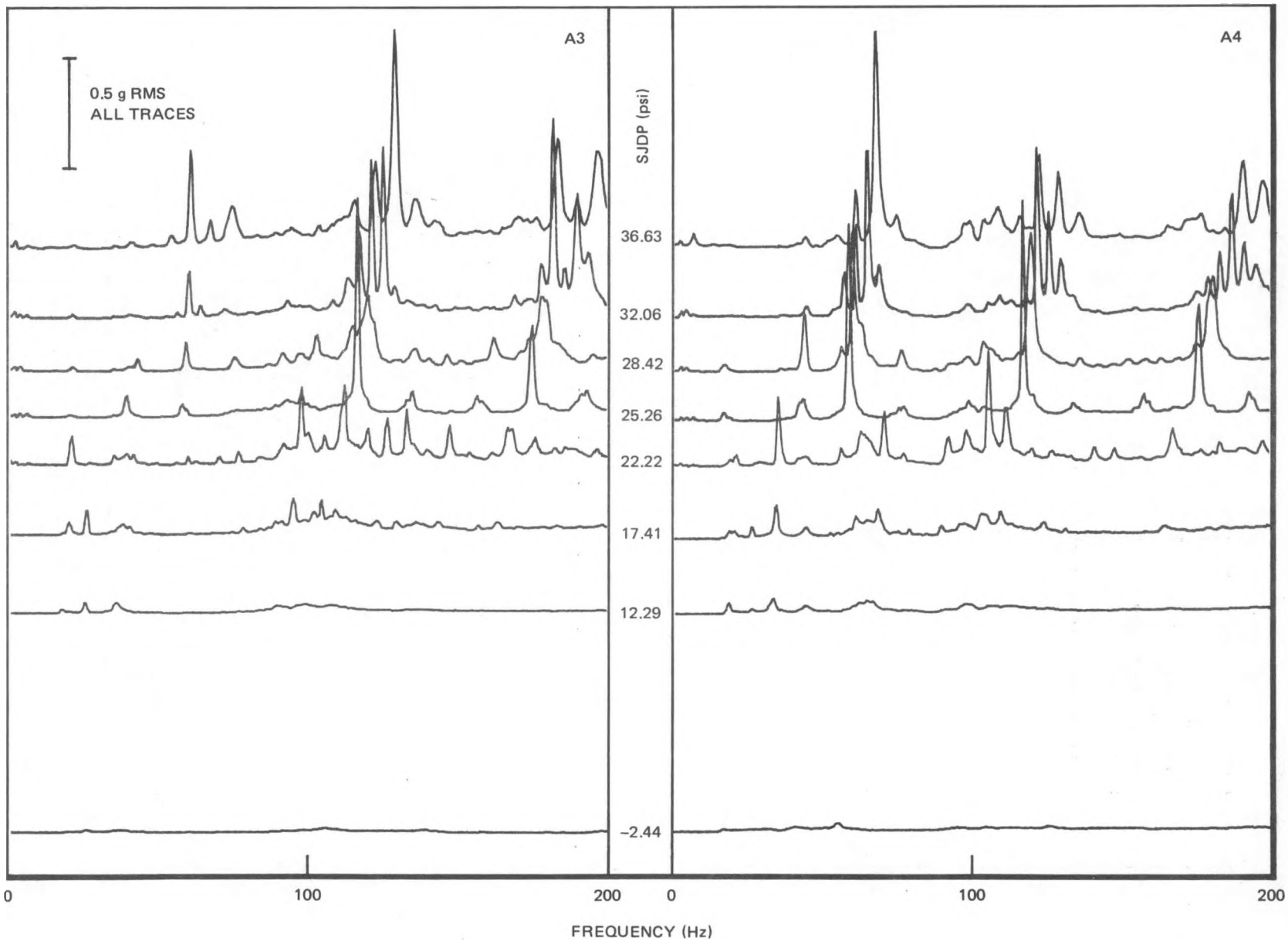

Figure 5-34. Vibration Progression for the BWR/6-218 Jet Pump

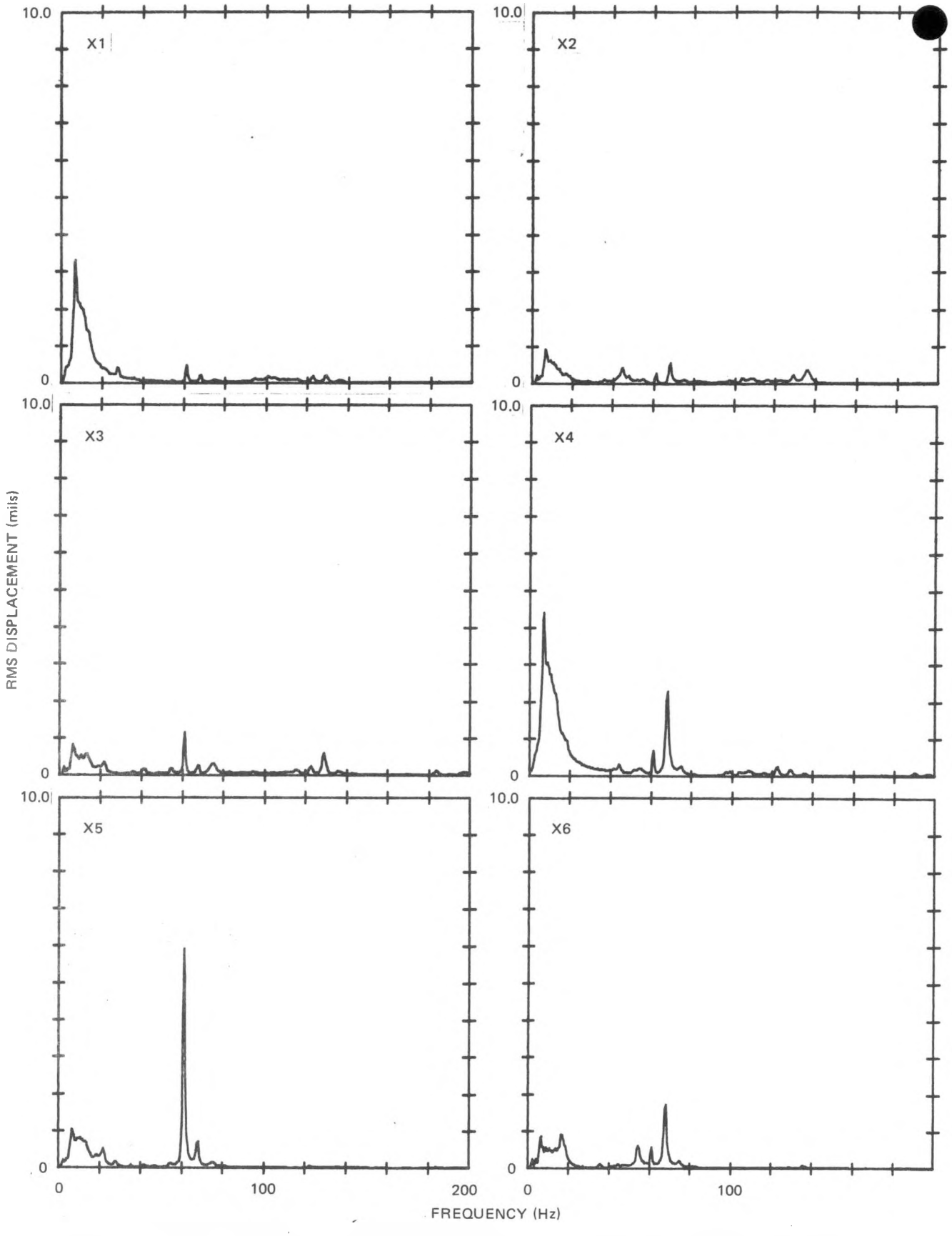

Figure 5-33. Displacement Amplitude Spectra for Test Condition 4208 (High Level FIV) M = 1.46

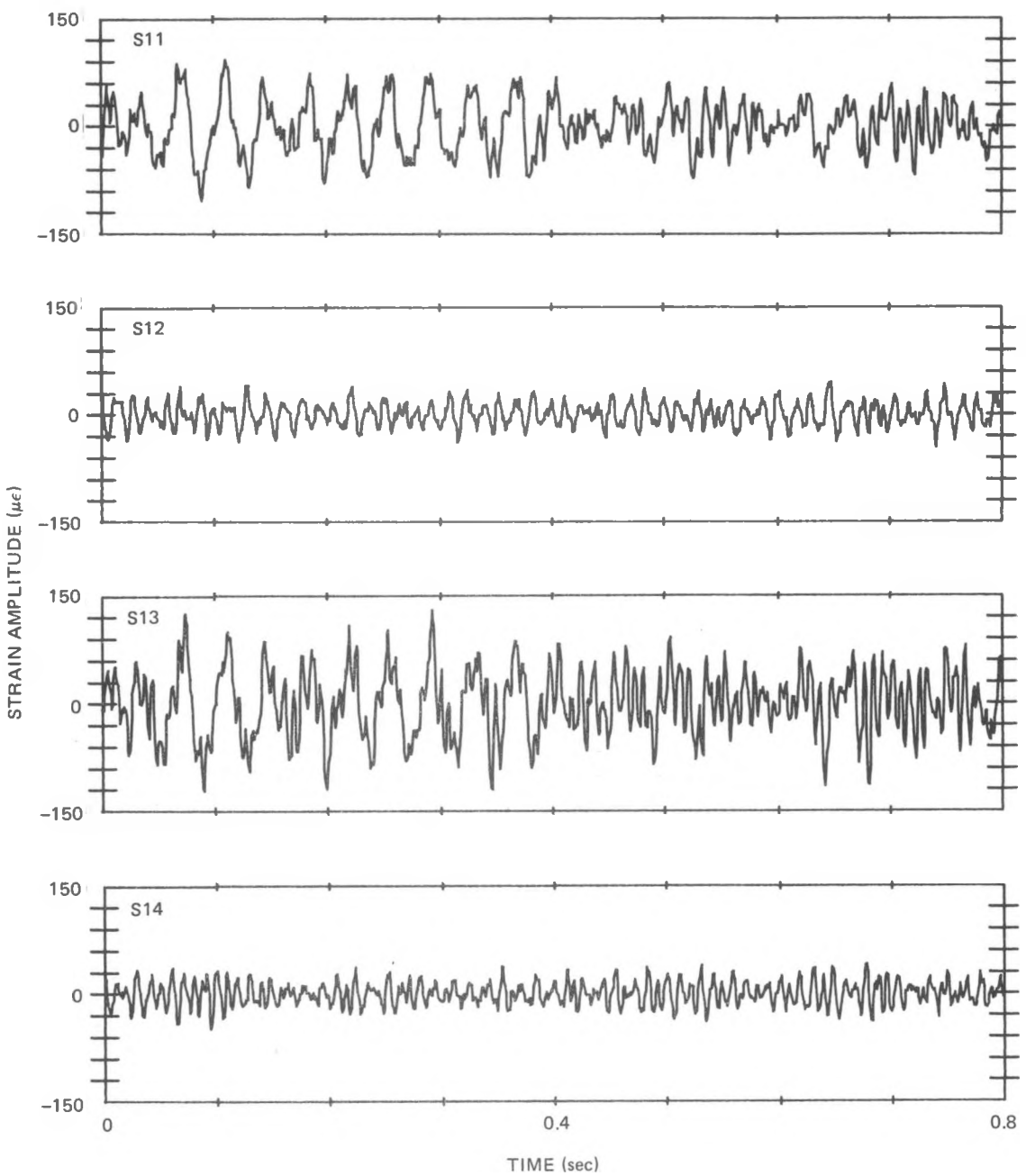

Figure 5-32. Instantaneous Strain Time Histories for Test Condition 4208 (High Level FIV) M = 1.46

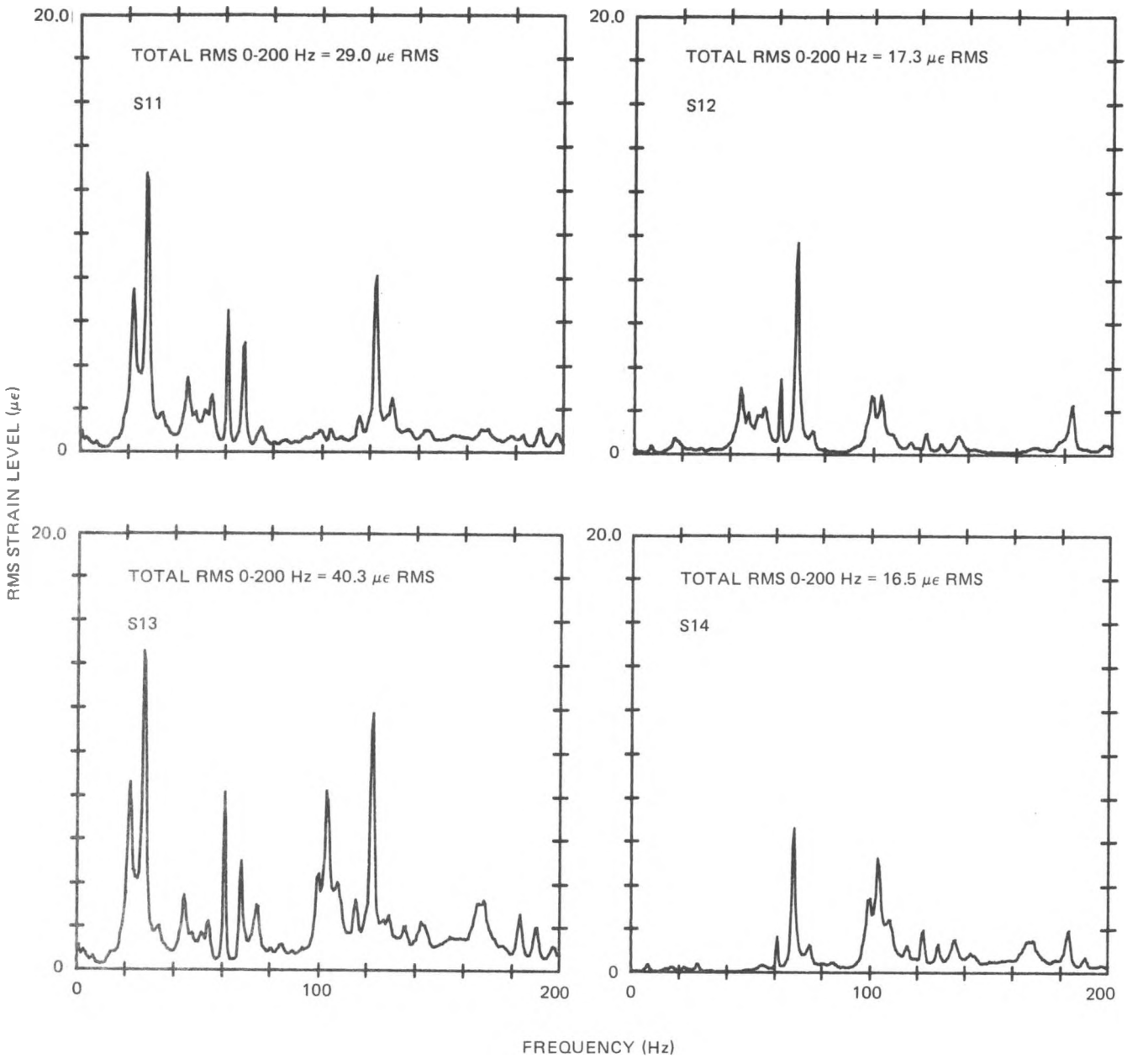

Figure 5-31. Strain Amplitude Spectra for Test Condition 4208 (High Level FIV) M = 1.46

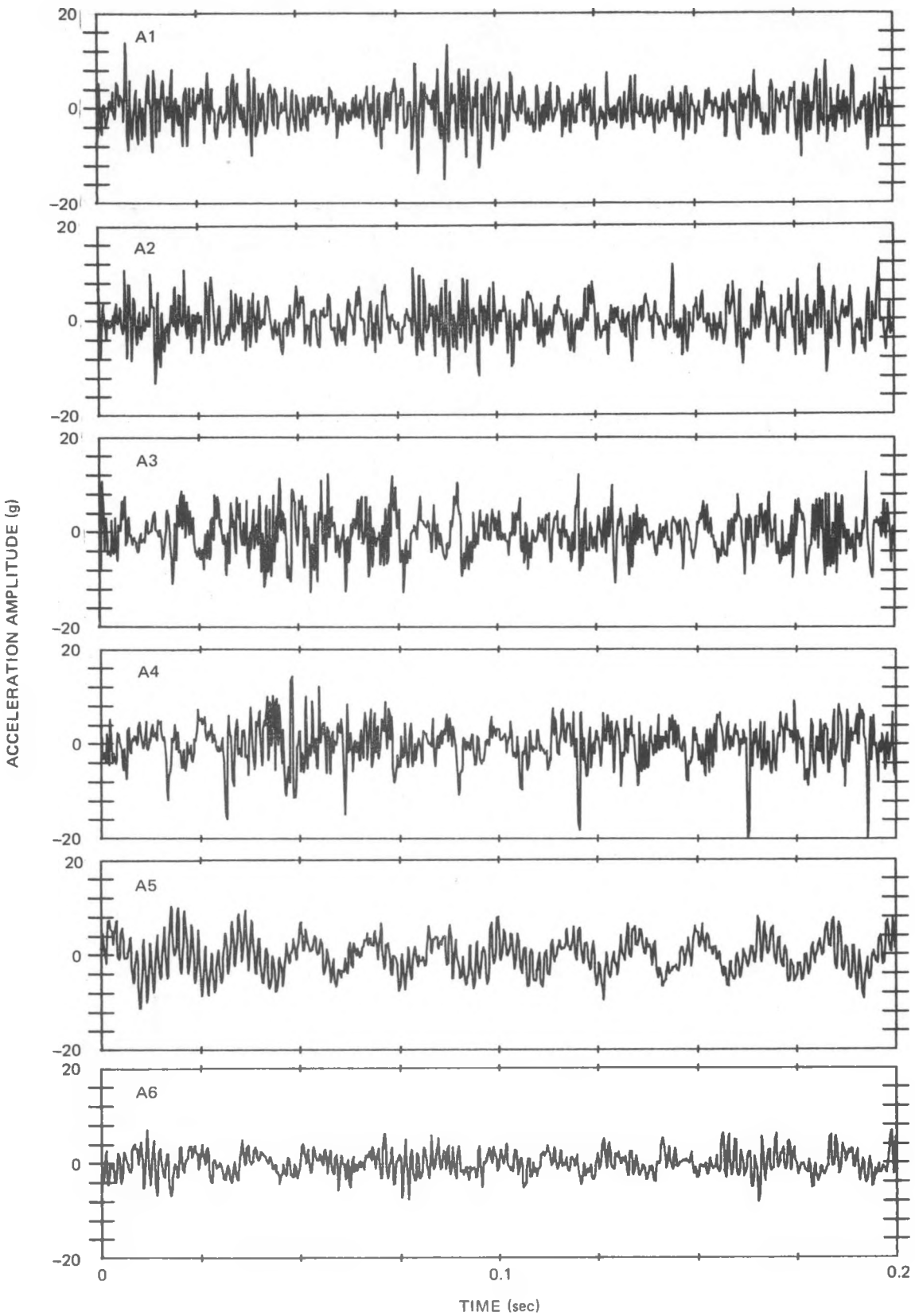

Figure 5-30. Instantaneous Acceleration Time Histories for Test Condition 4208 (High Level FIV) M = 1.46

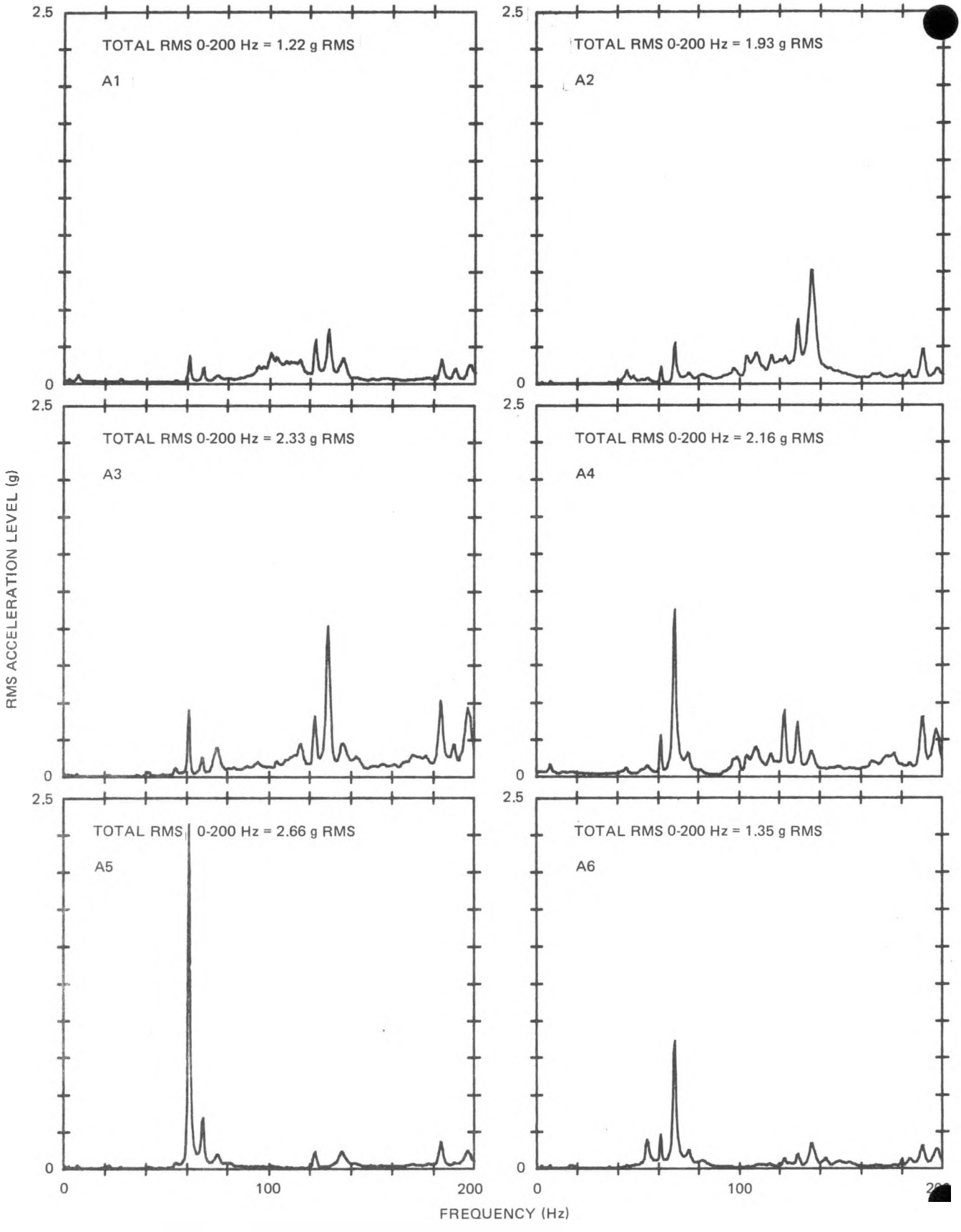

Figure 5-29. Acceleration Amplitude Spectra for Test Condition 4208 (High Level FIV) M = 1.46

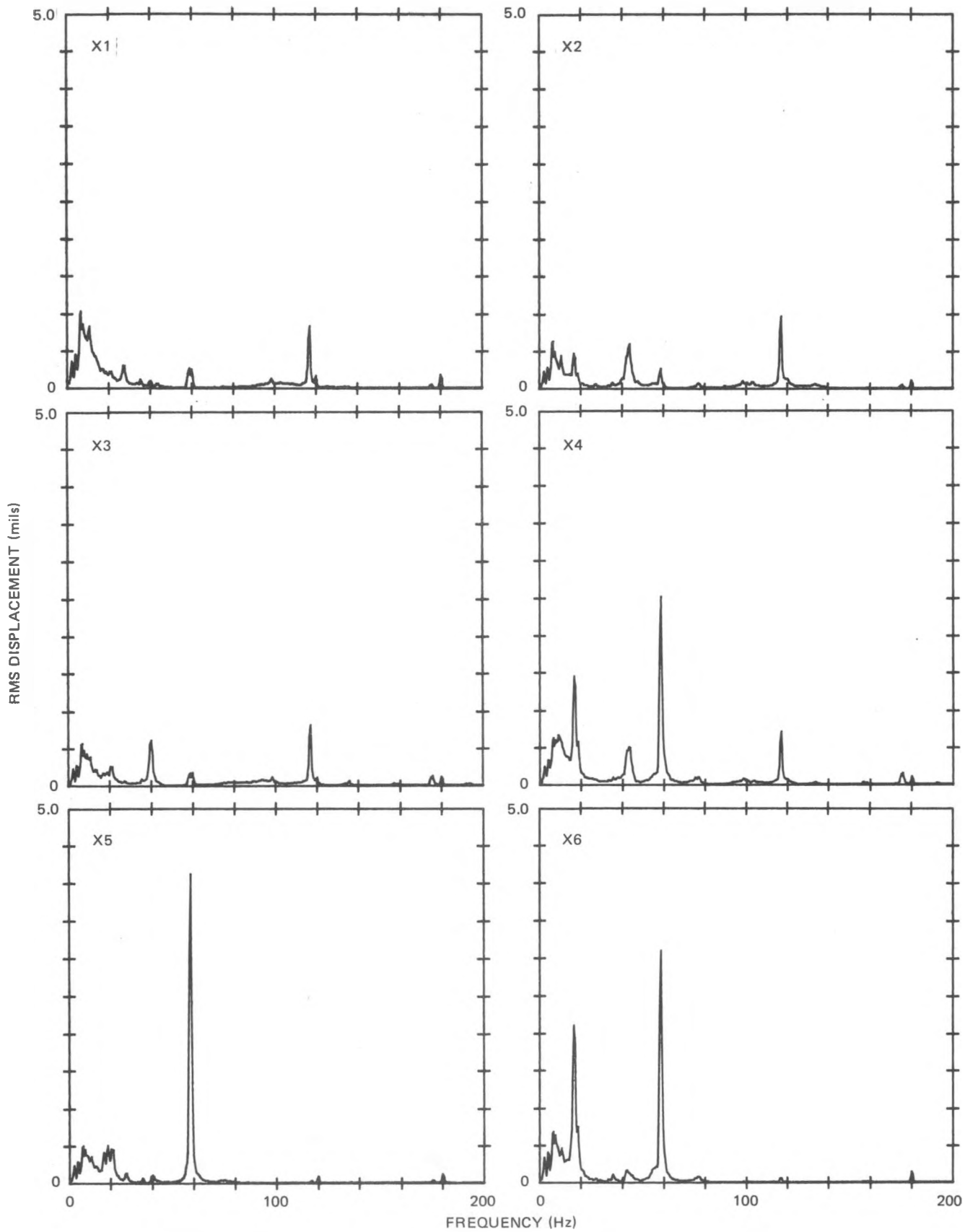

Figure 5-28. Displacement Amplitude Spectra for Test Condition 4205 (Intermediate Level FIV) M = 1.98

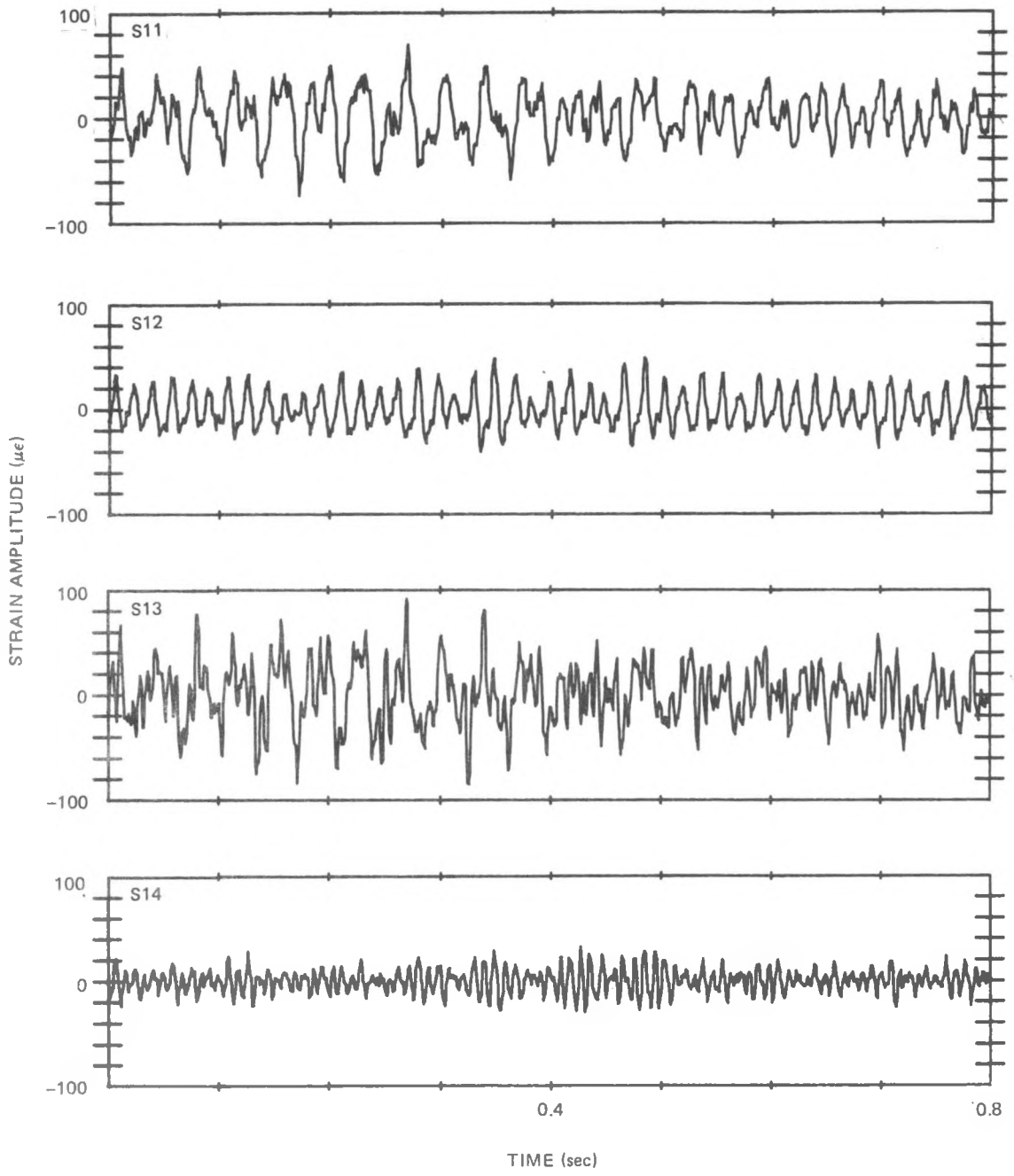

Figure 5-27. Instantaneous Strain Time Histories for Test Condition 4205 (Intermediate Level FIV) M = 1.98

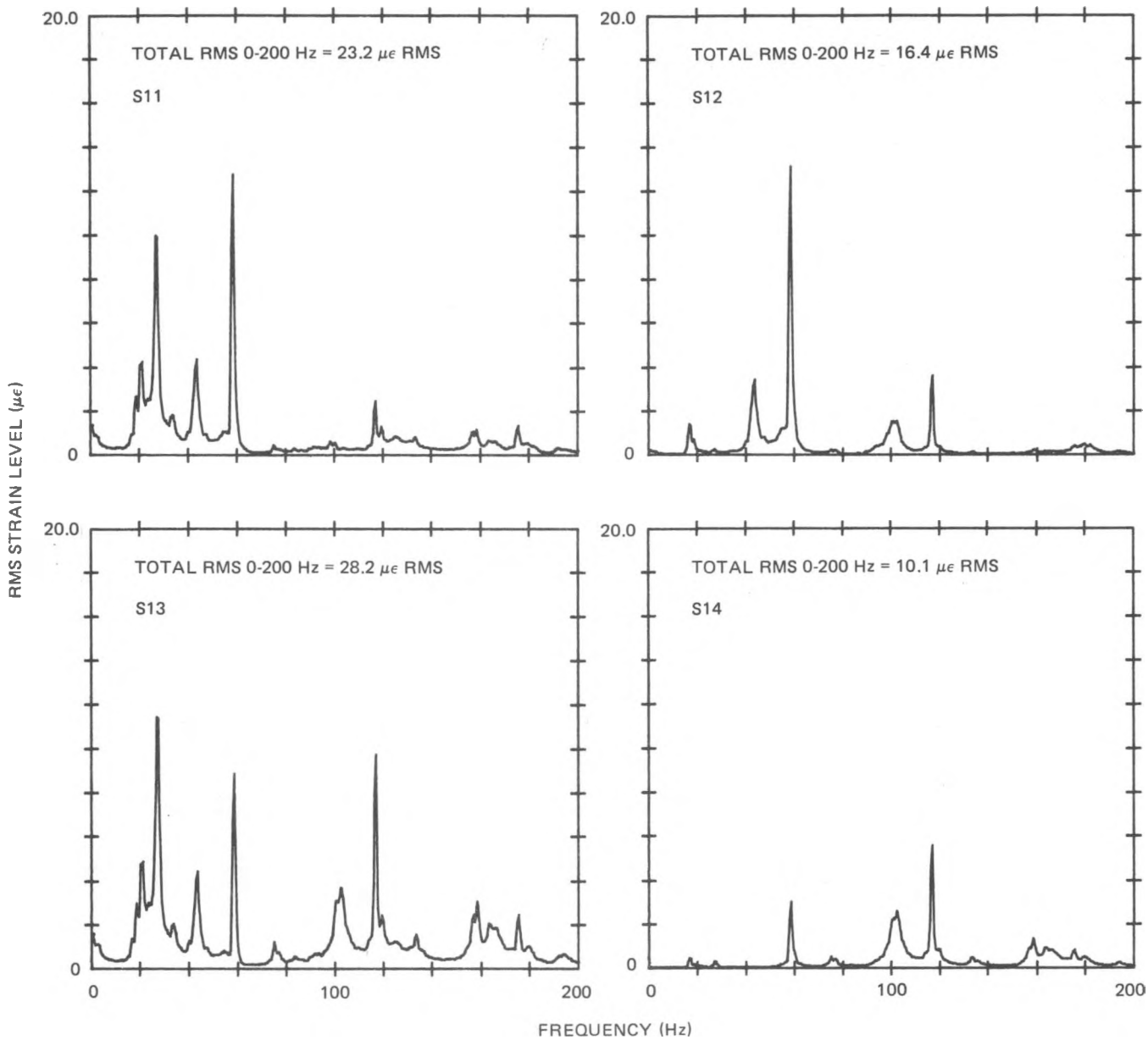

Figure 5-26. Strain Amplitude Spectra for Test Condition 4205 (Intermediate Level FIV) M = 1.98

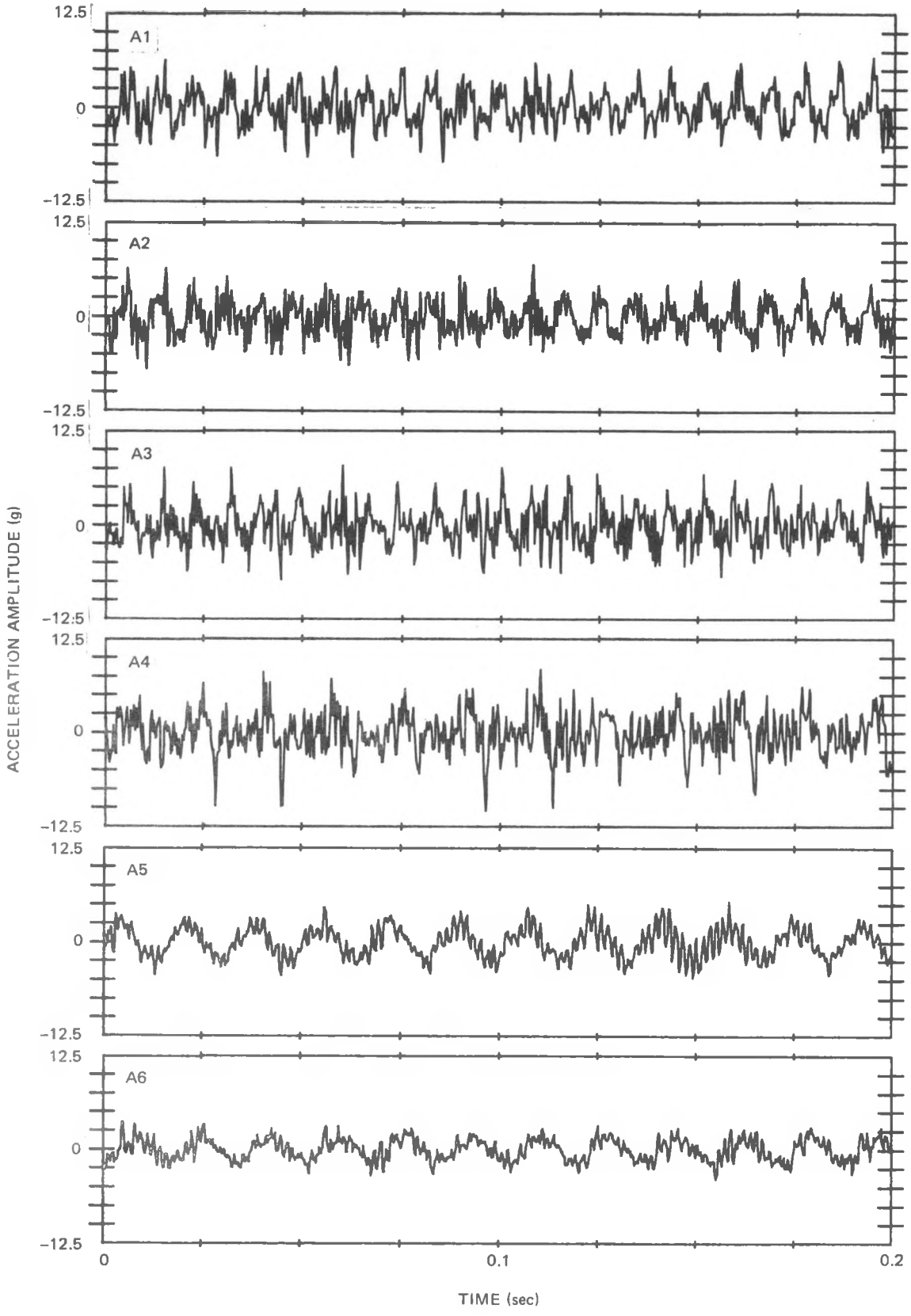

Figure 5-25. Instantaneous Acceleration Time Histories for Test Condition 4205 (Intermediate Level FIV) M = 1.98

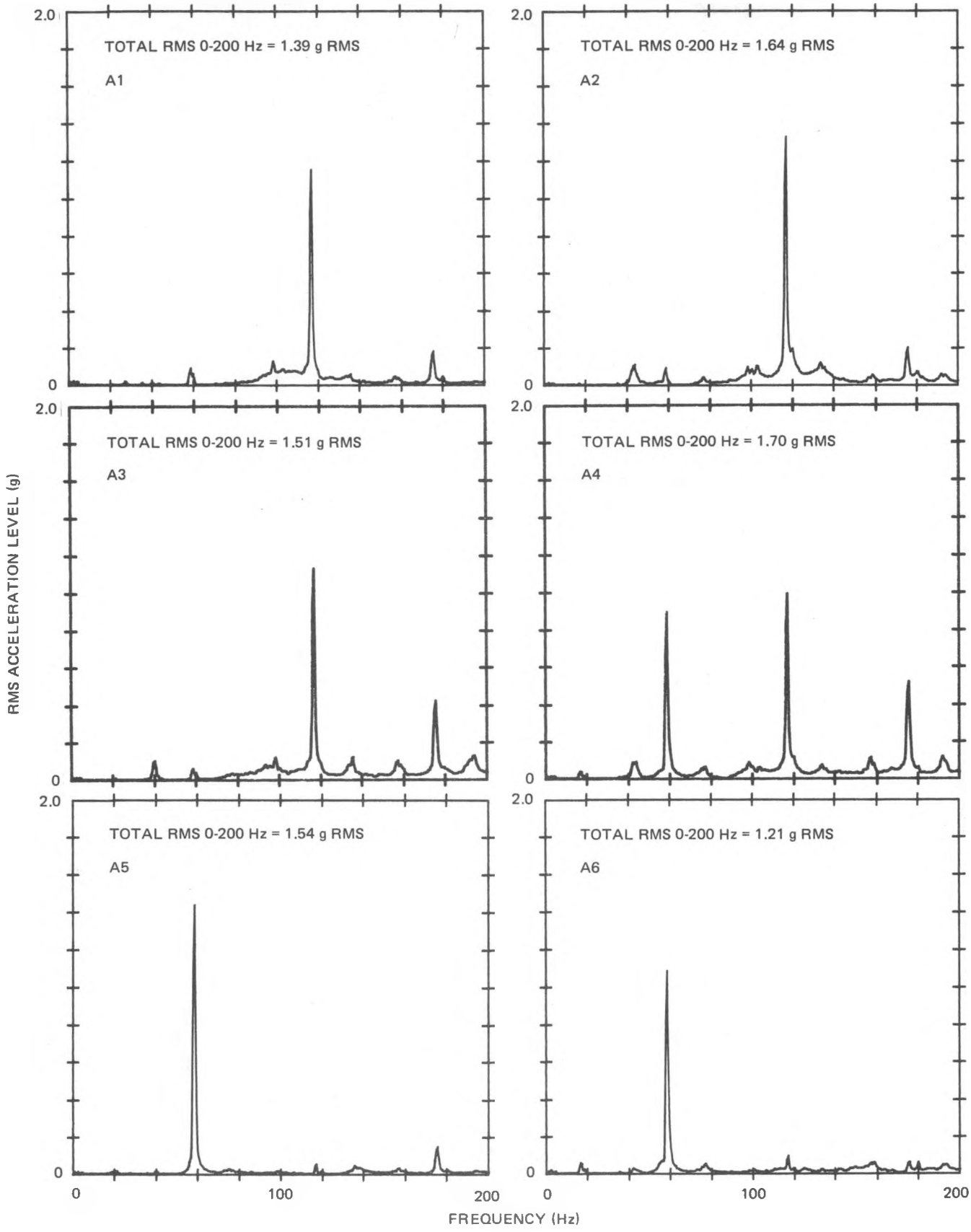

Figure 5-24. Acceleration Amplitude Spectra for Test Condition 4205 (Intermediate Level FIV) M = 1.98

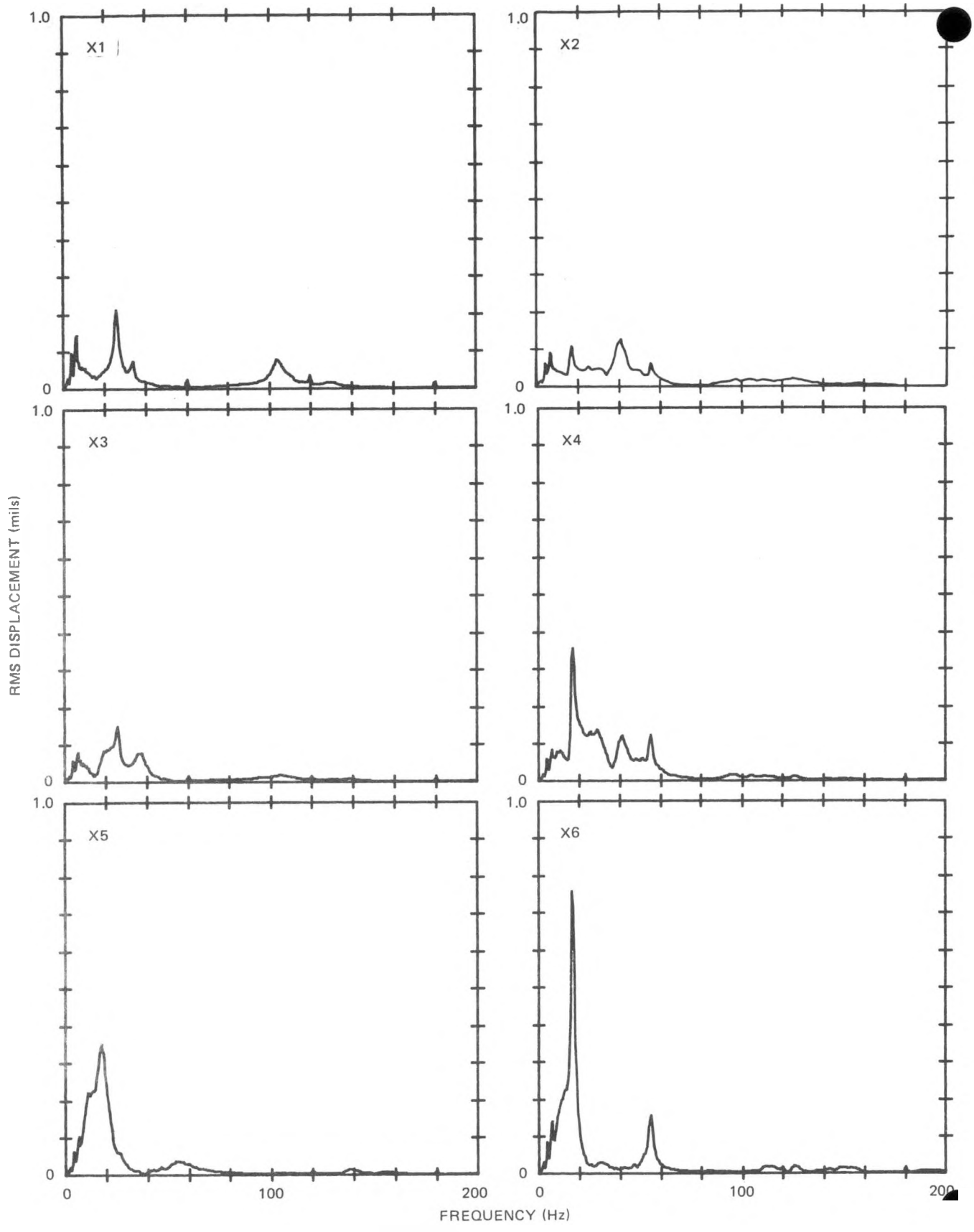

Figure 5-23. Displacement Amplitude Spectra for Test Condition 4201 (Low Level FIV) M = 3.23

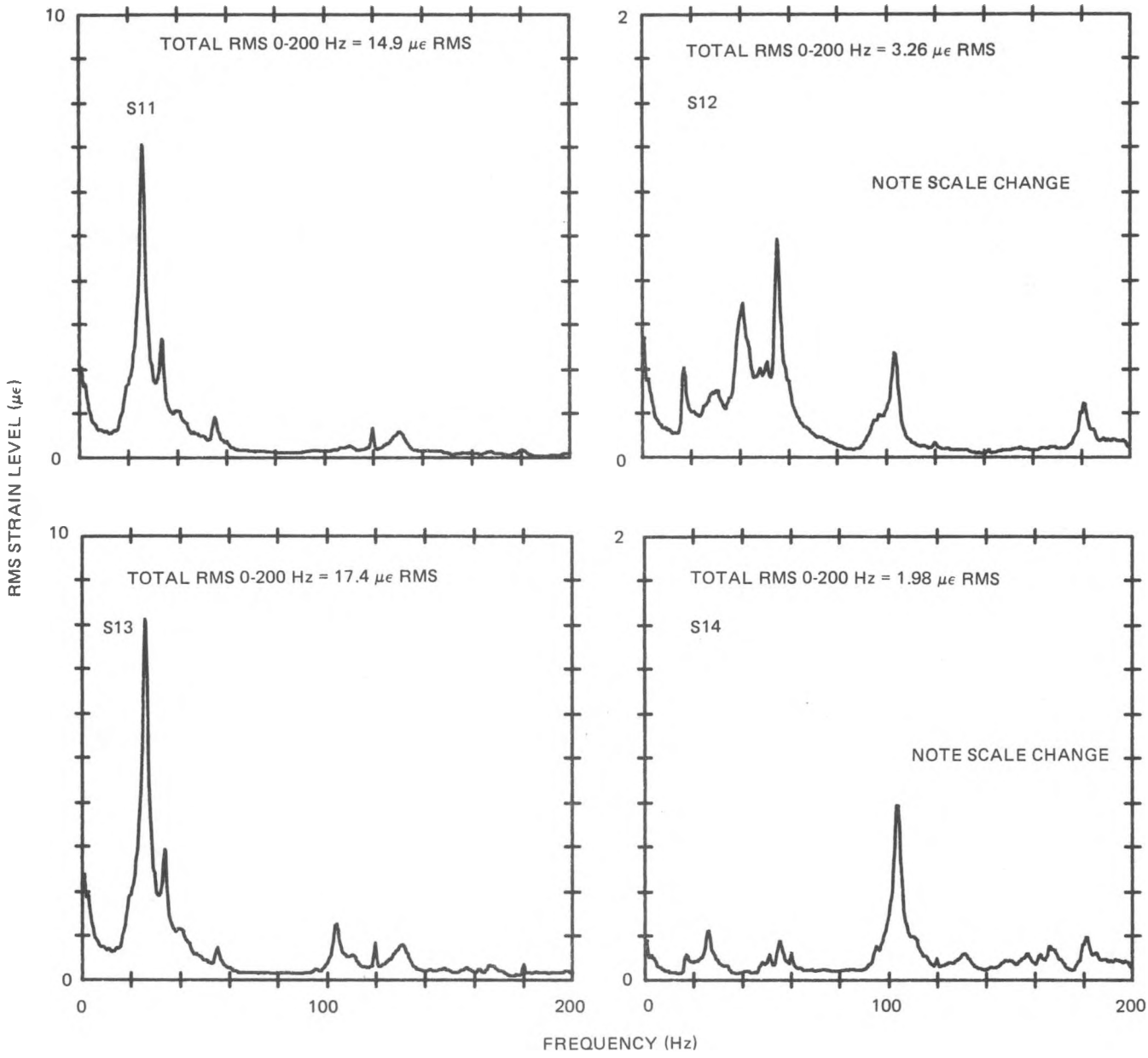

Figure 5-21. Strain Amplitude Spectra for Test Condition 4201 (Low Level FIV) M = 3.23

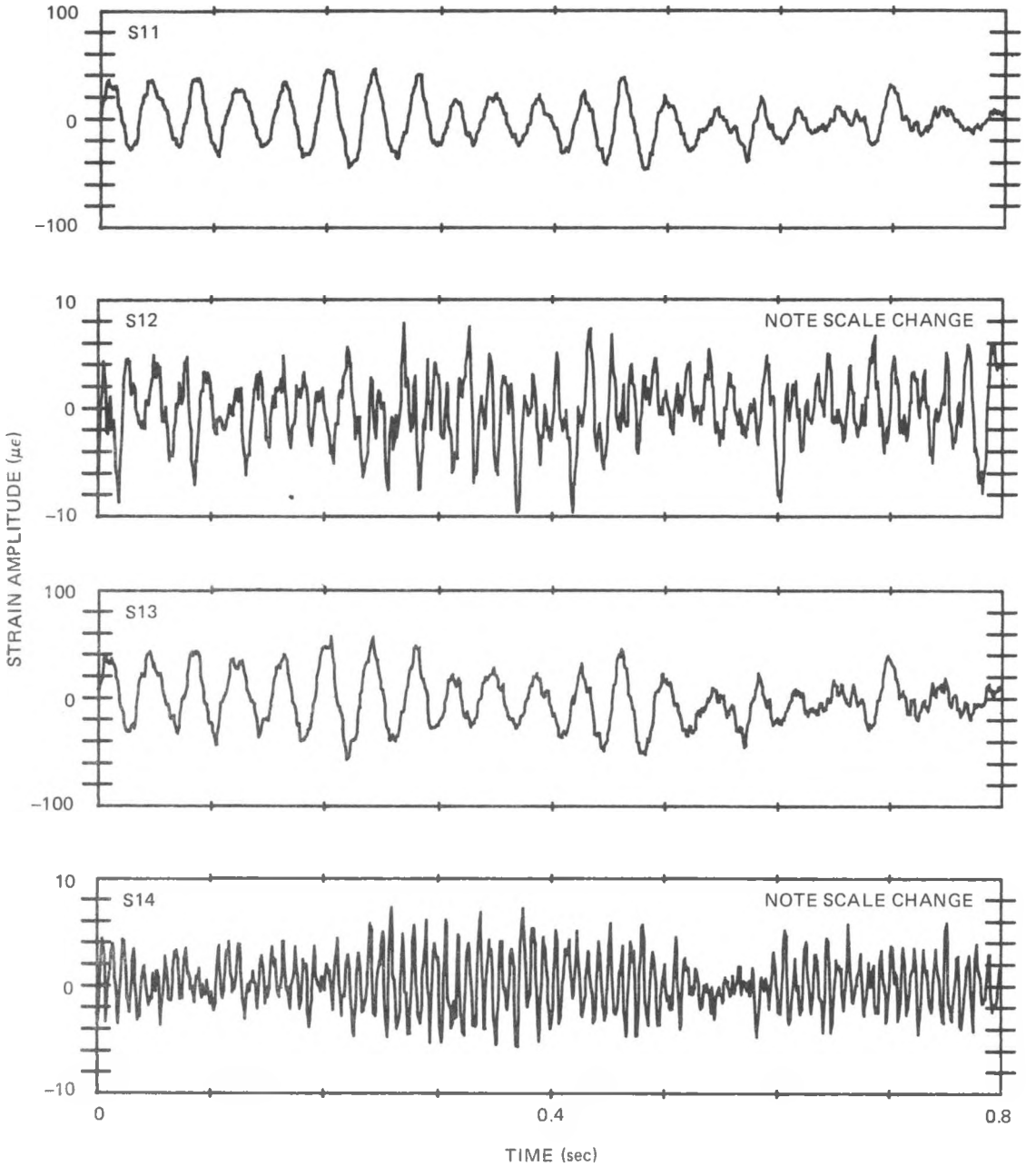

Figure 5-22. Instantaneous Strain Time Histories for Test Condition 4201 (Low Level FIV) M = 3.23

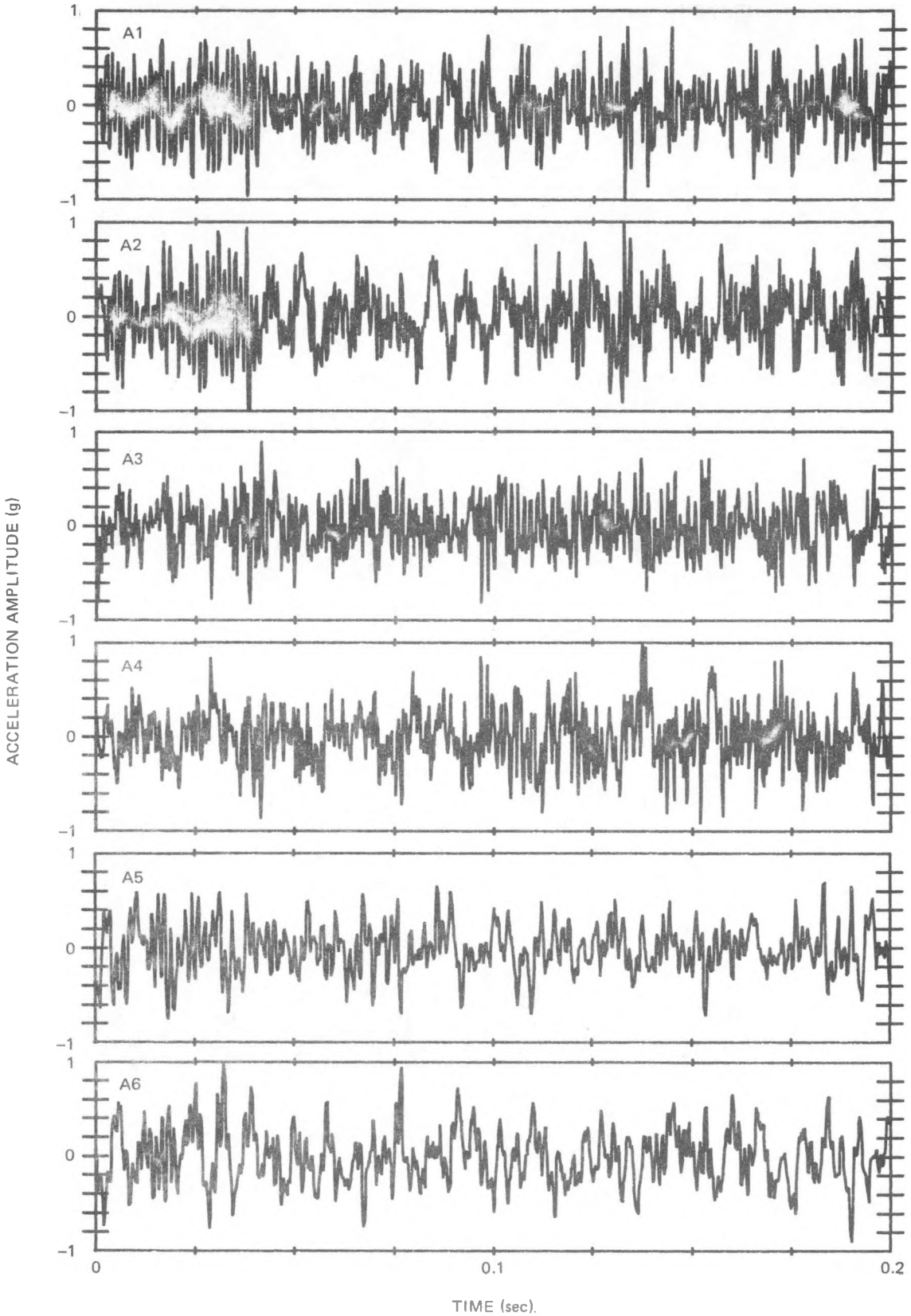

Figure 5-20. Instantaneous Acceleration Time Histories for Test Condition 4201 (Low Level FIV) M = 3.23

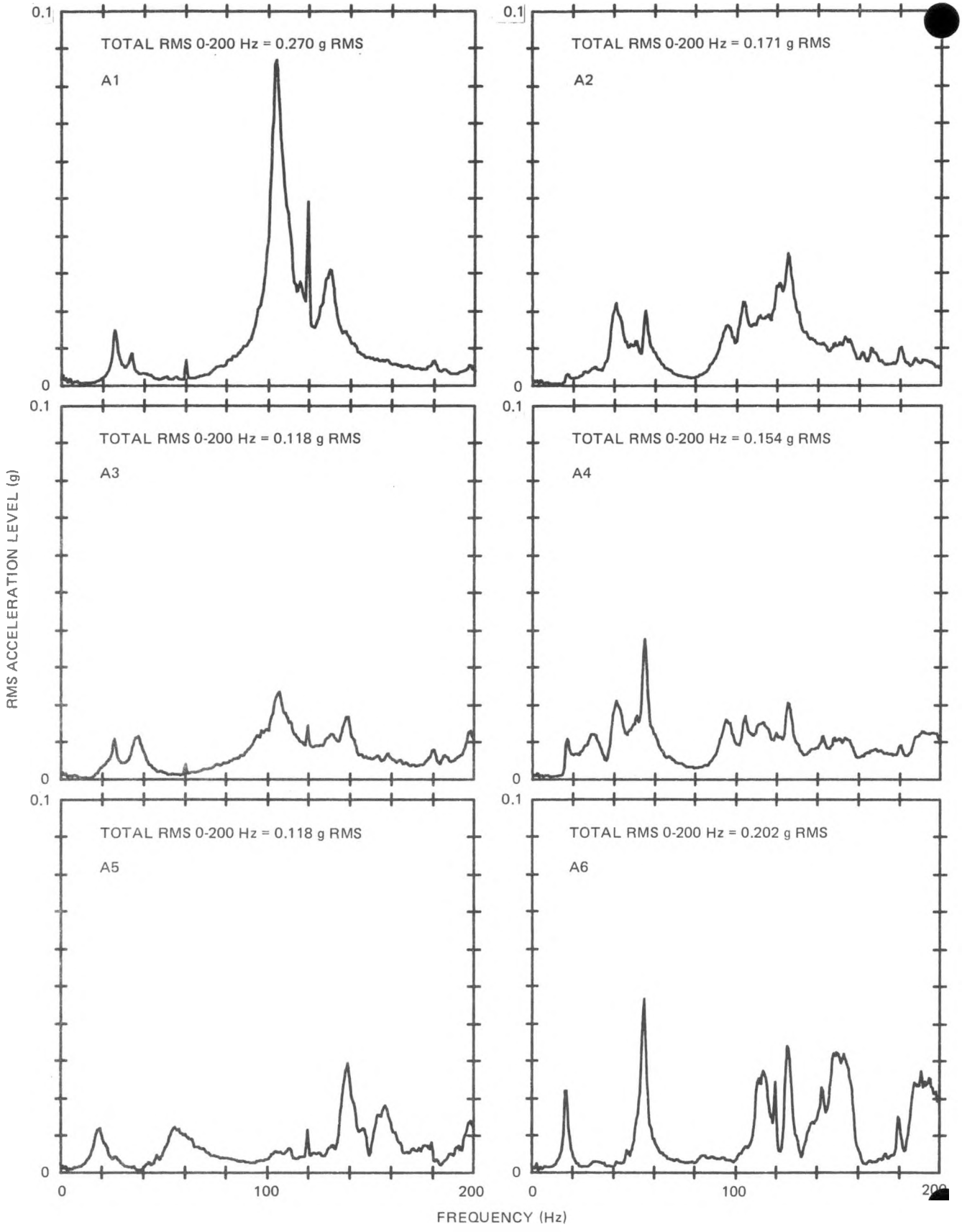

Figure 5-19. Acceleration Amplitude Spectra for Test Conditions 4201 (Low Level FIV) M = 3.23

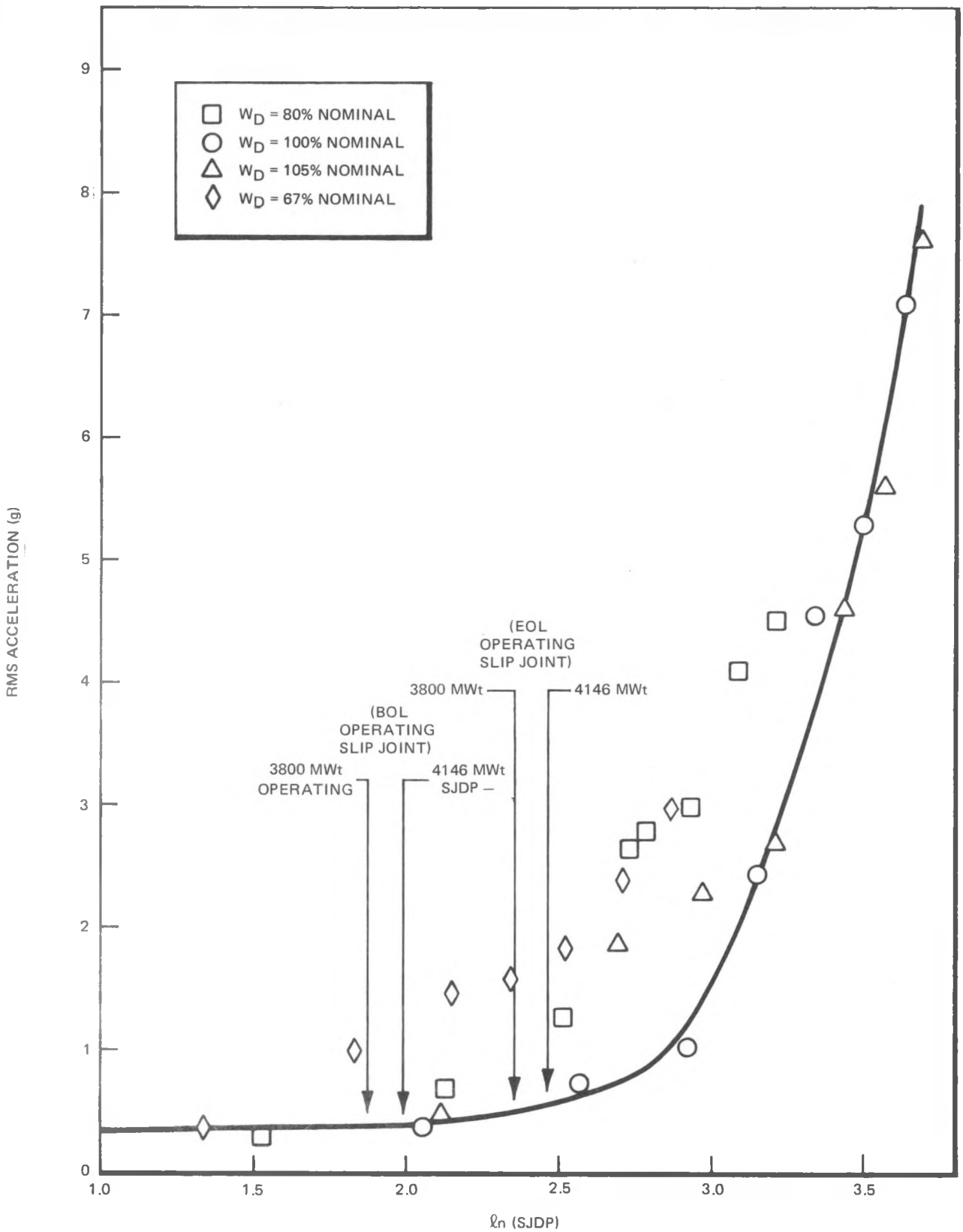

Figure 5-18. Vibration Characteristic for the BWR/6-251 Jet Pump

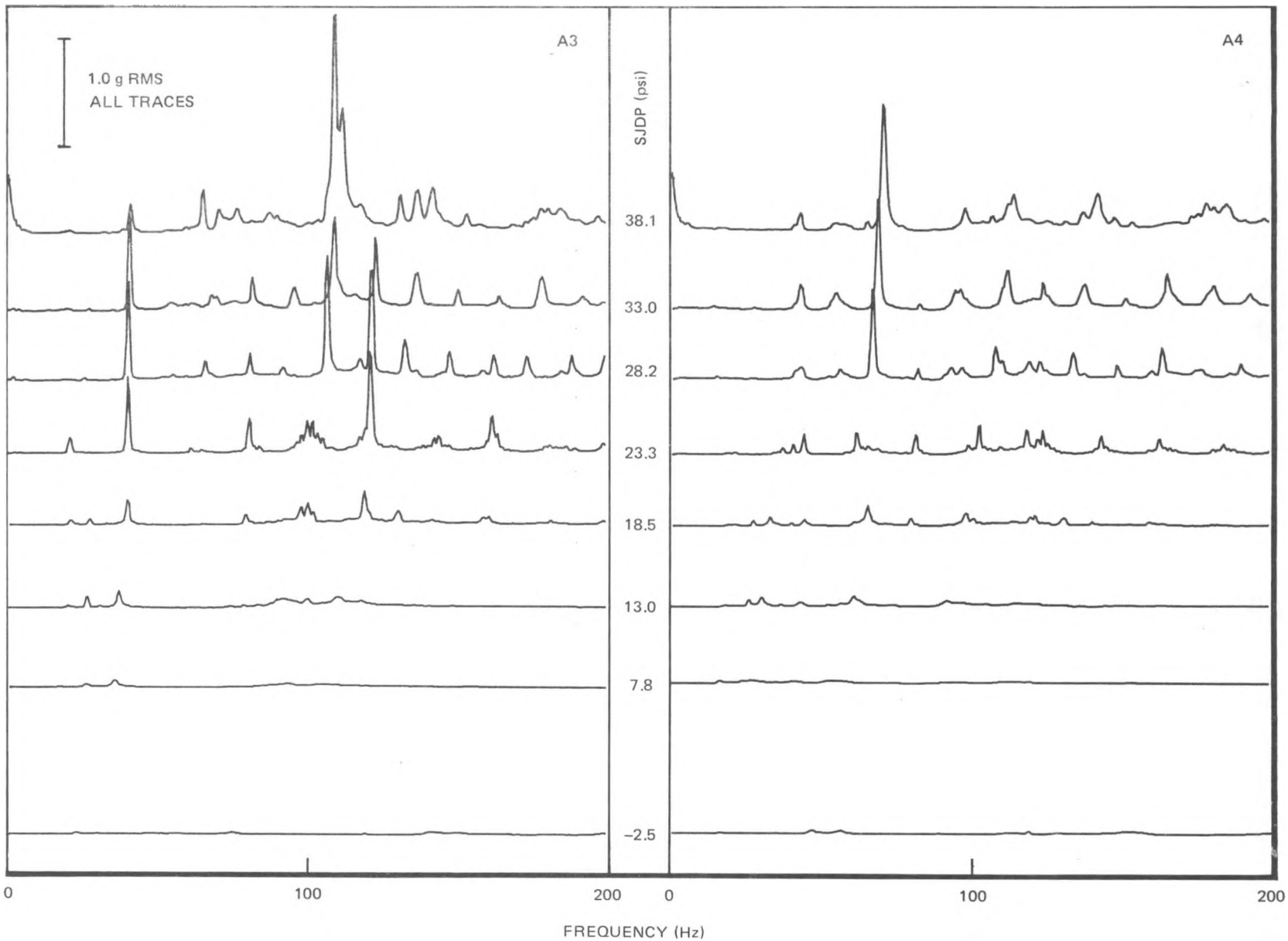

Figure 5-17. Vibration Progression for the BWR/6-251 Jet Pump

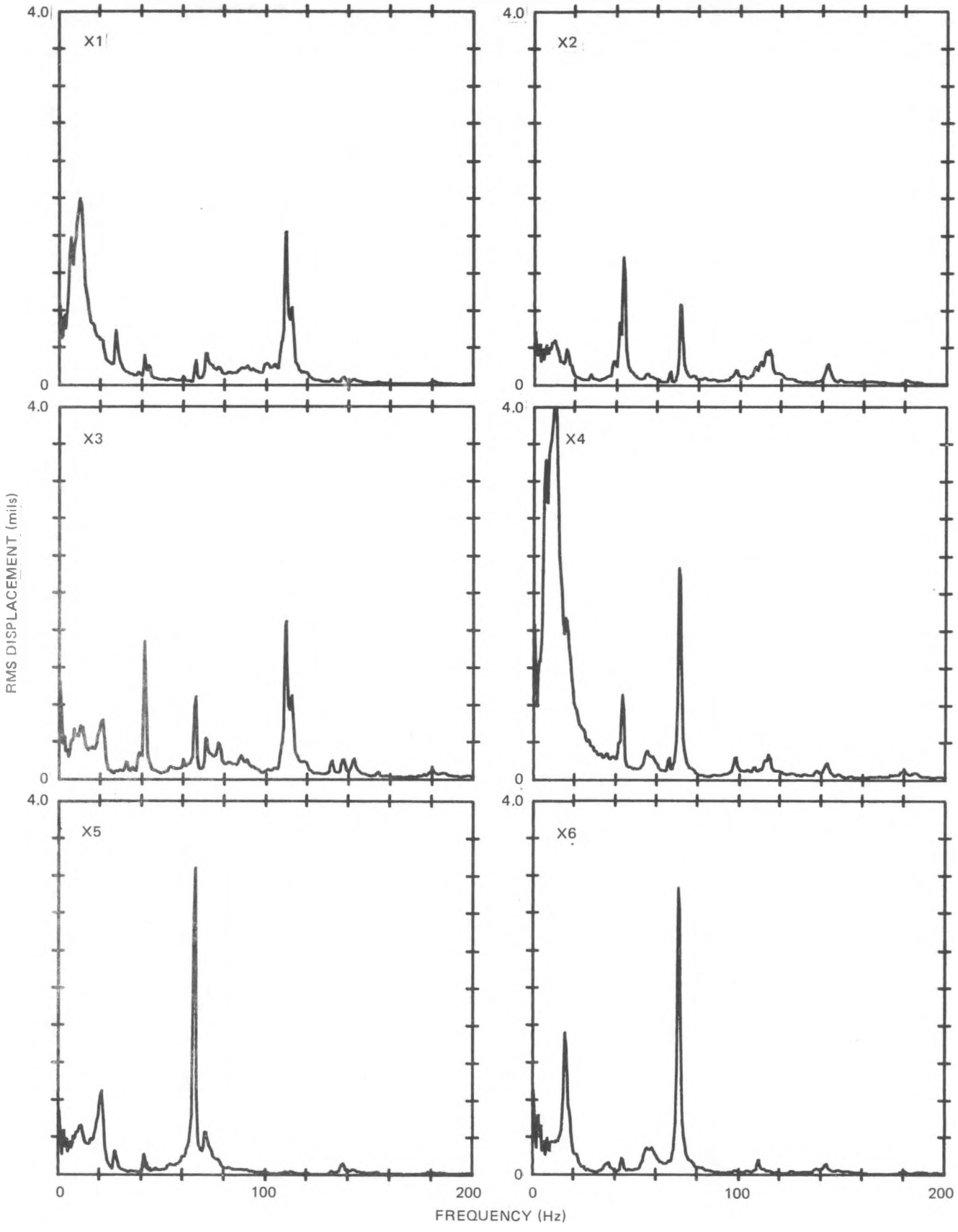

Figure 5-16. Displacement Amplitude Time Histories for Test Condition 0208 (High Level FIV) M = 1.32

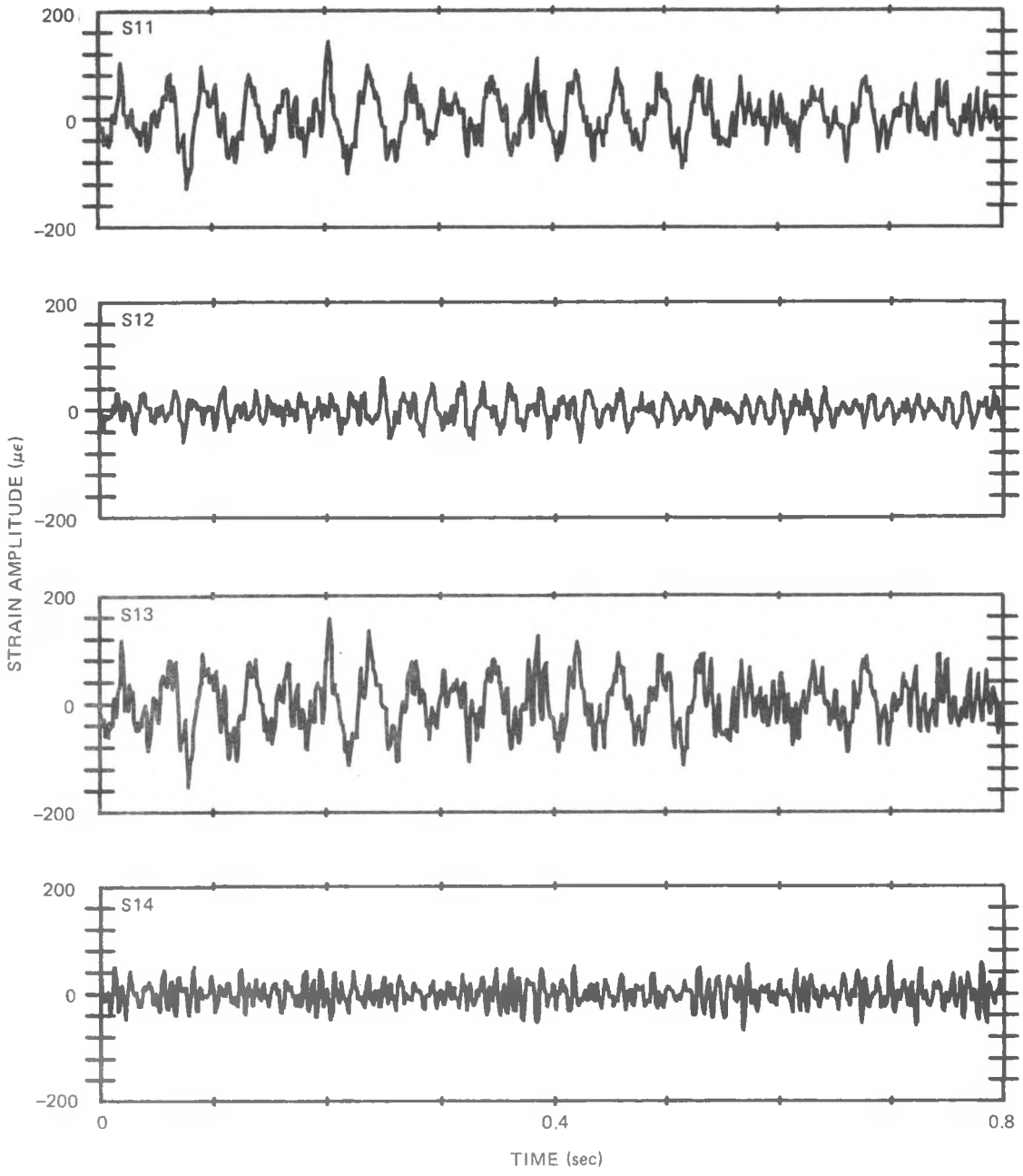

Figure 5-15. Instantaneous Strain Time Histories for Test Condition 0208 (High Level FIV) M = 1.32

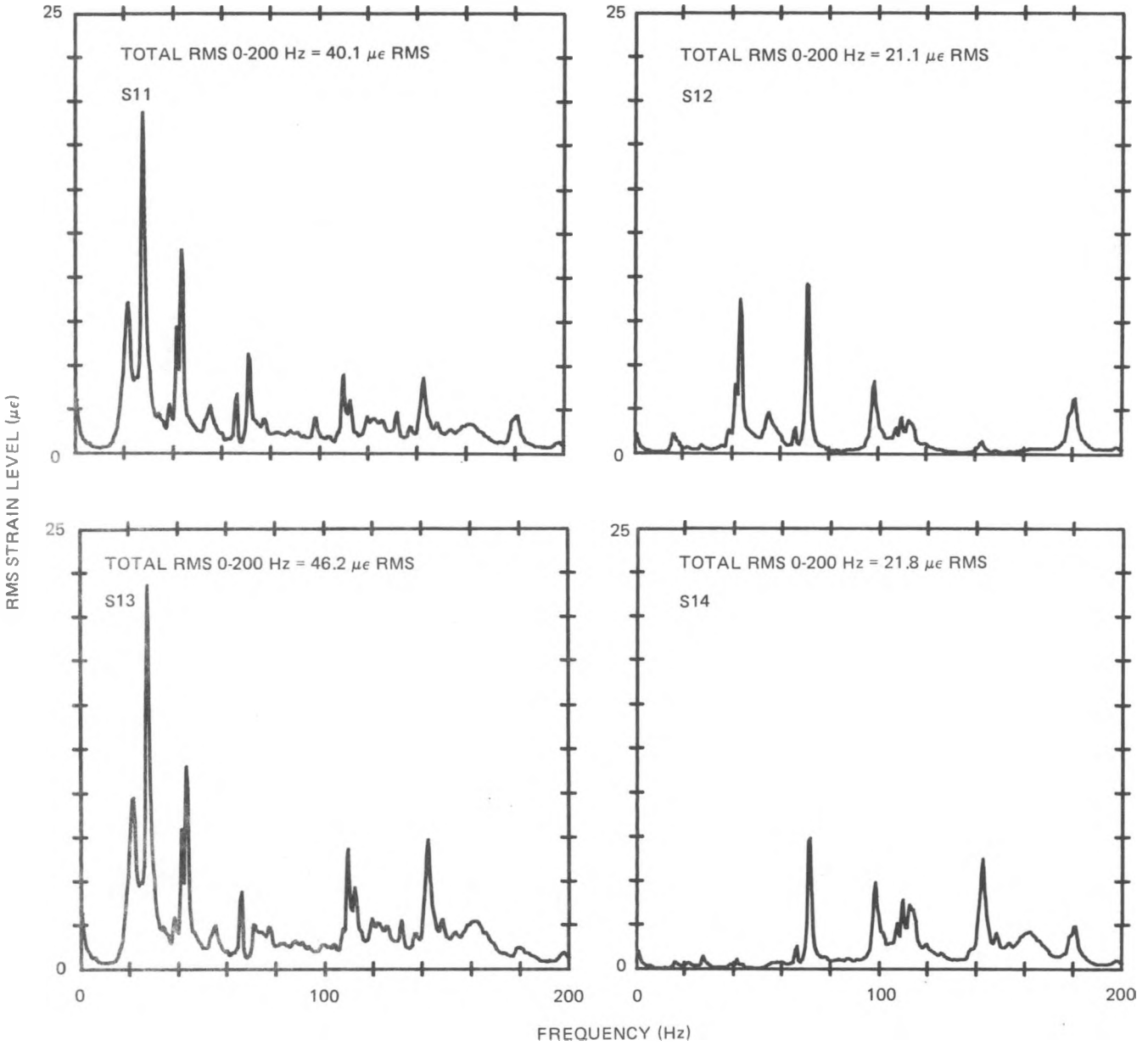

Figure 5-14. Strain Amplitude Spectra for Test Condition 0208 (High Level FIV) M = 1.32

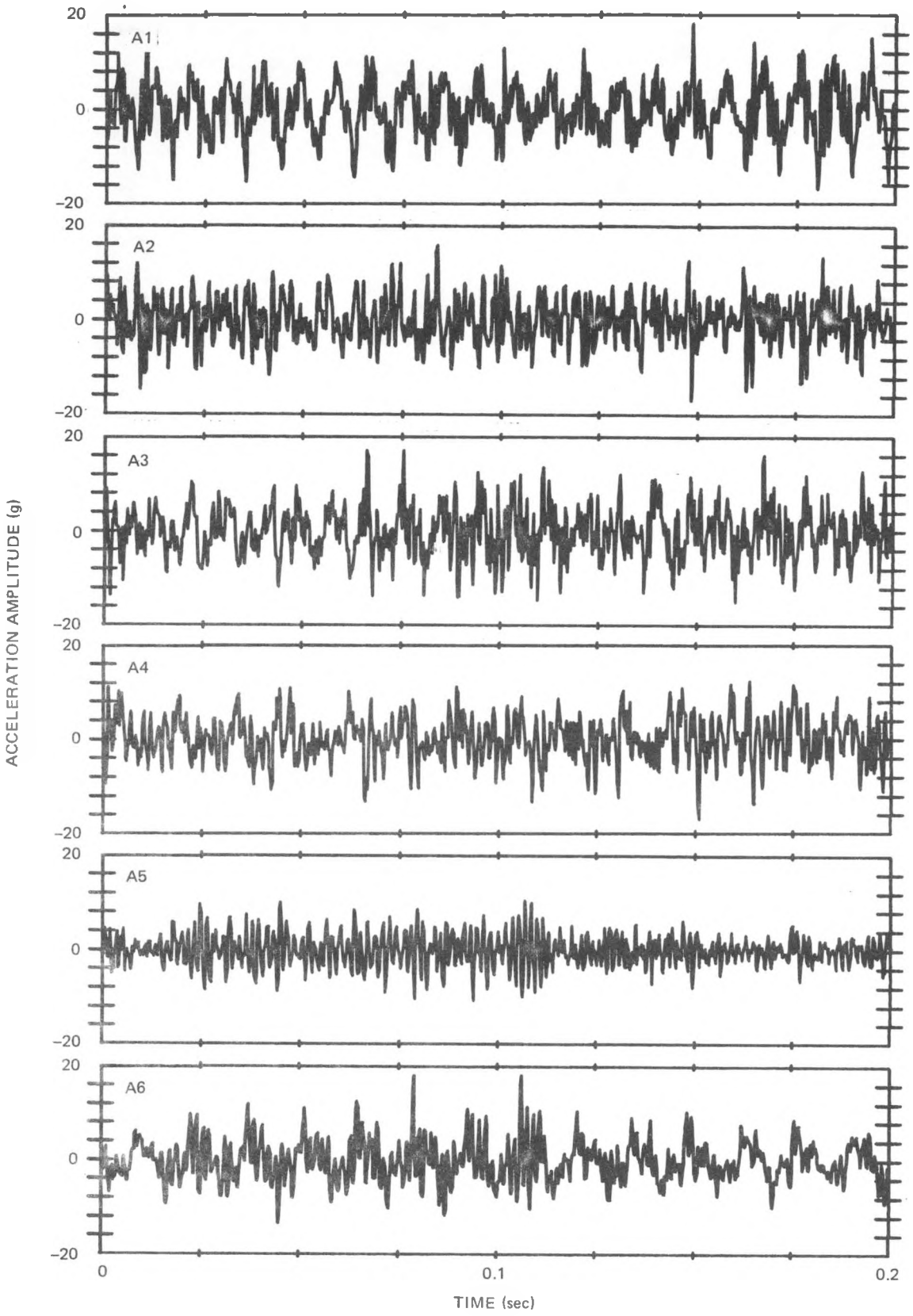

Figure 5-13. Instantaneous Acceleration Time Histories for Test Condition 0208 (High Level FIV) M = 1.32

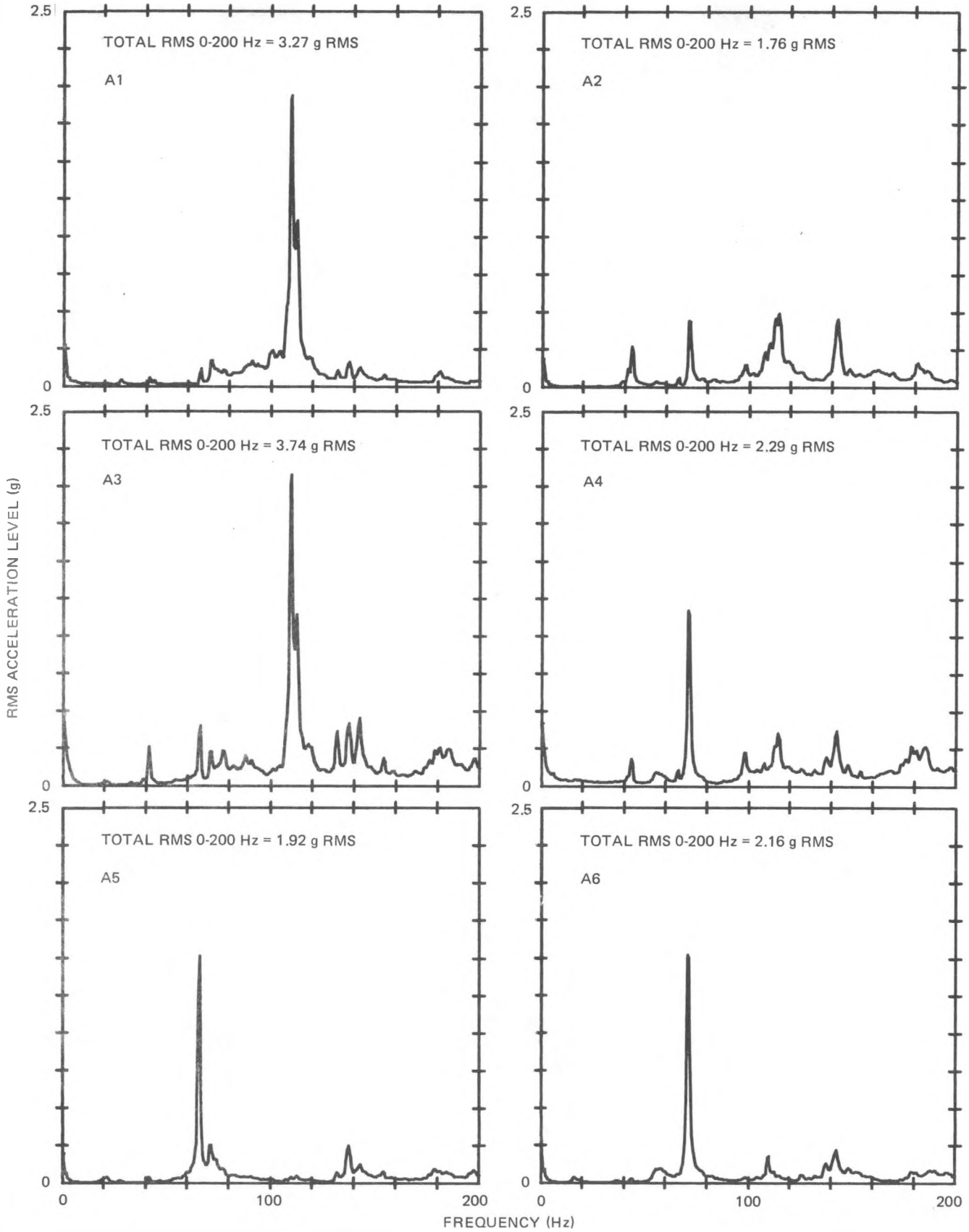

Figure 5-12. Acceleration Amplitude Spectra for Test Condition 0208 (High Level FIV) M = 1.32

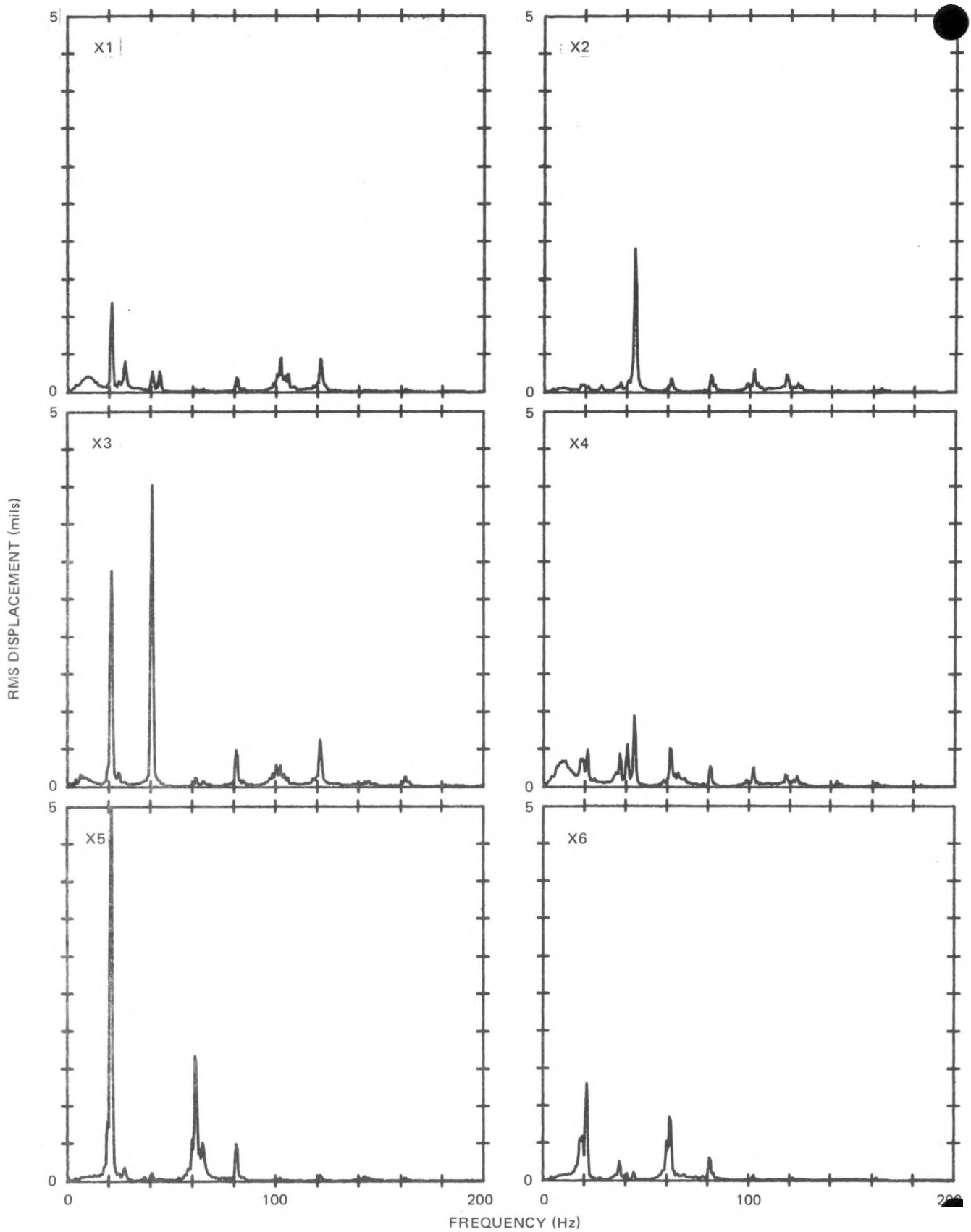

Figure 5-11. Displacement Amplitude Spectra for Test Condition 0205 (Intermediate Level FIV) M = 1.91

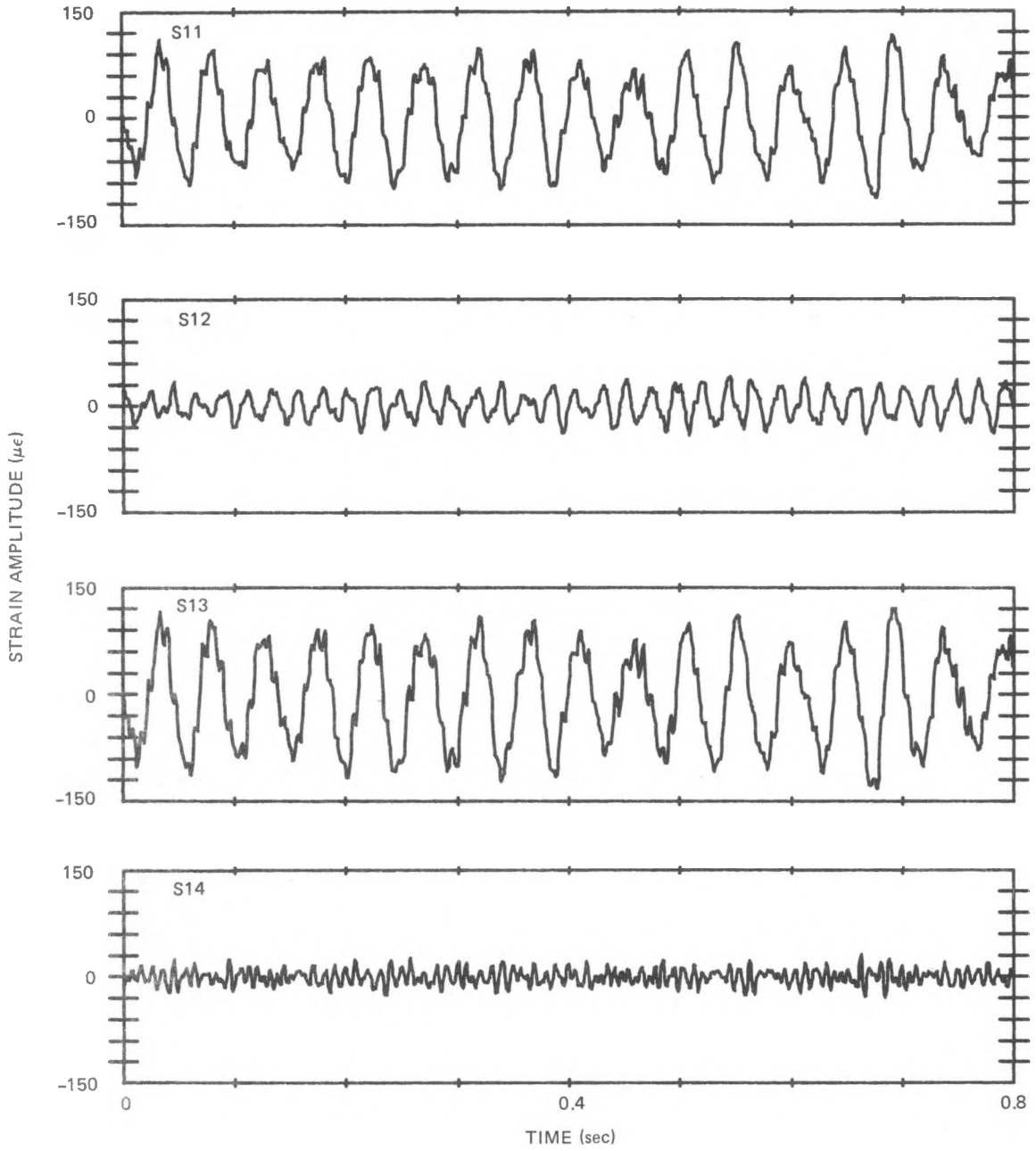

Figure 5-10. Instantaneous Strain Time Histories for Test Condition 0205 (Intermediate Level FIV) M = 1.91

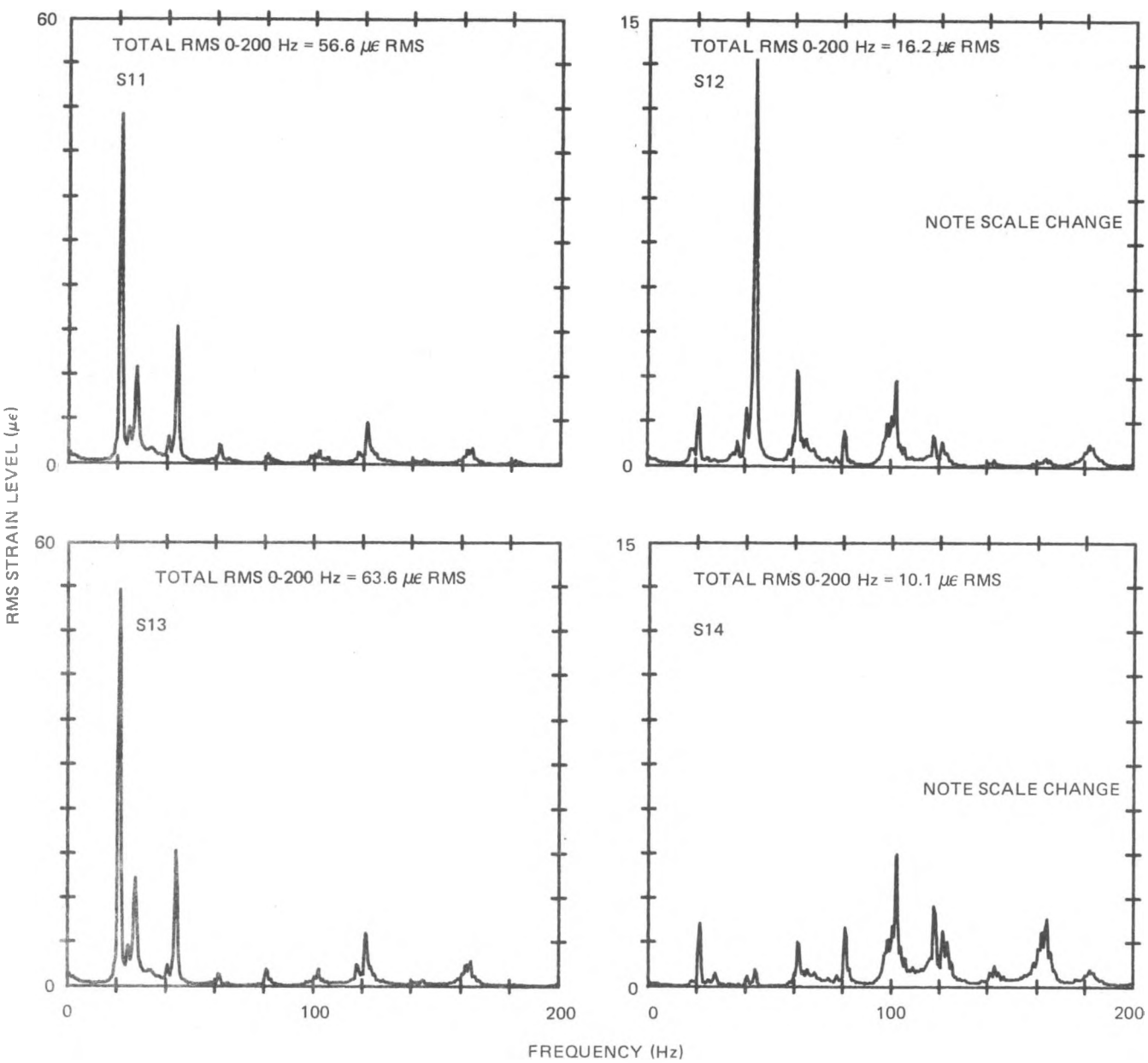

Figure 5-9. Strain Amplitude Spectra for Test Condition 0205 (Intermediate Level FIV) M = 1.91

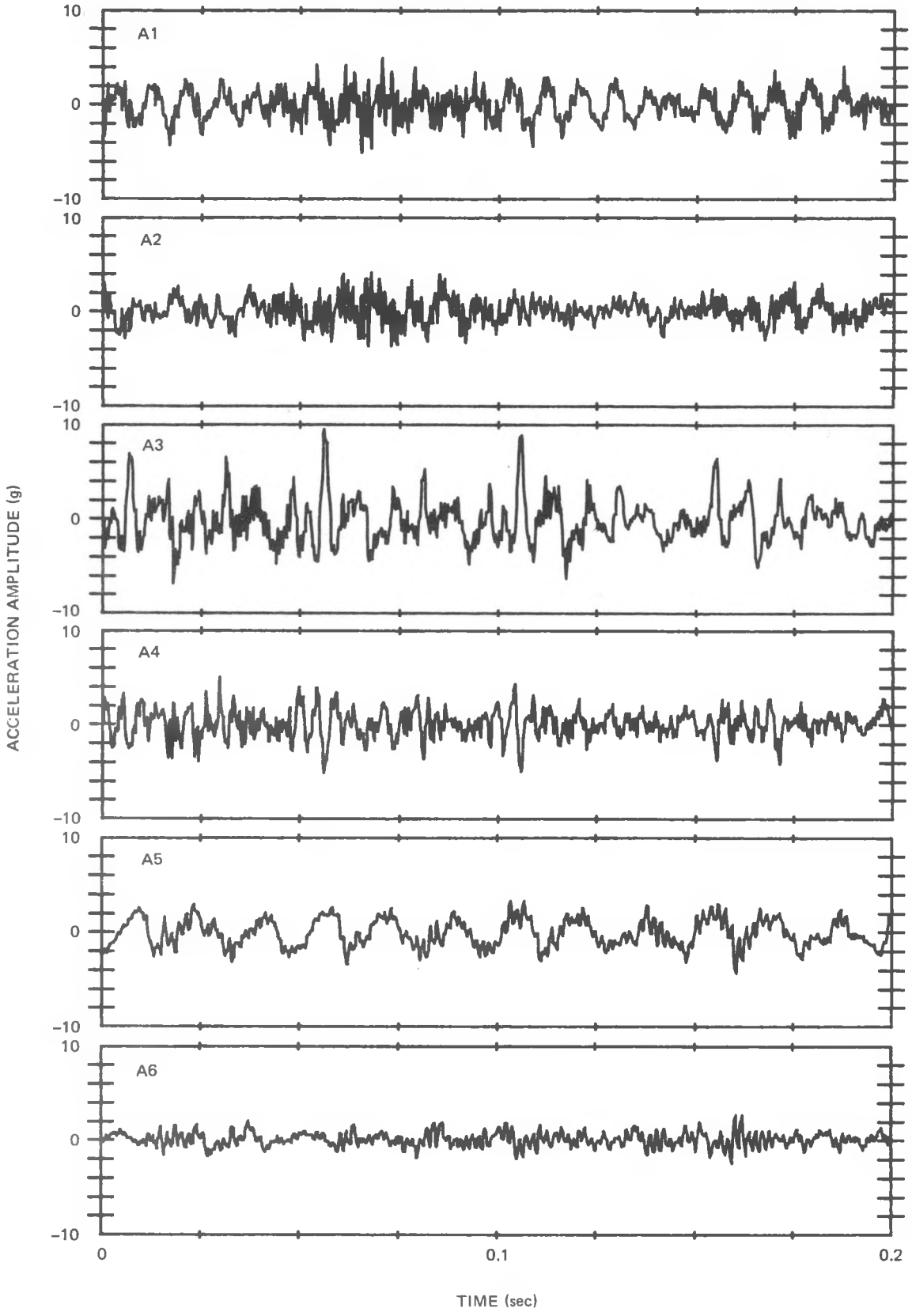

Figure 5-8. Instantaneous Acceleration Time Histories for Test Condition 0205 (Intermediate Level FIV) M = 1.91

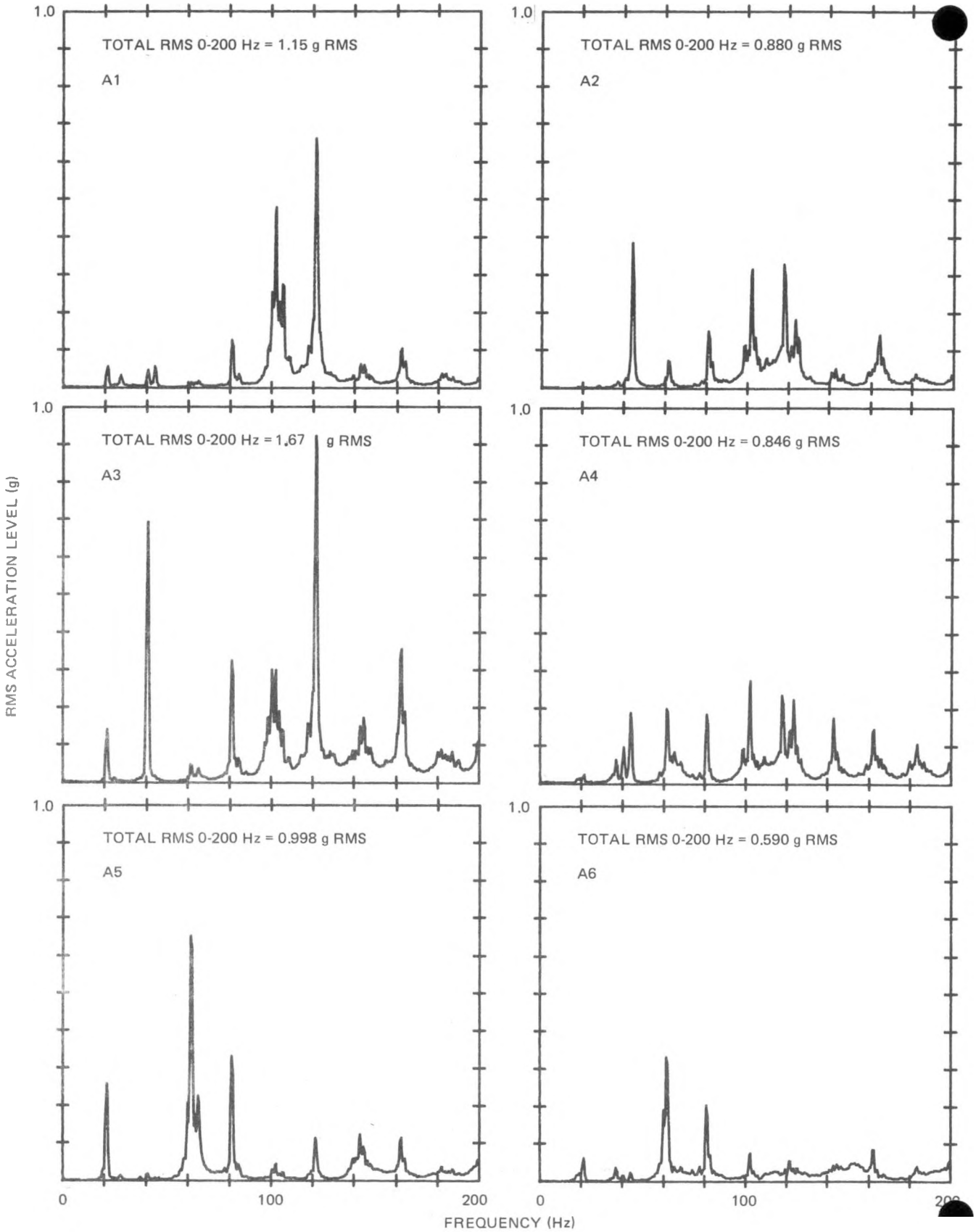

Figure 5-7. Acceleration Amplitude Spectra for Test Condition 0205 (Intermediate Level FIV) M = 1.91

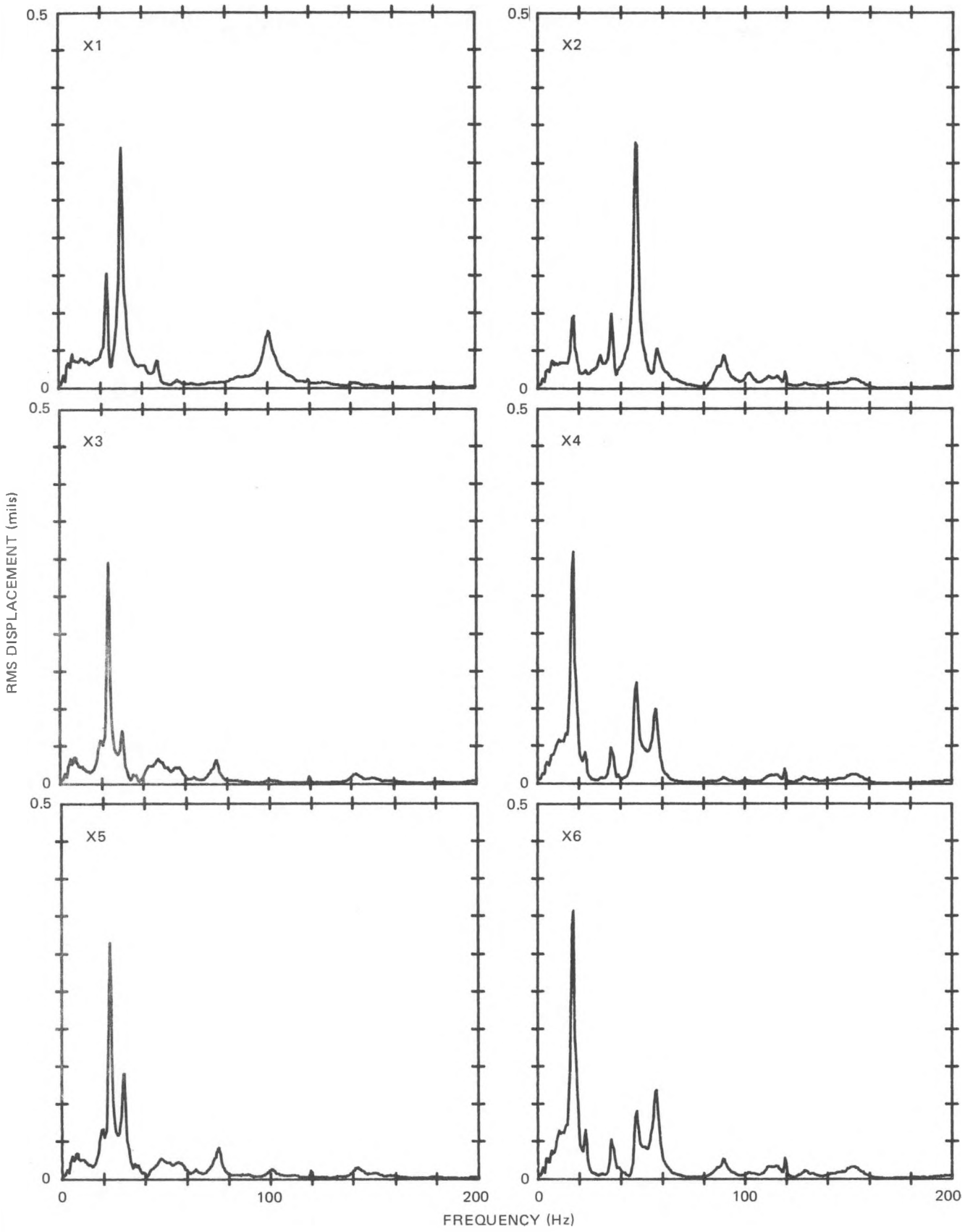

Figure 5-6. Displacement Amplitude Spectra for Test Condition 0201 (Low Level FIV) M = 2.90

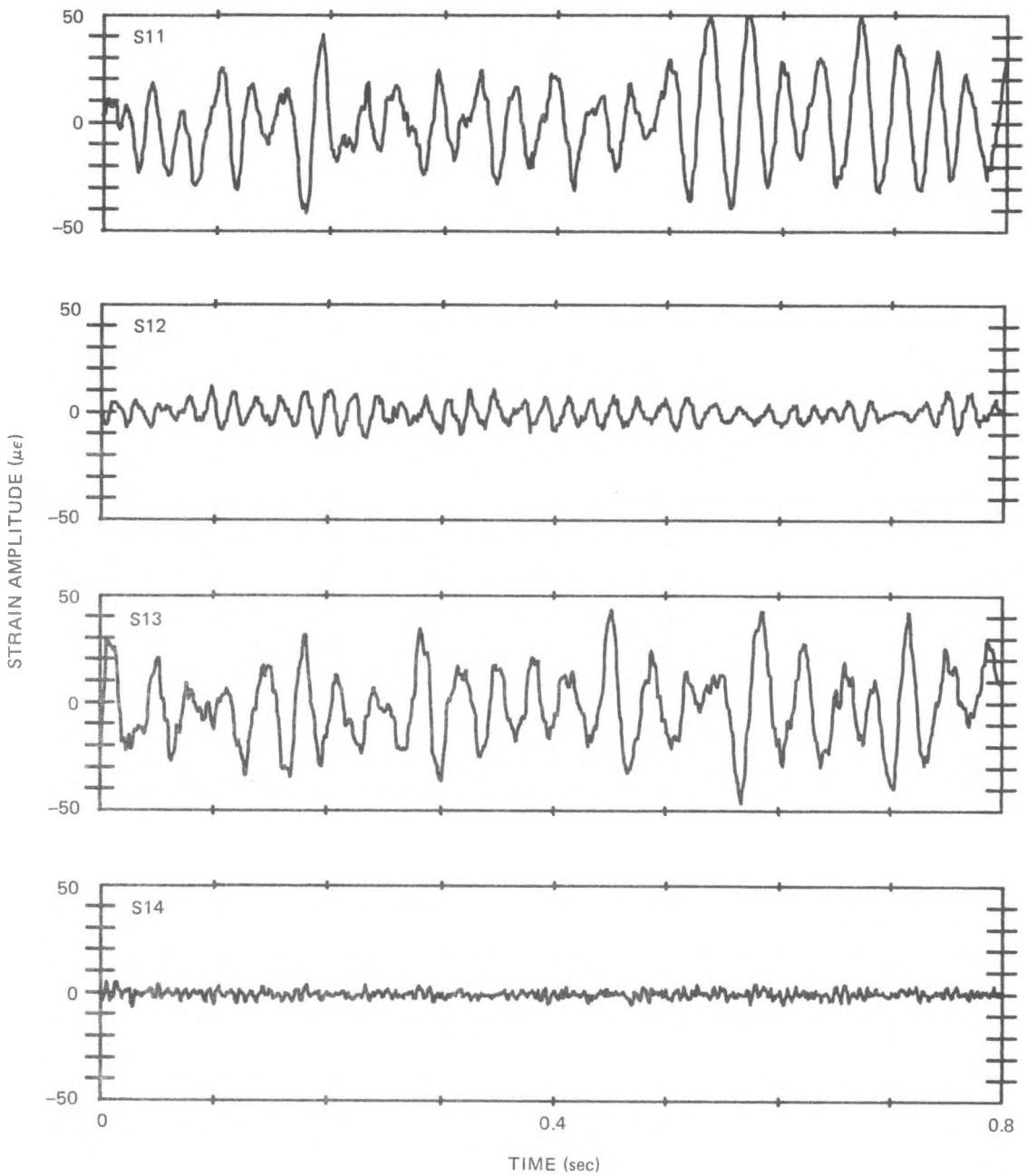

Figure 5-5. Instantaneous Strain Time Histories for Test Condition 0201 (Low Level FIV) M = 2.90

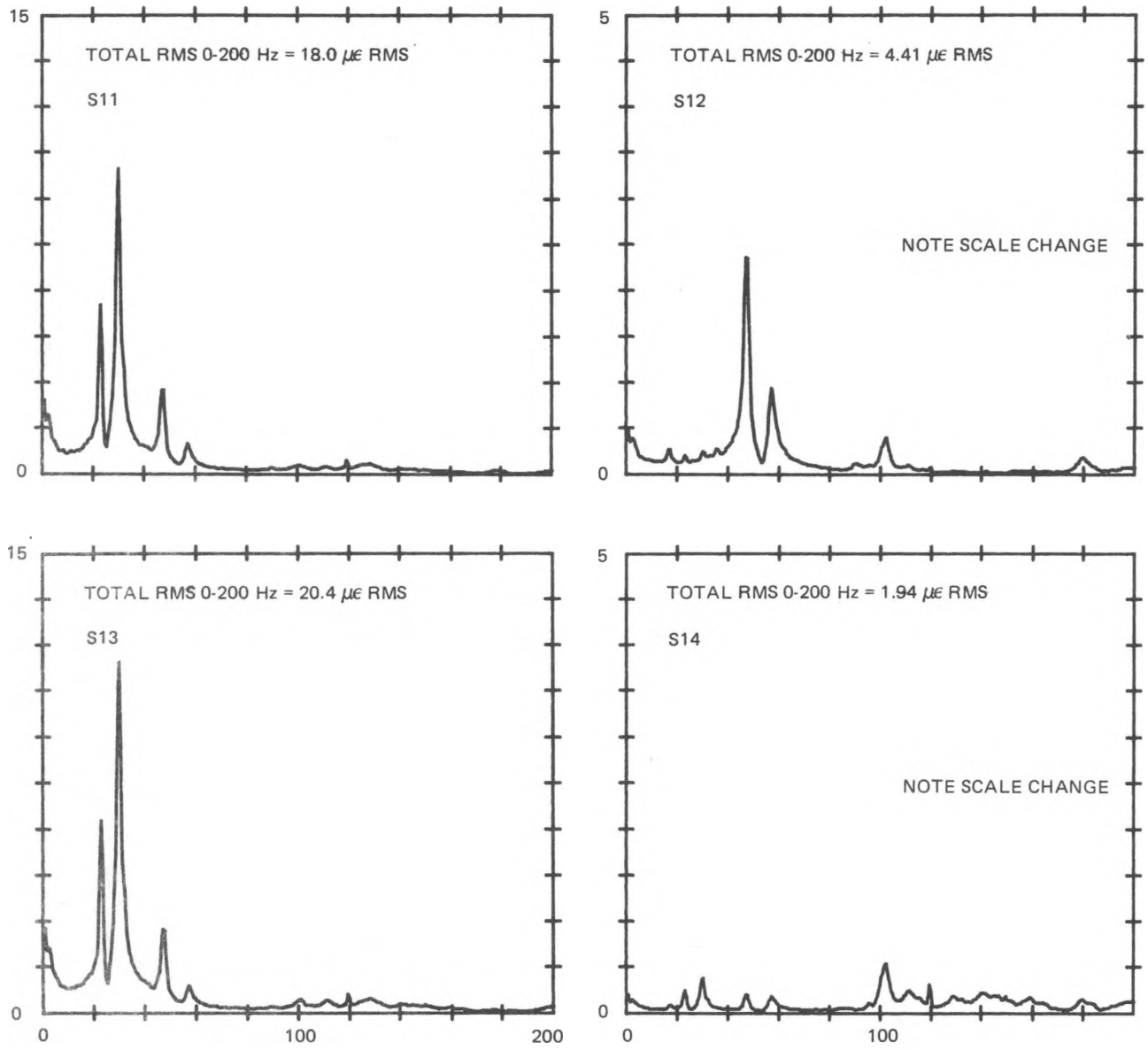

Figure 5-4. Strain Amplitude Spectra for Test Condition 0201 (Low Level FIV) M = 2.90

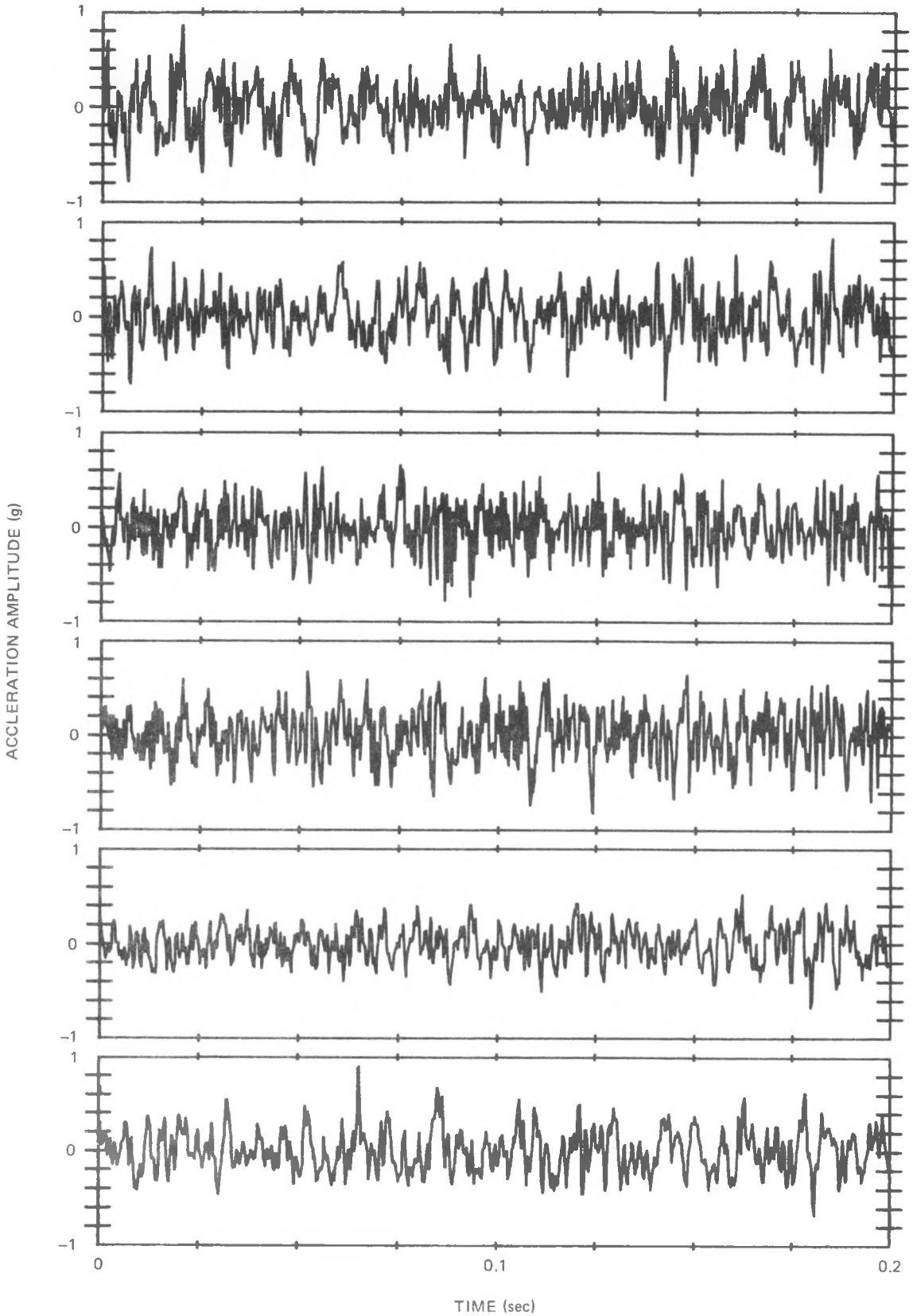

Figure 5-3. Instantaneous Acceleration Time Histories for Test Condition 0201 (Low Level FIV) M = 2.90

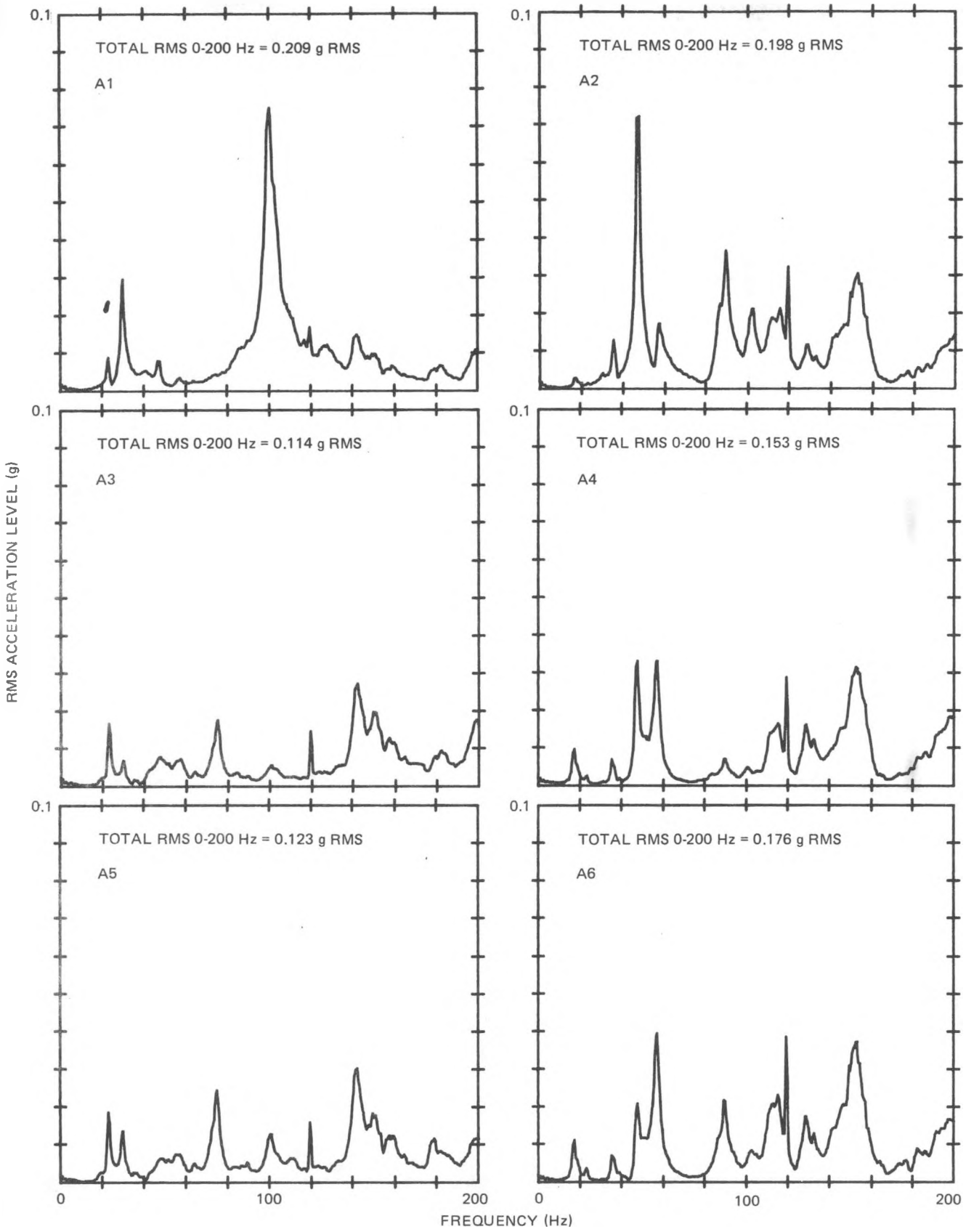

Figure 5-2. Acceleration Amplitude Spectra for Test Condition 0201 (Low Level FIV) M = 2.90

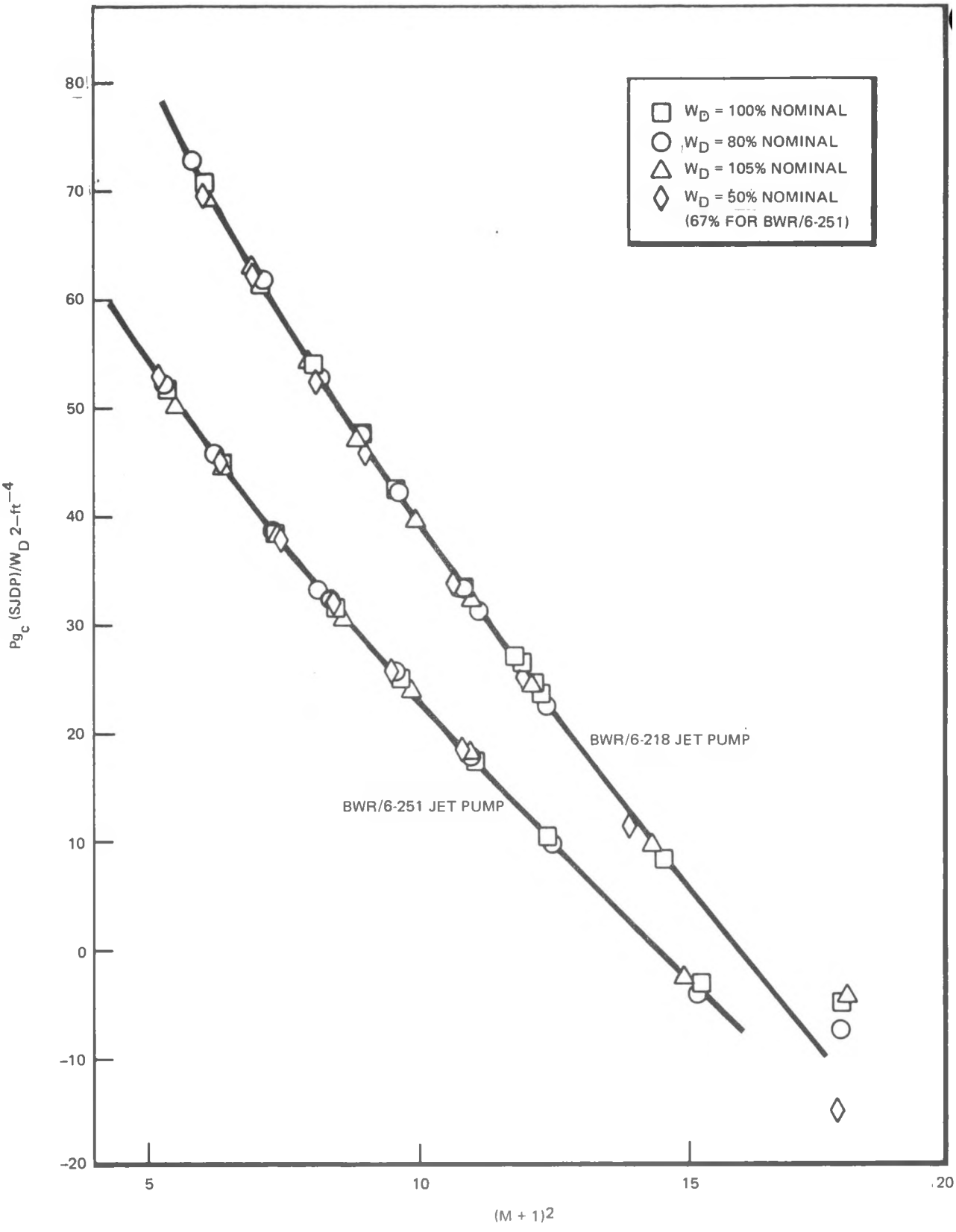

Figure 5-1. Jet Pump Hydraulic Characteristics

Table 5-7

TEST RESULTS FOR TEST CONDITION 43

BWR/6-218 TESTS AT 105% DRIVE FLOW

Run No.	Drive Flow Rate (% of 1.215 x 10^6 lb/hr)	Pressure (psia)	Temperature (^oF)	SJDP (psi)	M-Ratio
4302	105.3	1045.7	532.3	5.72	2.7849
4303	105.3	1045.4	532.4	14.26	2.4809
4304	104.8	1045.4	532.5	18.53	2.3170
4305	104.8	1045.6	532.5	22.73	2.1554
4306	104.3	1045.6	532.4	26.89	1.9813
4307	103.7	1045.5	532.6	30.44	1.8248
4308	103.9	1045.5	532.6	35.43	1.6269
4309	105.1	1045.3	532.4	39.89	1.4703
4310	105.4	1045.8	532.5	-2.51	3.2464

Table 5-8

TEST RESULTS FOR TEST CONDITION 46

BWR/6-218 TESTS AT 105% DRIVE FLOW

Run No.	Drive Flow Rate (% of 1.215 x 10^6 lb/hr)	Pressure* (psia)	Temperature* (^oF)	SJDP (psi)	M-Ratio
4601	49.8	1046	532.5	-1.90	3.2201
4602	50.2	1046	532.5	1.50	2.7312
4603	50.4	1046	532.5	3.34	2.4547
4604	50.4	1046	532.5	4.49	2.2662
4605	49.1	1046	532.5	5.75	2.0024
4606	50.2	1046	532.5	6.92	1.8505
4607	49.8	1046	532.5	8.05	1.6303
4608	49.8	1046	532.5	9.02	1.4570

*Nominal values - actual test data not available.

Table 5-5

TEST RESULTS FOR TEST CONDITION 41

BWR/6-218 TESTS AT 80% DRIVE FLOW

Run No.	Drive Flow Rate (% of 1.215 x 10^6 lb/hr)	Pressure (psia)	Temperature (°F)	SJDP (psi)	M-Ratio
4101	80.0	1044.0	532.0	-2.51	3.2311
4102	79.3	1043.6	532.1	7.40	2.5172
4103	79.5	1043.6	532.1	10.32	2.3340
4104	79.9	1048.3	532.2	11.15	2.2961
4105	79.7	1043.5	532.8	14.03	2.1035
4106	79.5	1044.9	532.9	15.65	1.9904
4107	79.4	1045.8	532.1	17.39	1.8659
4108	79.1	1044.4	532.7	20.14	1.6702
4109	79.7	1045.6	532.9	24.15	1.4124

Table 5-6

TEST RESULTS FOR TEST CONDITION 42

BWR/6-218 TESTS AT 100% DRIVE FLOW

Run No.	Drive Flow Rate (% of 1.215 x 10^6 lb/hr)	Pressure (psia)	Temperature (°F)	SJDP (psi)	M-Ratio
4201	99.9	1047.3	532.0	-2.44	3.2252
4202	99.8	1043.4	532.2	12.29	2.5047
4203	99.7	1043.5	532.6	17.41	2.2961
4204	100.2	1043.9	532.5	22.22	2.0968
4205	100.8	1043.9	532.3	25.26	1.9834
4206	100.3	1043.9	532.6	28.42	1.8384
4207	100.0	1049.3	532.6	32.06	1.6594
4208	99.6	1053.4	532.5	36.63	1.4599
4209	100.8	1048.2	532.7	14.03	2.4463
4210	100.9	1045.6	532.1	14.45	2.4316
4211	100.3	1045.8	532.7	12.89	2.4820
4212	99.9	1045.7	532.5	4.40	2.8106

Table 5-3

TEST RESULTS FOR TEST CONDITION 03

BWR/6-251 TESTS AT 105% DRIVE FLOW

Run No.	Drive Flow Rate (% of 1.45 x 10^6 lb/hr)	Pressure (psia)	Temperature (°F)	SJDP (psi)	M-Ratio
0301	105.5	1046.7	532.5	-2.19	2.8630
0302*	104.9	1045.8	N/A	8.3**	2.5345
0303	104.6	1045.9	531.7	14.70	2.3067
0304	104.8	1046.4	531.4	19.53	2.1393
0305	104.3	1046.4	531.4	24.97	1.9339
0306	104.4	1046.2	531.4	31.20	1.7055
0307	103.9	1046.2	531.5	35.72	1.5279
0308	103.4	1046.2	531.7	39.92	1.3451

*Questionable data.

**SJDP obtained by interpolation from Figure 5-1.

Table 5-4

TEST RESULTS FOR TEST CONDITION 03

BWR/6-251 TESTS AT 67% DRIVE FLOW

Run No.	Drive Flow Rate (% of 1.45 x 10^6 lb/hr)	Pressure* (psia)	Temperature* (°F)	SJDP (psi)	M-Ratio
0601	67.2	1046	532.5	17.69	1.2853
0602	67.3	1046	532.5	6.22	2.2899
0603	67.1	1046	532.5	8.59	2.0858
0604	66.2	1046	532.5	10.37	1.9070
0605	66.6	1046	532.5	12.44	1.7314
0606	66.9	1046	532.5	14.96	1.5200

*Nominal values - actual test data not available.

Table 5-1

TEST RESULTS FOR TEST CONDITION 01

BWR/6-251 TESTS AT 80% DRIVE FLOW

Run No.	Drive Flow Rate (% of 1.45×10^6 lb/hr)	Pressure (psia)	Temperature (°F)	SJDP (psi)	M-Ratio
0101	79.79	1043.0	531.6	-1.93	2.8950
0102	78.96	1042.8	531.4	4.59	2.5295
0103	79.50	1042.7	531.7	8.38	2.3132
0104	80.15	1042.6	531.8	12.29	2.0872
0105	79.93	1042.8	531.8	15.34	1.8945
0106	80.57	1046.9	532.0	15.94	1.8689
0107	80.66	1046.9	531.6	18.78	1.7019
0108	80.35	1046.7	532.0	21.96	1.4942
0109	80.17	1046.5	531.2	24.91	1.3031

Table 5-2

TEST RESULTS FOR TEST CONDITION 02

BWR/6-251 TESTS AT 100% DRIVE FLOW

Run No.	Drive Flow Rate (% of 1.45×10^6 lb/hr)	Pressure (psia)	Temperature (°F)	SJDP (psia)	M-Ratio
0201	100.7	1046.4	531.3	-2.50	2.9047
0202	100.1	1045.9	532.4	7.81	2.5188
0203	100.1	1046.3	531.2	13.00	2.3262
0204	99.9	1046.2	532.4	18.54	2.1103
0205	99.4	1046.2	531.8	23.33	1.9102
0206	99.5	1046.5	532.0	28.23	1.7150
0207	99.6	1046.7	532.1	33.00	1.5245
0208	99.6	1046.7	531.8	38.13	1.3152

Figure 5-42 shows the inside of the diffuser at the slip joint. Contact with the mixer is clearly apparent in the circumferential band just inside of the opening. This circumferential gouge was measured as 0.001-0.002 in. deep.

Representative photographs showing damage to the BWR/6-218 jet pump are shown in Figures 5-43 through 5-49. Figures 5-43 and 5-44 show the gouges in the mixer left by the adjusting screws, while Figure 5-45 shows the line of contact between the mixer and wedge. As with the BWR/6-251 jet pump, only enough torque to center the mixer within the diffuser was applied to the adjusting screws.

Figure 5-46 shows the tapered side of the wedge with wear marks and gouges left by contact with the restrainer bracket. Figure 5-47 shows the guide rod which prevents the wedge from tilting with respect to the mixer axis. The wear mark visible in this photograph is approximately 1/4-in. long, indicating the extent of wedge movement during the test.

Figures 5-48 and 5-49 show the slip-joint regions of the mixer and diffuser, respectively. The markings are the same as for the BWR/6-251 jet pump.

From these photographs it is apparent that, left unchecked, high-level FIV can cause substantial damage to the jet pump and associated support structures. The service time necessary to sustain the level of damage shown in these photographs was relatively short (50-100 hr). However, most, if not all, of the damage was caused by operation of the jet pumps at off-design hydraulic conditions.

The damage sustained by both jet pumps was similar in nature and extent. In both cases, gouges were observed at the points of contact between the mixer and adjusting screws (Figure 2-3). Additionally, wear was evident on the wedges at the points of contact with the mixer and the restrainer bracket. The wedges appeared to have vibrated vertically (axially) approximately 1/4-in. based on the wear pattern and did not return to their pre-test installation positions. During the BWR/6-218 jet pump test, tack welds between the restrainer bracket and one adjusting screw were broken and the screw had rotated completely out of the bracket, to be recovered at the bottom of the test vessel.

Further damage was found when the jet pumps were removed following each test. A circumferential gouge 0.001-0.002 in. deep was found on the inside of both diffuser collars. These gouges were caused by impacting with the mixers at the slip joint. The hardfaced (slip-joint) region of the mixers showed evidence of material pickup from the diffuser.

Representative photographs showing damage to the BWR/6-251 jet pump are shown in Figures 5-36 through 5-42. Figures 5-36 and 5-37 show the gouges in the mixer left by the adjusting screws. These gouges resulted from vibration rather than tightening torque, since only enough torque was applied during installation to center the mixer within the diffuser. Figure 5-38 shows the wear mark on the mixer left by contact with the wedge.

Figures 5-39 and 5-40 show the wear patterns on the tapered and flat side of the wedge, respectively. The tapered side of the wedge was in contact with the restrainer bracket. The light-colored areas of each side of the wedge show the stellite hardface inlay used to reduce wear. Despite this hardfacing, gouges in the tapered side of the wedge are visible.

Figure 5-41 shows the discharge end (slip-joint region) of the mixer. This region also was inlaid with stellite to minimize wear. The axial bands visible in the photograph show the areas of contact with the stellite strips on the inside of the diffuser. Between these bands are rough textured areas where material from the diffuser adhered to the stellite on the mixer.

Figures 5-24 through 5-28 show the FIV response of the jet pump at test condition 4205 (100% drive flow, 25.3 psi SJDP). These figures represent an "intermediate" level FIV response similar to the BWR/6-251 jet pump response. The dominant frequency for this jet pump, however, appears to be 58.5 Hz, with harmonics again indicating impacting between the mixer and diffuser at the slip joint.

Figures 5-29 through 5-33 show the FIV response of the jet pump at test condition 4208 (100% drive flow, 36.6 psi SJDP) and represent a high-level FIV response. The progression of FIV response from low-level to high-level is shown in Figure 5-34. The format and sensor identification is the same as for the BWR/6-251 jet pump. The transition from low-level to high-level FIV again appears to occur at a SJDP between 17 psi and 22 psi.

Figure 5-35 shows the FIV characteristic for the BWR/6-218 jet pump for all test conditions. The rms acceleration shown was calculated from Equation 5-3 using data averaged over a four-minute record (1000 averages) at a bandwidth of 1000 Hz. Also shown in this figure are the operating SJDP values for the BWR/6-218 jet pump at BOL and EOL. These values were again computed by combining the design data of Figure 2-7 with the jet pump hydraulic characteristic of Figure 5-1. As with the BWR/6-251 jet pump, operation of the BWR/6-218 jet pump for extended periods of time at high acceleration levels resulted in damage to the jet pump and support hardware. A detailed discussion of the damage to both jet pumps follows.

5.2.3 Jet Pump Damage

As mentioned previously, both BWR/6 jet pumps sustained damage as a consequence of several days' operation at high FIV levels. There exists no quantitative information which might be used to construct a damage history for either jet pump. However, both jet pumps were operated for approximately 50-100 hours at acceleration levels above 2 grms (Figures 5-18 and 5-35). At acceleration levels above approximately 4 grms, the jet pump vibration was clearly audible outside of the test vessel. At the highest acceleration levels (6-7 grms), the entire vessel, support structure and work platform were felt to vibrate.

each trace is the same and the spacing of the traces is proportional to the SJDP. From this figure, it is apparent that the harmonic FIV response becomes dominant at a SJDP between 18 psi and 23 psi (test conditions 0204 and 0205).

Figure 5-18 shows the FIV characteristic for the BWR/6-251 jet pump for all test conditions. The rms acceleration level shown represents an averaged value chosen to better represent the vectorial accelerations of the mixer at the slip joint. That is:

$$A^2_{rms} = A^2_{3rms} + A^2_{4rms} \qquad (5\text{-}3)$$

In Equation 5-3, A_{3rms} and A_{4rms} are the rms accelerations in the tangential and radial directions, respectively, averaged over a four-minute data record (1000 averages) at a bandwidth of 100 Hz. The rms accelerations are shown plotted against the natural logarithm of the SJDP to accentuate the asymptotic behavior at large SJDP.

Also shown in Figure 5-18 are the operating SJDP values for the 3800 MW and 4146 MW plants at BOL and EOL. These values were obtained by combining the design data of Figure 2-8 with the jet pump hydraulic characteristic of Figure 5-1. From Figure 5-18, it is apparent that the jet pump approaches the threshold of high-level FIV more closely with age (predicted).

For the BWR/6-251 jet pump, sustained operation at a SJDP above the threshold of high-level FIV resulted in damage to the jet pump and support hardware. A detailed discussion of this damage is presented in a later section of this report.

5.2.2 Vibration Characteristics of the BWR/6-218 Jet Pump

Figures 5-19 through 5-23 show the FIV response of the BWR/6-218 jet pump at test condition 4201 (100% drive flow, minimum SJDP). This test condition, as before, represents a base case jet pump response. The acceleration spectra (Figure 5-19) exhibit broad, low level peaks at the structural resonances. Figures 5-24 through 5-28 show the FIV response of the jet pump at test condition 4205 (100% drive flow, 25.3 psi SJDP). These figures represent an "intermediat

peaks in the 20-50 Hz range are natural frequencies associated with the riser/mixer combination, while the 17 Hz peak is the first mode frequency of the diffuser.

Figure 5-3 shows the corresponding instantaneous time histories for the six accelerometers. Little, if any, periodicity is evident in these time histories. Figures 5-4 and 5-5 show the strain amplitude spectra and instantaneous time histories, respectively, for the four strain gage pairs located on the riser brace arms (see Figure 4-3 for locations). Again, low amplitude structural resonances dominate the spectra. The instantaneous time histories, however, show considerable periodicity associated with the strong low frequency spectral lines and the absence of high frequency components.

Figure 5-6 shows the displacement amplitude spectra obtained by the double integration of the acceleration signals in the time domain. Note the similarity between the strain and displacement amplitude spectra.

Figures 5-7 through 5-11 show the FIV response of the jet pump at test condition 0205 (100% drive flow, 23.3 psi SJDP). These figures represent an "intermediate" level FIV response. The acceleration levels (Figure 5-7) are approximately 5 times the base level (Figure 5-2) and are strongly harmonic in nature. The sharpness of the spectral peaks is an indication of very low damping. The multiple harmonics of a 21 Hz fundamental frequency are evidence of impacting between the mixer and diffuser at the slip joint. Note that the 21 Hz frequency does not correspond to any of the natural structural frequencies apparent in the base case spectra.

Figures 5-12 through 5-16 show the FIV response of the jet pump at test condition 0208 (100% drive flow, 38.1 psi SJDP). This test condition represents a high-level FIV response. The acceleration levels (Figure 5-12) are approximately 15 times the base level (Figure 5-2) and differ considerably in character from the base case. Most of the vibrational energy is concentrated in a few dominant spectral lines.

Figure 5-17 shows the progression of the FIV response from the base case (test condition 0201) to the high-level case (test condition 0208) for the two accelerometers (A3, A4) located on the mixer near the slip joint. The vertical scale for

The vibration test data for the two jet pumps are presented separately. Each presentation consists of representative frequency and time domain graphs showing the dependence of vibration amplitude on SJDP. All test data were processed by a dual-channel spectrum analyzer which utilized a built-in microprocessor programmed with a highly efficient Fast Fourier Transform (FFT) algorithm. This instrument was capable of processing vibration data in both the time and frequency domains. A discussion of data analysis instrumentation and technique is given in Appendix B.

The vibration test data are presented as ensemble-averaged amplitude spectra and instantaneous time histories for each of the accelerometers and strain gages. Ensemble averaging was performed continuously over a four-minute data record (256 averages) to ensure that statistically accurate spectra were obtained. Additionally, the acceleration data were integrated twice in the time domain to produce displacement time histories from which ensemble-averaged displacement spectra were prepared. The integrating instrument had a high pass filter set at 10 Hz to minimize false low frequency displacement signals which result from the integration technique (Appendix B).

Throughout each presentation, the amplitude spectra are displayed over a frequency range of 0-200 Hz. This bandwidth was selected as being representative of the range of important displacement information as well as to provide adequate frequency resolution within the display. Furthermore, because of the harmonic nature of the high level FIV response, most of the information at frequencies above 200 Hz is redundant. However, the FIV response characterization graphs (amplitude versus SJDP) were constructed using data taken over a 1000 Hz bandwidth to ensure that all available information was utilized.

5.2.1 Vibration Characteristics of the BWR/6-251 Jet Pump

Figure 5-2 shows the ensemble-averaged acceleration amplitude spectra for the six accelerometers on the jet pump (see Figure 4-3 for locations) for test condition 0201 (100% drive flow, minimum SJDP). This test condition represents a base case with no slip joint leakage flow-related FIV. The fairly broad spectral peaks which are evident in each frame represent the highly damped response of the jet pump to the random excitation caused by the main flow through the jet pump. Based on experience with other jet pumps,[4] the spectral

5. TEST RESULTS

5.1 HYDRAULIC TEST RESULTS

At each steady-state test condition, a complete set of thermal-hydraulic test facility data was obtained. These data were independently analyzed[6,7] and are incorporated herein in order to establish a relationship between the hydraulic and mechanical characteristics of the jet pump.

Tables 5-1 through 5-4 list the thermal-hydraulic characteristics of the BWR/6-251 jet pump at the four test conditions indicated in Table 4-2.

From these hydraulic data, a relationship between the drive flow, M-ratio and SJDP is obtained. Since the internal jet pump pressure is a function of geometry and internal fluid velocity, it is reasonable to assume that the SJDP is also related to the fluid velocity (assuming constant pressure external to the jet pump). Thus, with ρ as the weight density,

$$SJDP \alpha \rho V^2/2g_c = W_T^2/2g_c \rho A^2. \qquad (5\text{-}1)$$

From the relationships among the jet pump hydraulic parameters developed earlier, it follows that:

$$SJDP \alpha (M+1)^2 W_D^2/2 \rho g_c A^2 \qquad (5\text{-}2)$$

This hydraulic characteristic for the two jet pumps tested is shown in Figure 5-1. This figure not only provides the useful relationship between SJDP and flow, but also demonstrates the consistency (reliability) of the hydraulic data.

5.2 VIBRATION TEST RESULTS

The vibration test results presented below are by no means exhaustive. These data have been selected as being representative of the character and magnitude of the FIV responses of the particular jet pumps tested.

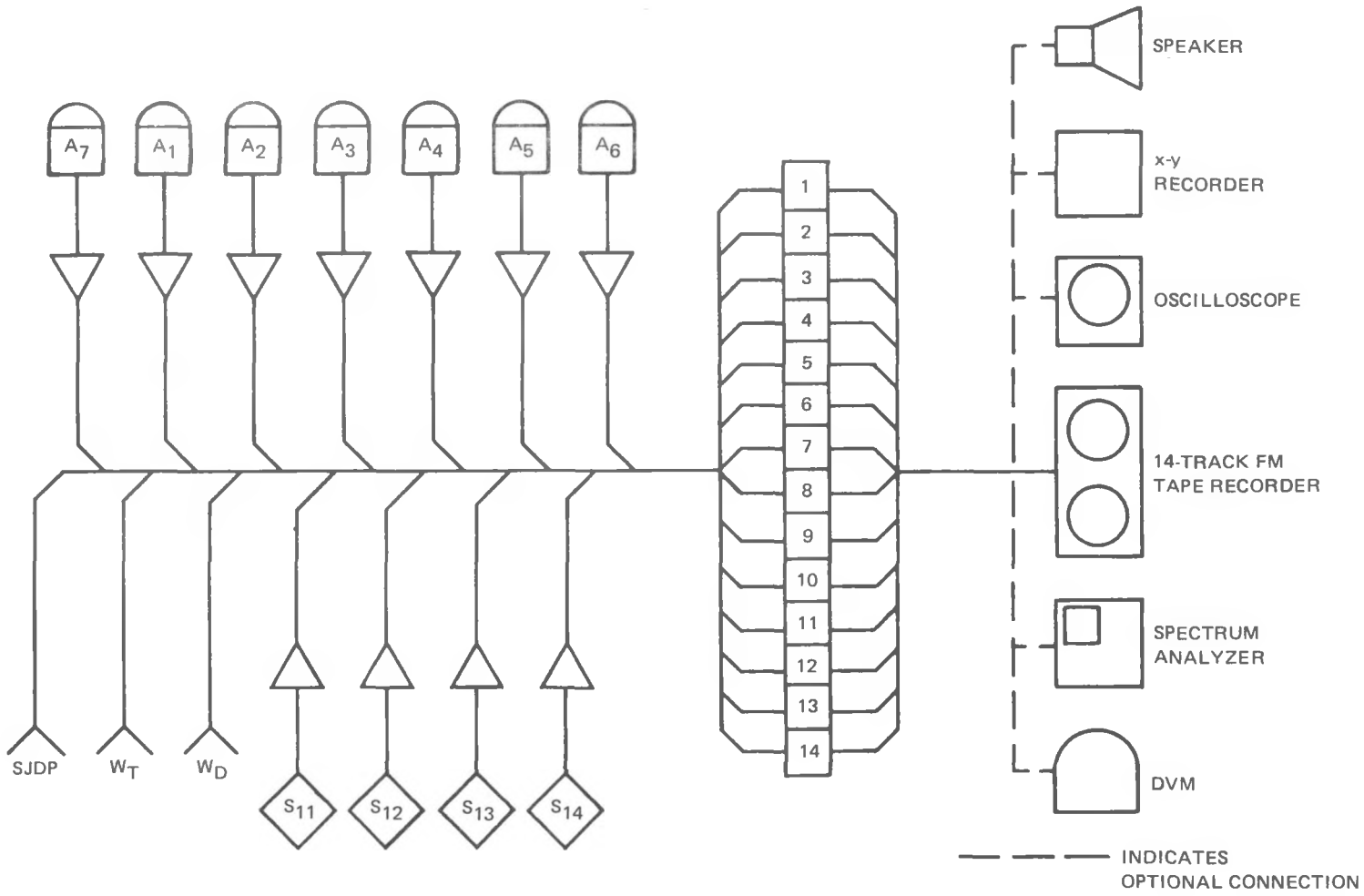

Figure 4-5. Jet Pump Test Data Acquisition Arrangement